

**ATTACHMENT 1**

---

**CDI REPORT NO. 10-11NP, "STRESS ASSESSMENT OF NINE  
MILE POINT UNIT 2 STEAM DRYER USING THE ACOUSTIC  
CIRCUIT MODEL REV. 4.1," REV. 0  
(NON-PROPRIETARY)**

---

Stress Assessment of Nine Mile Point  
Unit 2 Steam Dryer Using the Acoustic Circuit Model Rev. 4.1

Revision 0

Prepared by

Continuum Dynamics, Inc.  
34 Lexington Avenue  
Ewing, NJ 08618

Prepared under Purchase Order No. 7708631 for

Constellation Energy Group  
Nine Mile Point Nuclear Station, LLC  
P. O. Box 63  
Lycoming, NY 13093

Prepared by



---

Alexander H. Boschitsch

Approved by



---

Alan J. Bilanin

June 2010

This report complies with Continuum Dynamics, Inc. Nuclear Quality Assurance Program currently in effect.



## Executive Summary

The finite element model and analysis methodology, used to assess stresses induced by the flow of steam through the steam dryer at Nine Mile Point Unit 2 (NMP2), are described and applied to obtain stresses at CLTP conditions. The stress analysis is consistent with those carried out in the U.S. for prior dryer qualification to EPU conditions and the resulting stresses are assessed for compliance with the ASME B&PV Code 2007 [1], Section III, subsection NG, for the load combination corresponding to normal operation (the Level A Service Condition).

The stress analysis is carried out in the frequency domain, which confers a number of useful computational advantages over a time-accurate transient analysis including the ability to assess the effects of frequency scaling in the loads without the need for additional finite element calculations. The analysis develops a series of unit stress solutions corresponding to the application of a unit pressure at a MSL at specified frequency,  $f$ . Each unit solution is obtained by first calculating the associated acoustic pressure field using a separate analysis that solves the damped Helmholtz equation within the steam dryer [2]. This pressure field is then applied to a finite element structural model of the steam dryer and the harmonic stress response at frequency,  $f$ , is calculated using the commercial ANSYS 10.0 finite element analysis software. This stress response constitutes the unit solution and is stored as a file for subsequent processing. Once all unit solutions have been computed, the stress response for any combination of MSL pressure spectrums (obtained by Fast Fourier Transform of the pressure histories in the MSLs) is determined by a simple matrix multiplication of these spectrums with the unit solutions.

The acoustic loads for the results herein are prepared using an acoustic circuit model (ACM) that has recently been revised to version 4.1 [3]. This version reflects new biases and uncertainties obtained during re-benchmarking against available Quad Cities (QC) data carried out under the requirement that identical filtering methods be used on both QC data and new plant signal measurements. Also, the ACM acoustic load predictions are obtained using recently acquired main steam line strain gage measurements[4]. Other than the removal of known non-acoustic discrete frequencies (e.g., electrical noise at multiples of 60 Hz) and the application of coherence filtering (which was also invoked when processing the QC data) no other filtering methods are used. In particular, no noise subtraction using low power data is performed. Further details of the acoustic load processing procedure are given in [3].

The baseline calculation presented here pertains to the same steam dryer examined in [5]. That configuration included several modifications to meet margin under previous ACM Rev. 4.0 loads without low power subtraction. These modifications include: (i) the addition of reinforcement strips on the closure plates; (ii) reinforcements of the closure plate attachment welds and (iii) reinforcement welds for the lifting rod braces.

Results obtained from application of the methodology to this baseline NMP2 steam dryer show that at nominal CLTP operation (no frequency shift) the minimum alternating stress ratio (SR-a) anywhere on the steam dryer is  $SR-a=1.94$ . The loads used to obtain this value account for all the end-to-end biases and uncertainties in the loads model [4] and finite element analysis. To account for uncertainties in the modal frequency predictions of the finite element model, the stresses are also computed for loads that are shifted in the frequency domain by  $\pm 2.5\%$ ,  $\pm 5\%$ ,

$\pm 7.5\%$  and  $\pm 10\%$ . The minimum alternating stress ratio encountered at any frequency shift is found to be  $SR-a=1.56$  occurring at the  $-5\%$  shift and occurring on the weld connecting the lifting rod support brace to the side plate of the steam dryer. The stress ratio due to maximum stresses ( $SR-P$ ) is dominated by static loads and is  $SR-P=1.25$  with all frequency shifts considered.

Since flow-induced acoustic resonances are not anticipated in the steam dryer, the alternating stress ratios at EPU operation can be obtained by scaling the CLTP values by the steam flow velocity squared,  $(U_{EPU}/U_{CLTP})^2=1.1756^2=1.382$ . Under this approach, the limiting alternating stress ratio becomes  $SR-a=1.56/1.382=1.13$ . This is below the target value at EPU of  $SR-a=2$ .

Since the baseline configuration does not meet EPU margin, additional modifications are presented in Section 6 that ensure stresses remain below the target levels required for EPU operation. This section describes the modifications needed and provides calculations showing that these stresses meet margin. The reinforcements consist of: (i) a localized reinforcement of the lifting rod support braces and its attachment weld to the steam dryer side plate to eliminate the current high stress state; (ii) addition of a reinforcement plate over the outboard section of the middle hood located between the closure plate and existing middle hood reinforcement strip and (iii) addition of a total of four 20 lb masses on the inner hoods to alleviate high stresses on the inner hood/hood support welds. These three modifications are in addition to the previously planned reinforcement of the closure plates and its attachment welds. With these modifications in place the limiting alternating stress ratio on the dryer increases to greater than 2.76 for all locations identified as warranting modification.

The review of the stress margin identifies a group of locations (referred to as group 4 in Section 6) that has a minimum stress ratio of  $SR-a=2.65$  which corresponds to the steam flow for 117.5% EPU conditions. No additional modifications are considered mandatory to meet the required factor of two to the endurance limit for 120% EPU based on the application of the curve B of Fig I-9.2.2 in Appendix I of Section III in the ASME B&PV Code for the group 4 locations. In addition supplemental measurements using the [(3)] installed on MSL-D described in [6] and discussed in [7] indicate that noise in the frequency intervals when scaled using the velocity squared rule is biasing the stress ratios high. Under the premise that noise is a significant contributor to the load, then the load is not expected to increase with velocity squared scaling and the final margin at 120% EPU is expected to remain well above 2. While modification concepts are presented and feasible, complete stress evaluations for these modifications are not considered warranted as a factor of 2 margin is demonstrated using the ASME code endurance limits applicable to this location. It is also anticipated, based on the [(3)] supplemental data on MSL-D, that power ascension testing will demonstrate substantial margin without modification of the group 4 locations.

## Table of Contents

Section	Page
Executive Summary .....	i
Table of Contents .....	iii
1. Introduction and Purpose .....	1
2. Methodology .....	3
2.1 Overview .....	3
2.2 [[..... <sup>(3)</sup> ]] .....	5
2.3 Computational Considerations.....	6
3. Finite Element Model Description.....	9
3.1 Steam Dryer Geometry .....	9
3.2 Material Properties.....	12
3.3 Model Simplifications.....	12
3.4 Perforated Plate Model .....	13
3.5 Vane Bank Model .....	15
3.6 Water Inertia Effect on Submerged Panels.....	16
3.7 Structural Damping.....	16
3.8 Mesh Details and Element Types .....	16
3.9 Connections Between Structural Components.....	16
3.10 Pressure Loading.....	28
4. Structural Analysis.....	31
4.1 Static Analysis .....	31
4.2 Harmonic Analysis.....	31
4.3 Post-Processing .....	37
4.4 Computation of Stress Ratios for Structural Assessment .....	37
4.5 Finite Element Sub-modeling .....	40
5. Results.....	48
5.1 General Stress Distribution and High Stress Locations.....	49
5.2 Load Combinations and Allowable Stress Intensities .....	63
5.3 Frequency Content and Filtering of the Stress Signals.....	91
6. Proposed Modifications to Achieve EPU Target Stress Levels.....	101
7. Conclusions.....	118
8. References.....	119
Appendix A Sub-modeling and Modification of Closure Plates .....	121
Sub model Node 101175.....	126
Sub model node 91605.....	133
Sub model node 95172.....	141
Sub model node 100327.....	150
Appendix B. Scoping Evaluation of Hood Support Cutout to Alleviate Stress in the Hood/Hood Support/Base Plate Weld .....	157

## 1. Introduction and Purpose

Plans to qualify the Nine Mile Point nuclear plant for operation at Extended Power Uprate (EPU) operating condition require an assessment of the steam dryer stresses experienced under the increased loads. The steam dryer loads due to pressure fluctuations in the main steam lines (MSLs) are potentially damaging and the cyclic stresses from these loads can produce fatigue cracking if loads are sufficiently high. The industry has addressed this problem with physical modifications to the dryers, as well as a program to define steam dryer loads and their resulting stresses. The purpose of the stress analysis discussed here is to calculate the maximum and alternating stresses generated during Current Licensed Thermal Power (CLTP) and Extended Power Uprate (EPU) and to determine the margins that exist when compared to stresses that comply with the ASME Code (ASME B&PV Code, Section III, subsection NG).

The stress analysis of the modified NMP2 steam dryer establishes whether the existing and proposed modifications are adequate for sustaining structural integrity and preventing future weld cracking under planned EPU operating conditions. The load combination considered here corresponds to normal operation (the Level A Service Condition) and includes fluctuating pressure loads developed from NMP2 main steam line data, and weight. The fluctuating pressure loads, induced by the flowing steam, are predicted using a separate acoustic circuit analysis of the steam dome and main steam lines [8]. Level B service conditions, which include seismic loads, are not included in this evaluation.

[[

<sup>(3)</sup>]] This approach also affords a number of additional computational advantages over transient simulations including:

<sup>(3)</sup>]] This last advantage is realized through the use of “unit” solutions representing the stress distribution resulting from the application of a unit fluctuating pressure at one of the MSLs at a particular frequency. [[  
<sup>(3)</sup>]]

Prior stress evaluations of the NMP2 steam dryer [5] used the ACM Rev. 4.0 acoustic analysis to estimate the loads on the dryer. An important aspect of the acoustic prediction is the filtering of the strain gage signals measured on the main steam lines. Contamination of these

signals by various sources of noise including discrete electrical frequencies (60, 120, 180 and 240 Hz), pipe bending, EIC and mechanical pump frequencies, all lead to fictitious and potentially excessive stress predictions. Therefore removal of non-acoustic noise in the signal is performed to obtain more accurate acoustic loads and steam dryer stresses. In earlier work, noise subtraction was performed using signals collected at low power where acoustic sources are negligible. However, technical considerations including how to process the signals in frequency ranges where the low power data exceeded CLTP levels and the legitimacy of bias and uncertainty estimates procured using QC data without noise subtraction in place led to an effort to re-benchmark the ACM model. The new re-benchmarking activity dispensed with low power subtraction and instead utilized an improved coherence filtering scheme. Also, the overall methodology requires that the same filtering methods employed when benchmarking the ACM against QC data be used in subsequent plant evaluations. This benchmarking activity resulted in ACM Rev. 4.1 [3], which, together with a recently acquired and complete series of strain gage measurements [4] is used herein to obtain new steam dryer stress predictions.

This report describes the overall methodology used to obtain the unit solutions in the frequency domain and how to assemble them into a stress response for a given combination of pressure signals in the MSLs. This is followed by details of the NMP2 steam dryer finite element model including the elements used and overall resolution, treatment of connections between elements, the hydrodynamic model, the implementation of structural damping and key idealizations/assumptions inherent to the model. Post-processing procedures are also reviewed including the computation of maximum and alternating stress intensities, identification of high stress locations, adjustments to stress intensities at welds and evaluation of stress ratios used to establish compliance with the ASME Code. The results in terms of stress intensity distributions and stress ratios are presented next together with PSDs of the dominant stress components.

Application of the new ACM Rev. 4.1 acoustic loads results in several locations requiring reinforcements to meet target EPU stress levels (i.e., an alternating stress ratio of 2.0). Two of these locations involve the closure plates and the lifting rod support braces that were also identified in [5] as requiring reinforcement when dryer loads were estimated using ACM Rev. 4.0 *without* noise subtraction. The reinforcements recommended in [5] remain in place. Stiffening strips are added to the closure plate to simultaneously increase the frequency and lower stresses [9]; also the closure plate attachment weld is strengthened by placing an additional weld on the interior side of the junction where the closure plate meets the hood or vane bank. For the lifting rod braces, the existing 1/4 in weld is increased to 1/2 in. In addition to these prior locations, the ACM Rev. 4.1 loads warrant additional reinforcements. These are described in detail in Section 6 and include: (i) further reinforcement of the lifting rod support braces by welding additional plates to the braces and connected side-plates; (ii) overlaying of a 3/8" thick reinforcement sheet on the middle hood section lying outboard of the closure plates to suppress stresses occurring adjacent to the existing 3/8" reinforcement strip; (iii) the addition of four 20 lb masses on the center-most sections of the inner hoods to suppress stresses on the hood/hood support weld. With these reinforcements in place the dryer meets the EPU target stress levels.

## 2. Methodology

### 2.1 Overview

Based on previous analysis undertaken at Quad Cities Units 1 and 2, the steam dryer can experience strong acoustic loads due to the fluctuating pressures in the MSLs connected to the steam dome containing the dryer. C.D.I. has developed an acoustic circuit model (ACM) that, given a collection of strain gage measurements [10] of the fluctuating pressures in the MSLs, predicts the acoustic pressure field anywhere inside the steam dome and on the steam dryer [2, 8, 11]. The ACM is formulated in frequency space and contains two major components that are directly relevant to the ensuing stress analysis of concern here. [[

<sup>(3)</sup>]]

[[

<sup>(3)</sup>]]

[[

<sup>(3)</sup>]]

2.2 [[  
[[

<sup>(3)</sup>]]

<sup>(3)</sup>]]



[[

(3)]]

### 2.3 Computational Considerations

Focusing on the structural computational aspects of the overall approach, there are a number of numerical and computational considerations requiring attention. The first concerns the transfer of the acoustic forces onto the structure, particularly the spatial and frequency resolutions. The ANSYS finite element program inputs general distributed pressure differences using a table format. This consists of regular 3D rectangular (i.e., block)  $n_x \times n_y \times n_z$  mesh where  $n_\alpha$  is the number of mesh points in the  $i$ -th Cartesian direction and the pressure difference is provided at each mesh point (see Section 3.10). These tables are generated separately using a program that reads the loads provided from the ACM software, distributes these loads onto the finite element mesh using a combination of interpolation procedures on the surface and simple diffusion schemes off the surface (off-surface loads are required by ANSYS to ensure proper interpolation of forces), and written to ASCII files for input to ANSYS. A separate load file is written at each frequency for the real and imaginary component of the complex force.

The acoustic field is stored at 5 Hz intervals from 0 to 250 Hz. While a 5 Hz resolution is sufficient to capture frequency dependence of the acoustic field (i.e., the pressure at a point varies gradually with frequency), it is too coarse for representing the structural response especially at low frequencies. For 1% critical structural damping, one can show that the frequency spacing needed to resolve a damped resonant peak at natural frequency,  $f_n$ , to within 5% accuracy is  $\Delta f = 0.0064 \times f_n$ . Thus for  $f_n = 10$  Hz where the lowest structural response modes occur, a frequency interval of 0.064 Hz or less is required. In our calculations we require that 5% maximum error be maintained over the range from  $f_n = 5$  Hz to 250 Hz resulting in a finest frequency interval of 0.0321 Hz at the low frequency end (this adequately resolves all structural modes up to 250 Hz). Since there are no structural modes between 0 to 5 Hz, a 0.5 Hz spacing is used over this range with minimal (less than 5%) error. The unit load,  $\hat{f}_n(\omega, \mathbf{R})$ , at any frequency,  $\omega_k$ , is obtained by linear interpolation of the acoustic solutions at the two nearest frequencies,  $\omega_i$  and  $\omega_{i+1}$ , spaced 5 Hz apart. Linear interpolation is sufficient since the pressure load varies slowly over the 5 Hz range (linear interpolation of the structural response would not be acceptable over this range since it varies much more rapidly over the same interval). Details regarding the frequency resolution have been provided in [13].

#### *Solution Management*

[[

(3)]]

[[

(3)]]

### *Structural Damping*

In harmonic analysis one has a broader selection of damping models than in transient simulations. A damping factor,  $z$ , of 1% critical damping is used in the structural analysis. In transient simulations, this damping can only be enforced exactly at two frequencies (where the damping model is “pinned”). Between these two frequencies the damping factor can be considerably smaller, for example 0.5% or less depending on the pinning frequencies. Outside the pinning frequencies, damping is higher. With harmonic analysis it is straightforward to enforce very close to 1% damping over the entire frequency range. In this damping model, the damping matrix,  $\mathbf{D}$ , is set to

$$\mathbf{D} = \frac{2z}{\omega} \mathbf{K} \quad (7)$$

where  $\mathbf{K}$  is the stiffness matrix and  $\omega$  the forcing frequency. When comparing the response obtained with this model against that for a constant damping ratio, the maximum difference at any frequency is less than 0.5%, which is far smaller than the 100% or higher response variation obtained when using the pinned model required in transient simulation.

### *Load Frequency Rescaling*

One way to evaluate the sensitivity of the stress results to approximations in the structural modeling and applied loads is to rescale the frequency content of the applied loads. In this procedure the nominal frequencies,  $\omega_k$ , are shifted to  $(1+\lambda)\omega_k$ , where the frequency shift,  $\lambda$ , ranges between  $\pm 10\%$ , and the response recomputed for the shifted loads. The objective of the frequency shifting can be explained by way of example. Suppose that in the actual dryer a strong structural-acoustic coupling exists at a particular frequency,  $\omega^*$ . This means that the following conditions hold simultaneously: (i) the acoustic signal contains a significant signal at  $\omega^*$ ; (ii) the structural model contains a resonant mode of natural frequency,  $\omega_n$ , that is near  $\omega^*$ ; and (iii) the associated structural mode shape is strongly coupled to the acoustic load (i.e., integrating the product of the mode shape and the surface pressure over the steam dryer surface produces a significant modal force). Suppose now that because of discretization errors and modeling idealizations that the predicted resonance frequency differs from  $\omega^*$  by a small amount (e.g., 1.5%). Then condition (ii) will be violated and the response amplitude therefore significantly diminished. By shifting the load frequencies one re-establishes condition (ii) when  $(1+\lambda)\omega^*$  is

near  $\omega_n$ . The other two requirements also hold and a strong structural acoustic interaction is restored.

[[

(3)]]

*Evaluation of Maximum and Alternating Stress Intensities*

Once the unit solutions have been obtained, the most intensive computational steps in the generation of stress intensities are: (i) the FFTs to evaluate stress time histories from (5); and (ii) the calculation of alternating stress intensities. [[

(3)]]

The high computational penalty incurred in calculating the alternating stress intensities is due to the fact that this calculation involves comparing the stress tensors at every pair of points in the stress history. This comparison is necessary since in general the principal stress directions can vary during the response, thus for N samples in the stress history, there will be  $(N-1)N/2$  such pairs or, for  $N=64K$  (the number required to accurately resolve the spectrum up to 250 Hz in 0.01 Hz intervals),  $2.1 \times 10^9$  calculations per node each requiring the determination of the roots to a cubic polynomial. [[

(3)]]

### 3. Finite Element Model Description

A description of the ANSYS model of the nine Mile Point Unit 2 steam dryer follows.

#### 3.1 Steam Dryer Geometry

A geometric representation of the Nine Mile Point Unit 2 steam dryer was developed from available drawings (provided by Constellation Energy Group and included in the design record file, DRF-C-279C) within the Workbench module of ANSYS. The completed model is shown in Figure 1. This model includes on-site modifications to the Nine Mile Point Unit 2 steam dryer. These are as follows.

##### *On-Site Modifications*

- (i) The top tie rods are replaced with thicker ones.
- (ii) Inner side plates are replaced with thicker ones.
- (iii) Middle hoods are reinforced with additional strips.
- (iv) Lifting rods are reinforced with additional gussets.
- (v) Per FDDR KG1-0265 the support conditions are adjusted to ensure that the dryer is supported 100% on the seismic blocks.

These additional modifications have been incorporated into the NMP2 steam dryer model and are reflected in the results presented in this report. The affected areas are shown in Figure 2.

##### *Modifications Planned for EPU Operation – Set 1.*

In [5] several modifications were proposed to meet target EPU stress margins using a previous acoustic loads model (ACM Rev. 4.0) without noise subtraction. As described in [5] reinforcement of the closure plates and increases in selected weld sizes were recommended since analysis showed that the acoustic loads elicit a strong response of the original closure plates. These structures were therefore modified using stiffening strips to simultaneously reinforce them and shift their frequencies away from significant acoustic loads [9]. Updated analysis of these components and their incorporation into the full steam dryer analysis are summarized in Appendix A. Modifications to welds are analyzed using sub-models to minimize computational cost. These analyses are performed at the following locations as discussed further in Section 4.5: (i) the lifting rod support braces; (ii) closure plate welds; (iii) the ends of selected tie bars; (iv) the hood/hood support welds. All of the modifications summarized here and in Section 4.5 are implemented in what constitutes the baseline dryer model used to generate all results in Section 5.

##### *Supplementary Modifications Considered for EPU Operation – Set 2.*

When the dryer is subjected to the acoustic loads processed using the ACM Rev. 4.1 analysis, new locations emerge that do not meet EPU target levels. These locations are summarized in Section 6 together with proposed modification strategies. Briefly these modifications include: (a) further reinforcement of the lifting rod braces; (b) addition of a curved plate over the section of the middle hood lying between the closure plate and reinforcement strip and (c) addition of 20lb masses on the inner-most panels of the inner hoods to eliminate high stresses on the

hood/hood support junctions. These modifications are not reflected in the Section 5 results; instead, a stress evaluation of the steam dryer with these modifications in place is carried out in Section 6 using the [(3)] stress evaluation method.

#### *Reference Frame*

The spatial coordinates used herein to describe the geometry and identify limiting stress locations are expressed in a reference frame whose origin is located at the intersection of the steam dryer centerline and the plane containing the base plates (this plane also contains the top of the upper support ring and the bottom edges of the hoods). The y-axis is parallel to the hoods, the x-axis is normal to the hoods pointing from MSL C/D to MSL A/B, and the z-axis is vertical, positive up.

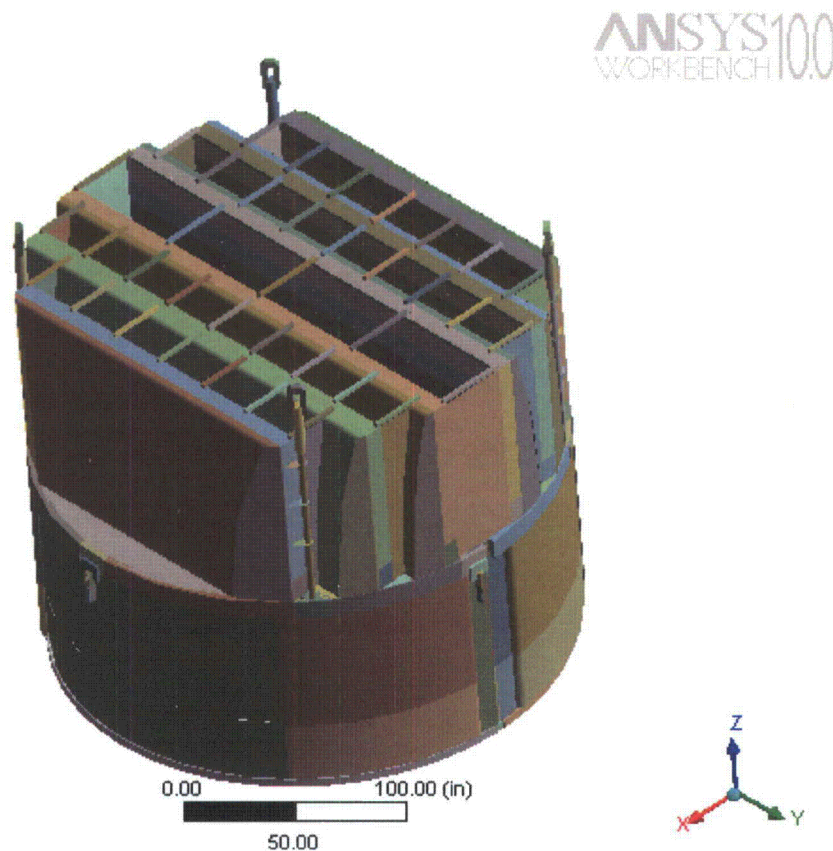


Figure 1. Overall geometry of the Nine Mile Point Unit 2 steam dryer model.

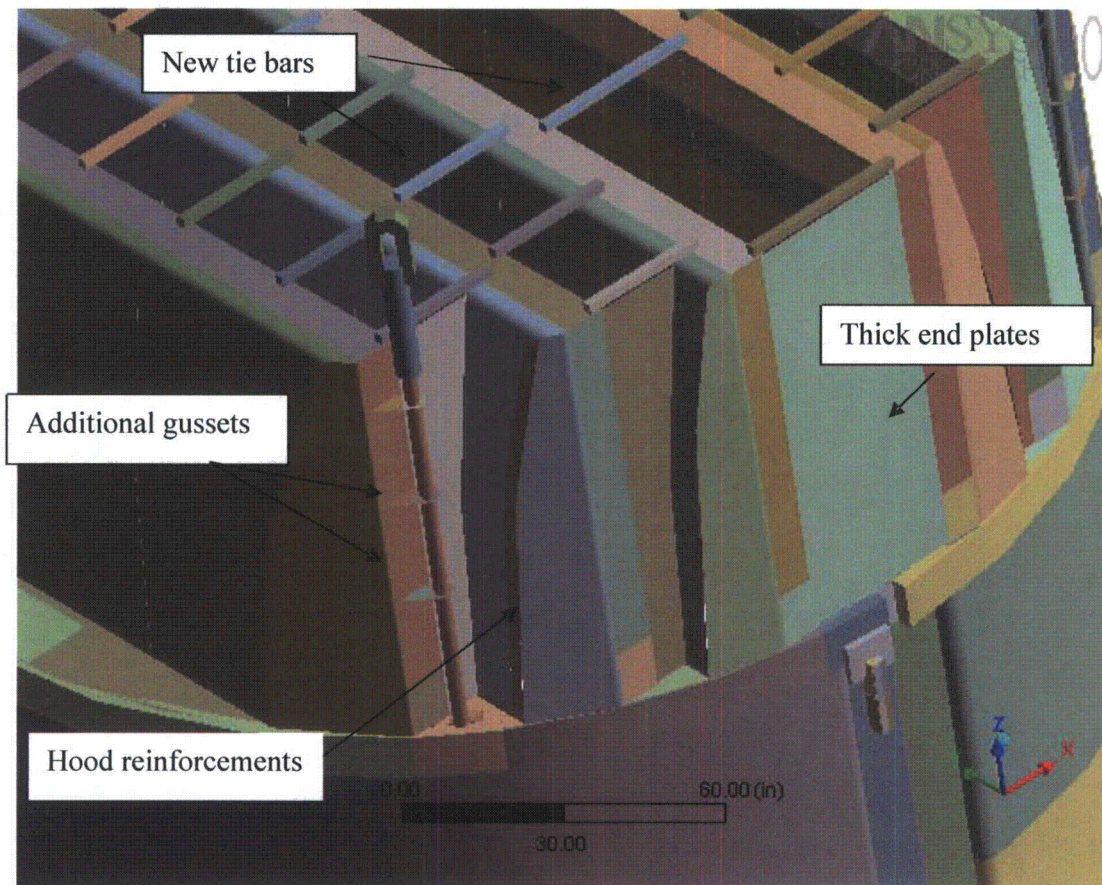


Figure 2. Modify the figure to eliminate inner hood strips. On-site modifications accounted for in the model and associated geometrical details.



### 3.2 Material Properties

The steam dryer is constructed from Type 304 stainless steel and has an operating temperature of 550°F. Properties used in the analysis are summarized below in Table 1.

Table 1. Material properties.

	Young's Modulus ( $10^6$ psi)	Density (lbm/in <sup>3</sup> )	Poisson Ratio
stainless steel	25.55	0.284	0.3
structural steel with added water inertia effect	25.55	0.856	0.3

The structural steel modulus is taken from Appendix A of the ASME Code for Type 304 Stainless Steel at an operating temperature 550°F. The effective properties of perforated plates and submerged parts are discussed in Sections 3.4 and 3.6. Note that the increased effective density for submerged components is only used in the harmonic analysis. When calculating the stress distribution due to the static dead weight load, the unmodified density of steel (0.284 lbm/in<sup>3</sup>) is used throughout.

Inspections of the NMP Unit 2 dryer have revealed IGSCC cracks in the upper support ring (USR) and skirt. A separate analysis of these cracks [16] has been performed to determine whether: (i) they will propagate further into the structure and (ii) their influence upon structural response frequencies and modes must be explicitly accounted for. To establish (i) the stress calculated in the global stress analysis is used in conjunction with the crack geometry to calculate the stress intensity factor which is then compared to the threshold stress intensity. For the USR and skirt cracks the highest stress intensity factors are 1.47 ksi-in<sup>0.5</sup> and 2.75 ksi-in<sup>0.5</sup> respectively; both values are below the threshold value (3 ksi-in<sup>0.5</sup>) implying that fatigue crack growth will not occur.

To determine (ii) the change in modal response frequencies due to the presence of a flaw is predicted by analytical means (in the case of the USR) or using finite element analysis (for the skirt). In each case, the flaw size used in these calculations is increased to ensure conservative estimates (for example, in the case of the skirt flaws extending up to ½ the panel width are considered). For the USR, the change in modal frequencies due to the presence of the cracks is less than 0.5%. For the skirt, using a conservative estimate for the crack to panel width of 0.3 (the measured value is less than 0.17) the change in modal frequency is also less than 0.5%. In both cases such small changes in modal frequencies are considered negligible and are readily accounted for when performing frequency shifting.

### 3.3 Model Simplifications

The following simplifications were made to achieve reasonable model size while maintaining good modeling fidelity for key structural properties:

- Perforated plates were approximated as continuous plates using modified elastic properties designed to match the static and modal behaviors of the perforated plates. The

perforated plate structural modeling is summarized in Section 3.4 and Appendix C of [17].

- The drying vanes were replaced by point masses attached to the corresponding trough bottom plates and vane bank top covers (Figure 4). The bounding perforated plates, vane bank end plates, and vane bank top covers were explicitly modeled (see Section 3.5).
- The added mass properties of the lower part of the skirt below the reactor water level were obtained using a separate hydrodynamic analysis (see Section 3.6).
- [[  
(3)]]
- Four steam dryer support brackets that are located on the reactor vessel and spaced at 90° intervals were explicitly modeled (see Section 3.9).
- Most welds were replaced by node-to-node connections; interconnected parts share common nodes along the welds. In other locations the constraint equations between nodal degrees of freedom were introduced as described in Section 3.9.

### 3.4 Perforated Plate Model

The perforated plates were modeled as solid plates with adjusted elastic and dynamic properties. Properties of the perforated plates were assigned according to the type and size of perforation. Based on [18], for an equilateral square pattern with given hole size and spacing, the effective moduli of elasticity were found.

The adjusted properties for the perforated plates are shown in Table 2 as ratios to material properties of structural steel, provided in Table 1. Locations of perforated plates are classified by steam entry / exit vane bank side and vertical position.

Tests were carried out to verify that this representation of perforated plates by continuous ones with modified elastic properties preserves the modal properties of the structure. These tests are summarized in Appendix C of [17] and compare the predicted first modal frequency for a cantilevered perforated plate against an experimentally measured value. The prediction was obtained for 40% and 13% open area plates (these are representative of the largest and lowest open area ratios of the perforated plates at NMP2, as seen in Table 2) using the analytical formula for a cantilevered plate and the modified Young's modulus and Poisson's ratio given by O'Donnell [18]. The measured and predicted frequencies are in close agreement, differing by less than 3%.

[[

(3)]]



[[

<sup>(3)</sup>]]

[[

<sup>(3)</sup>]]

Figure 3. [[

<sup>(3)</sup>]]

Table 2. Material properties of perforated plates.

[[

<sup>(3)</sup>]]

### 3.5 Vane Bank Model

The vane bank assemblies consist of many vertical angled plates that are computationally expensive to model explicitly, since a prohibitive number of elements would be required. These parts have significant weight which is transmitted through the surrounding structure, so it is important to capture their gross inertial properties. Here the vane banks are modeled as a collection of point masses located at the center of mass for each vane bank section (Figure 4). The following masses were used for the vane bank sections, based on data found on provided drawings:

inner banks, 1618 lbm, 4 sections per bank;  
middle banks, 1485 lbm, total 4 sections per bank; and  
outer banks, 1550 lbm, 3 sections per bank.

These masses were applied to the base plates and vane top covers using the standard ANSYS point mass modeling option, element MASS21. ANSYS automatically distributes the point mass inertial loads to the nodes of the selected structure. The distribution algorithm minimizes the sum of the squares of the nodal inertial forces, while ensuring that the net forces and moments are conserved. Vane banks are not exposed to main steam lines directly, but rather shielded by the hoods.

The collective stiffness of the vane banks is expected to be small compared to the surrounding support structure and is neglected in the model. In the static case it is reasonable to expect that this constitutes a conservative approach, since neglecting the stiffness of the vane banks implies that the entire weight is transmitted through the adjacent vane bank walls and supports. In the dynamic case the vane banks exhibit only a weak response since (i) they have large inertia so that the characteristic acoustically-induced forces divided by the vane masses and inertias yield small amplitude motions, velocities and accelerations; and (ii) they are shielded from acoustic loads by the hoods, which transfer dynamic loads to the rest of the structure. Thus, compared to the hoods, less motion is anticipated on the vane banks so that

approximating their inertial properties with equivalent point masses is justified. Nevertheless, the bounding parts, such as perforated plates, side panels, and top covers, are retained in the model. Errors associated with the point mass representation of the vane banks are compensated for by frequency shifting of the applied loads.

### **3.6 Water Inertia Effect on Submerged Panels**

Water inertia was modeled by an increase in density of the submerged structure to account for the added hydrodynamic mass. This added mass was found by a separate hydrodynamic analysis (included in DRF-C-279C supporting this report) to be  $0.143 \text{ lbm/in}^2$  on the submerged skirt area. This is modeled by effectively increasing the material density for the submerged portions of the skirt. Since the skirt is 0.25 inches thick, the added mass is equivalent to a density increase by  $0.572 \text{ lbm/in}^3$ . This added water mass was included in the ANSYS model by appropriately modifying the density of the submerged structural elements when computing harmonic response. For the static stresses, the unmodified density of steel is used throughout.

### **3.7 Structural Damping**

Structural damping was defined as 1% of critical damping for all frequencies. This damping is consistent with guidance given on pg. 10 of NRC RG-1.20 [22].

### **3.8 Mesh Details and Element Types**

Shell elements were employed to model the skirt, hoods, perforated plates, side and end plates, trough bottom plates, reinforcements, base plates and cover plates. Specifically, the four-node, Shell Element SHELL63, was selected to model these structural components. This element models bending and membrane stresses, but omits transverse shear. The use of shell elements is appropriate for most of the structure where the characteristic thickness is small compared to the other plate dimensions. For thicker structures, such as the upper and lower support rings, solid brick elements were used to provide the full 3D stress. The elements SURF154 are used to assure proper application of pressure loading to the structure. Mesh details and element types are shown in Table 3 and Table 4.

The mesh is generated automatically by ANSYS with refinement near edges. The maximum allowable mesh spacing is specified by the user. Here a 2.5 inch maximum allowable spacing is specified with refinement up to 1.5 inch in the following areas: drain pipes, tie rods, the curved portions of the drain channels and the hoods. Details of the finite element mesh are shown in Figure 5. Numerical experiments carried out using the ANSYS code applied to simple analytically tractable plate structures with dimensions and mesh spacings similar to the ones used for the steam dryer, confirm that the natural frequencies are accurately recovered (less than 1% errors for the first modes). These errors are compensated for by the use of frequency shifting.

### **3.9 Connections Between Structural Components**

Most connections between parts are modeled as node-to-node connections. This is the correct manner (i.e., within the finite element framework) of joining elements away from discontinuities. At joints between shells, this approach omits the additional stiffness provided by the extra weld material. Also, locally 3D effects are more pronounced. The latter effect is accounted for using weld factors. The deviation in stiffness due to weld material is negligible, since weld dimensions are on the order of the shell thickness. The consequences upon modal

frequencies and amplitude are, to first order, proportional to  $t/L$  where  $t$  is the thickness and  $L$  a characteristic shell length. The errors committed by ignoring additional weld stiffness are thus small and readily compensated for by performing frequency shifts.

When joining shell and solid elements, however, the problem arises of properly constraining the rotations, since shell element nodes contain both displacement and rotational degrees of freedom at every node whereas solid elements model only the translations. A node-to-node connection would effectively appear to the shell element as a simply supported, rather than (the correct) cantilevered restraint and significantly alter the dynamic response of the shell structure.

To address this problem, constraint equations are used to properly connect adjacent shell- and solid-element modeled structures. Basically, all such constraints express the deflection (and rotation for shell elements) of a node,  $R_1$ , on one structural component in terms of the deflections/rotations of the corresponding point,  $P_2$ , on the other connected component. Specifically, the element containing  $P_2$  is identified and the deformations at  $P_2$  determined by interpolation between the element nodes. The following types of shell-solid element connections are used in the steam dryer model including the following:

1. Connections of shell faces to solid faces (Figure 6a). While only displacement degrees of freedom are explicitly constrained, this approach also implicitly constrains the rotational degrees of freedom when multiple shell nodes on a sufficiently dense grid are connected to the same solid face.
2. Connections of shell edges to solids (e.g., connection of the bottom of closure plates with the upper ring). Since solid elements do not have rotational degrees of freedom, the coupling approach consisted of having the shell penetrate into the solid by one shell thickness and then constraining both the embedded shell element nodes (inside the solid) and the ones located on the surface of the solid structure (see Figure 6b). Numerical tests involving simple structures showed that this approach and penetration depth reproduce both the deflections and stresses of the same structure modeled using only solid elements or ANSYS' bonded contact technology. Continuity of rotations and displacements is achieved.

The use of constraint conditions rather than the bonded contacts advocated by ANSYS for connecting independently meshed structural components confers better accuracy and useful numerical advantages to the structural analysis of the steam dryer including better conditioned and smaller matrices. The smaller size results from the fact that equations and degrees of freedom are eliminated rather than augmented (in Lagrange multiplier-based methods) by additional degrees of freedom. Also, the implementation of contact elements relies on the use of very high stiffness elements (in penalty function-based implementations) or results in indefinite matrices (Lagrange multiplier implementations) with poorer convergence behavior compared to positive definite matrices.

The steam dryer rests on four support blocks which resist vertical and lateral displacement. The support blocks contact the seismic blocks welded to the USR so that 100% of the dryer weight is transmitted through the seismic blocks per the FDDR KG1-265. Because the contact region between the blocks and steam dryer is small, the seismic blocks are considered free to

rotate about the radial axis. Specifically nodal constraints (zero relative displacement) are imposed over the contact area between the seismic blocks and the support blocks. Two nodes on each support block are fixed as indicated in Figure 7. One node is at the center of the support block surface facing the vessel and the other node is 0.5" offset inside the block towards the steam dryer, half way to the nearest upper support ring node. This arrangement approximates the nonlinear contact condition where the ring can tip about the block.

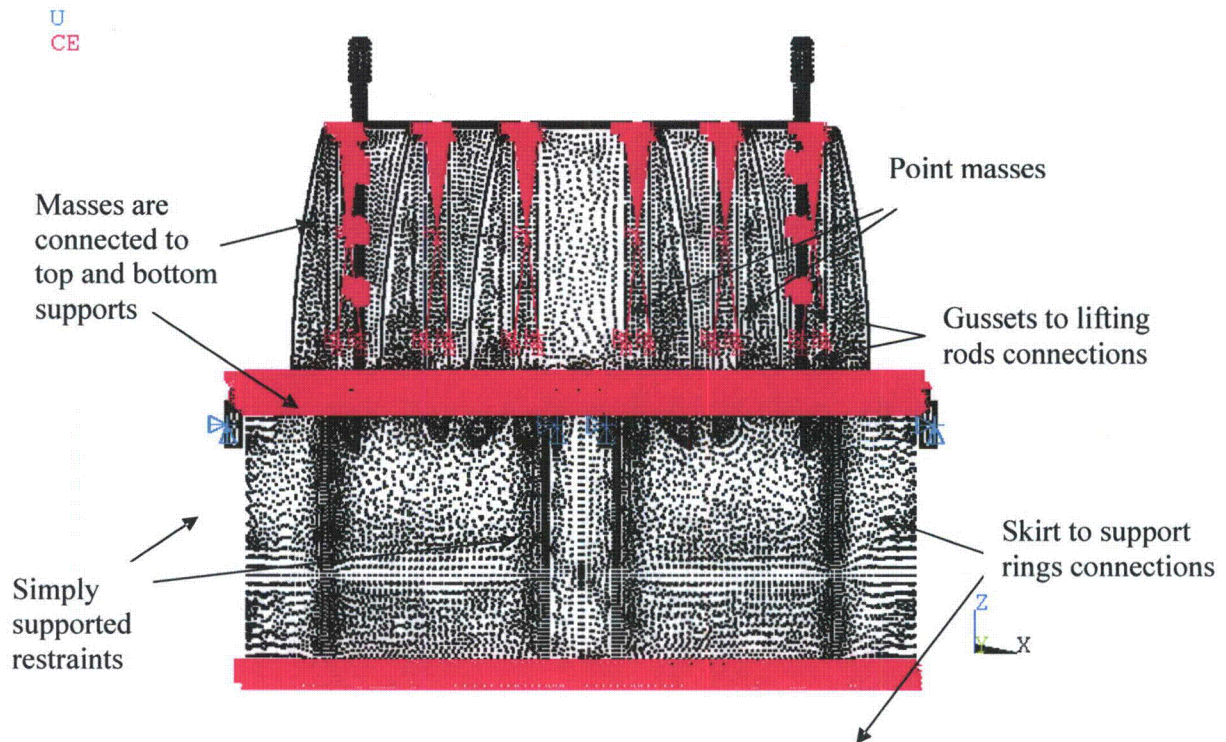


Figure 4. Point masses representing the vanes. The pink shading represents where constraint equations between nodes are applied (generally between solid and shell elements, point masses and nodes and  $[[^{(3)}]]$ ).

Table 3. FE Model Summary.

Description	Quantity
Total Nodes <sup>1</sup>	159,793
Total Elements	124,496

1. Not including additional damper nodes and elements.

Table 4. Listing of Element Types.

Generic Element Type Name	Element Name	ANSYS Name
20-Node Quadratic Hexahedron	SOLID186	20-Node Hexahedral Structural Solid
10-Node Quadratic Tetrahedron	SOLID187	10-Node Tetrahedral Structural Solid
4-Node Elastic Shell	SHELL63	4-Node Elastic Shell
Mass Element	MASS21	Structural Mass
Pressure Surface Definition	SURF154	3D Structural Surface Effect
Damper element	COMBIN14	Spring-Damper



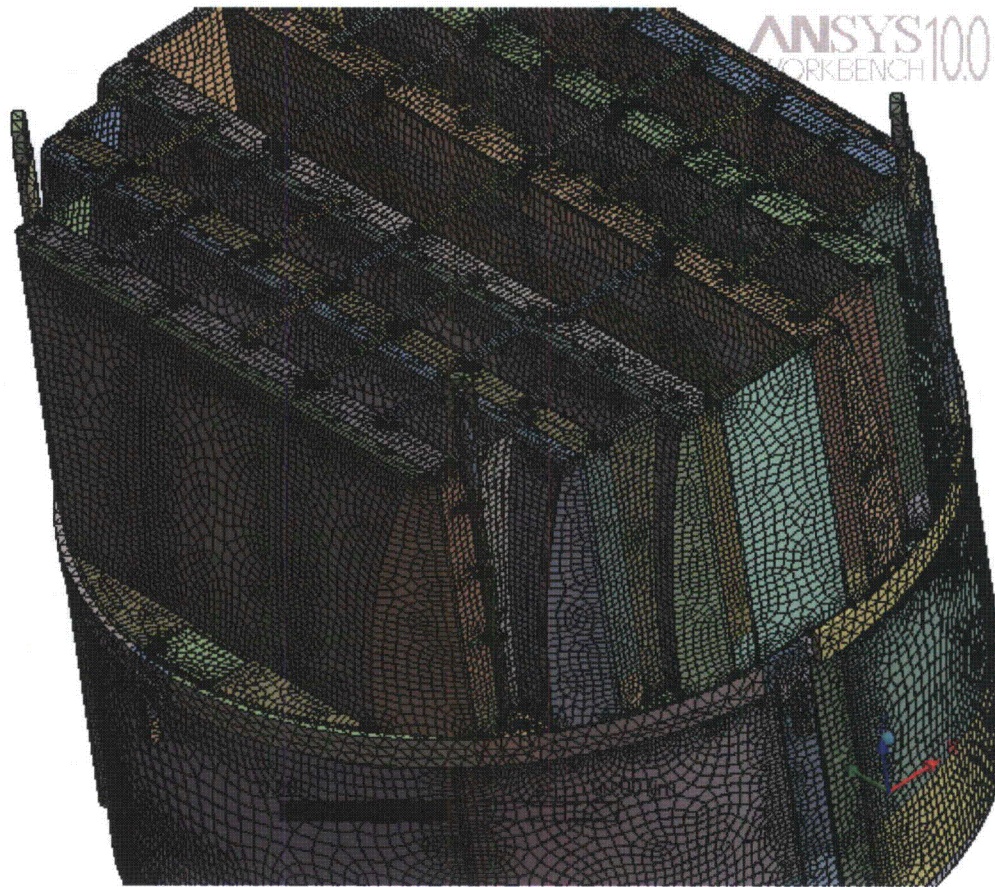


Figure 5a. Mesh overview.

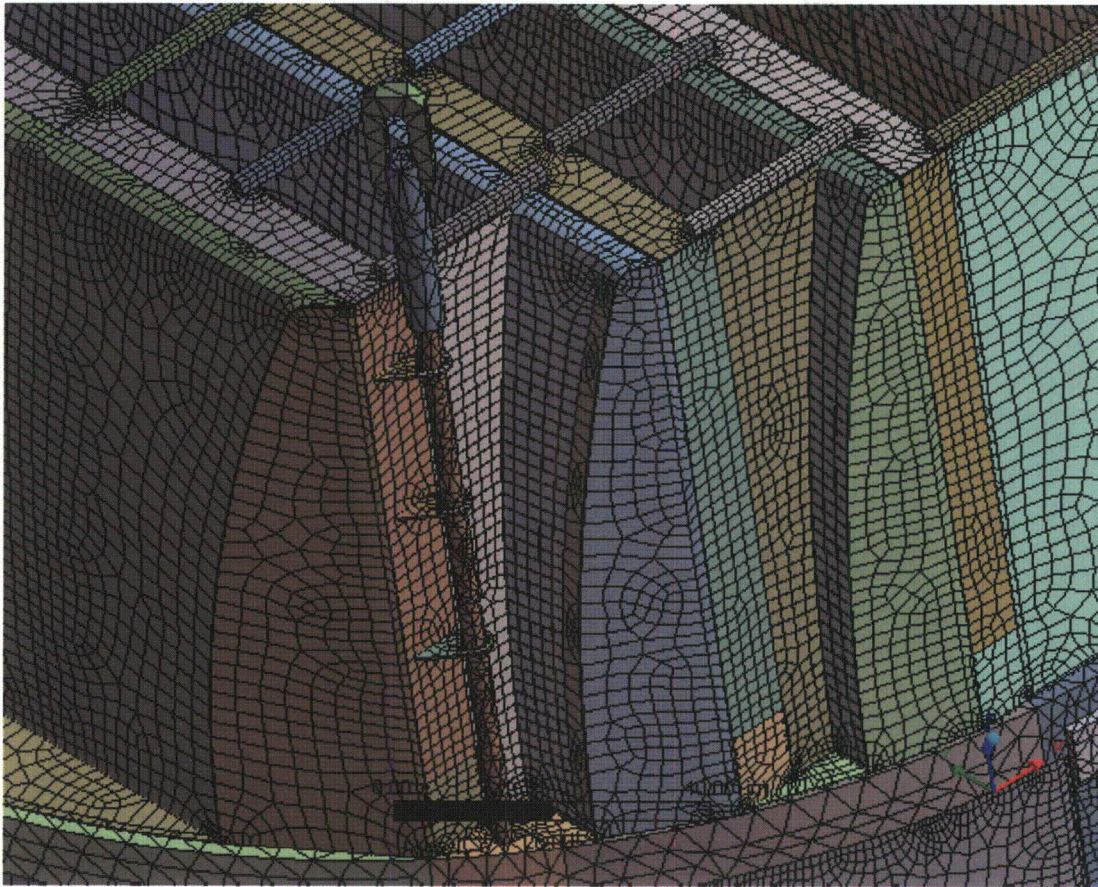


Figure 5b. Close up of mesh showing on-site modifications.





Figure 5c. Close up of mesh showing drain pipes and hood supports.



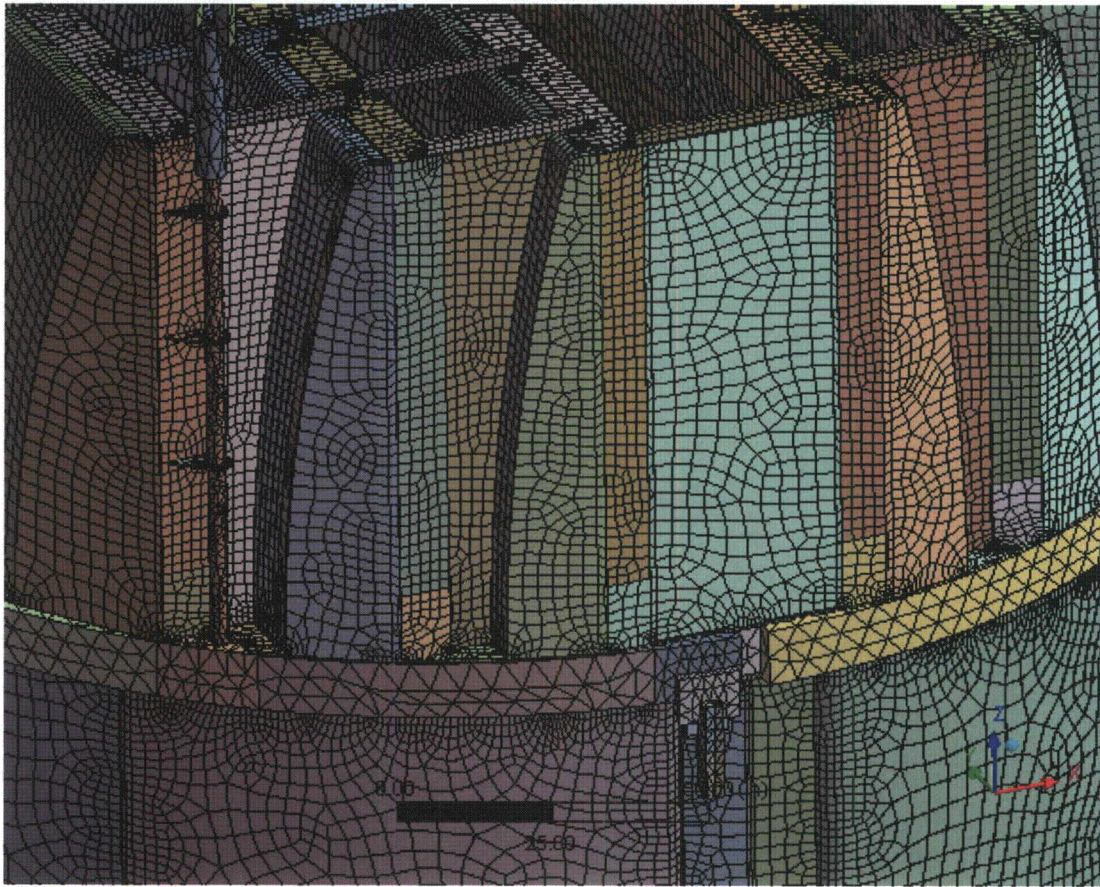


Figure 5d. Close up of mesh showing node-to-node connections between various plates.



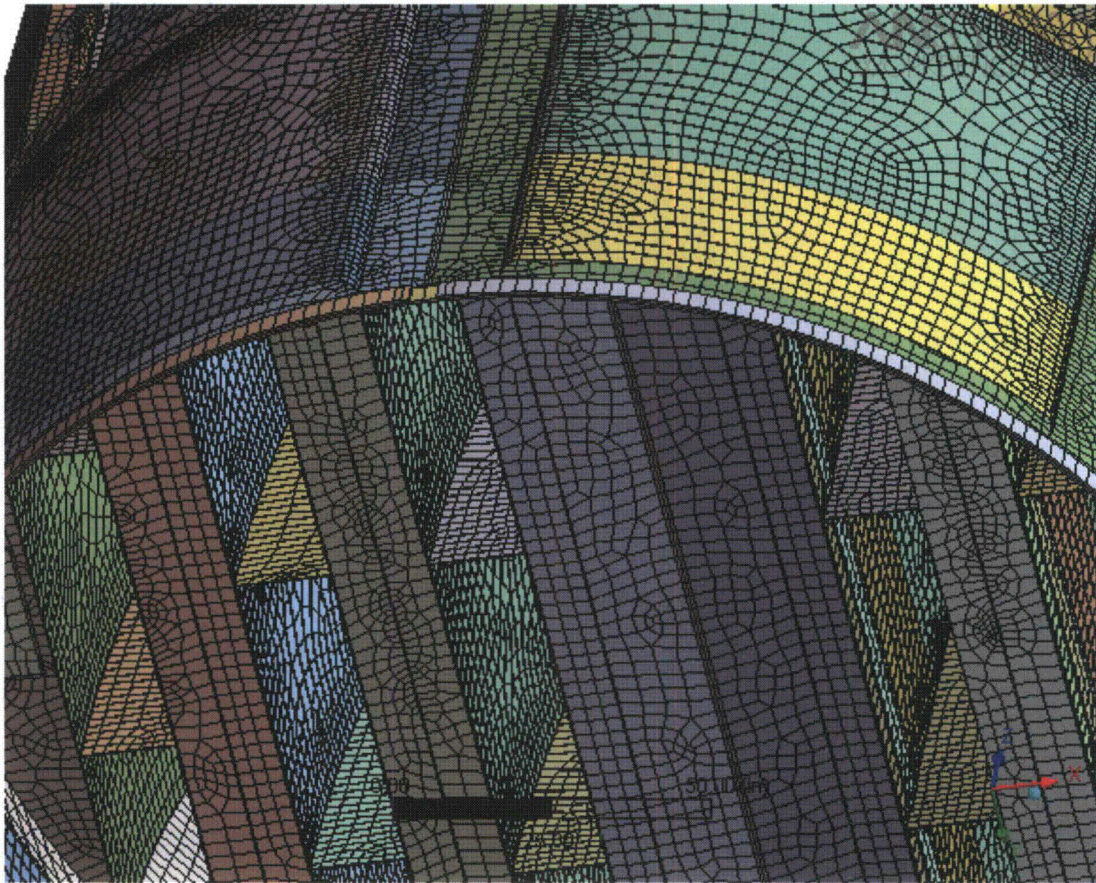


Figure 5e. Close up of mesh showing node-to-node connections between the skirt and drain channels; hood supports and hoods; and other parts.



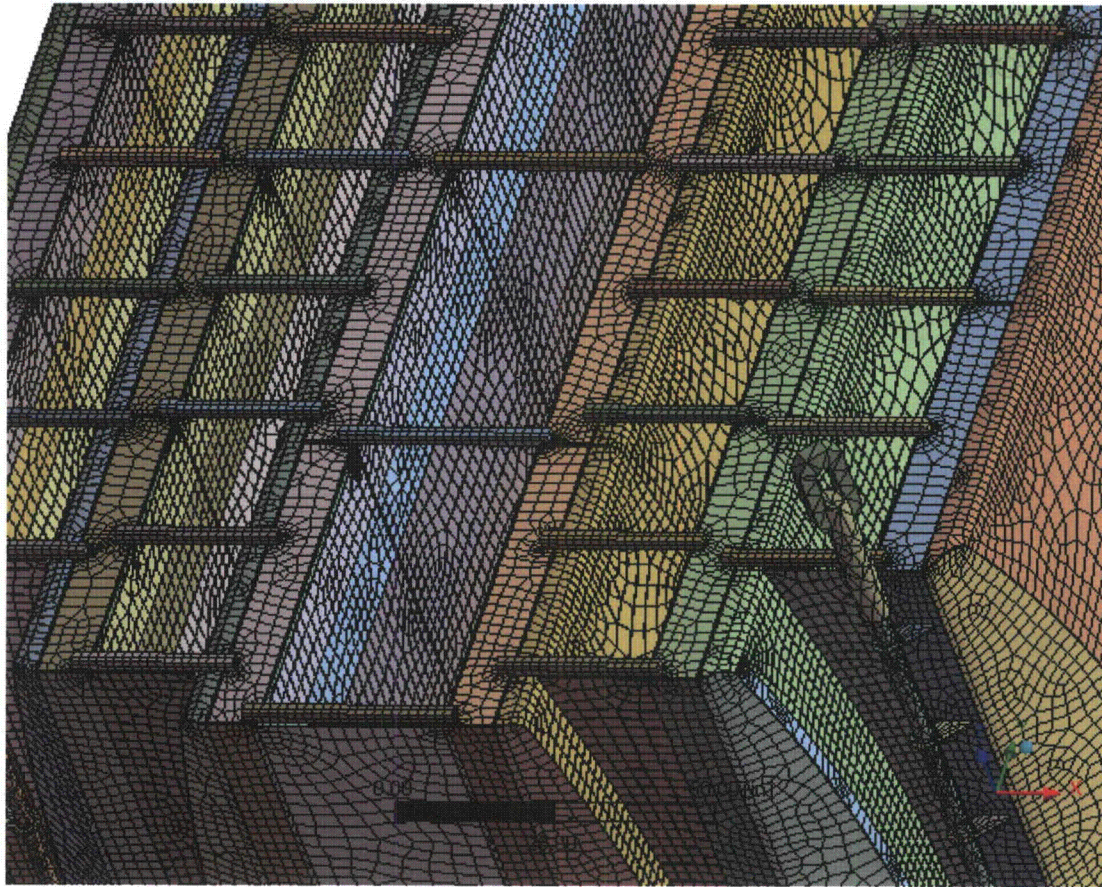


Figure 5f. Close up view of tie bars.

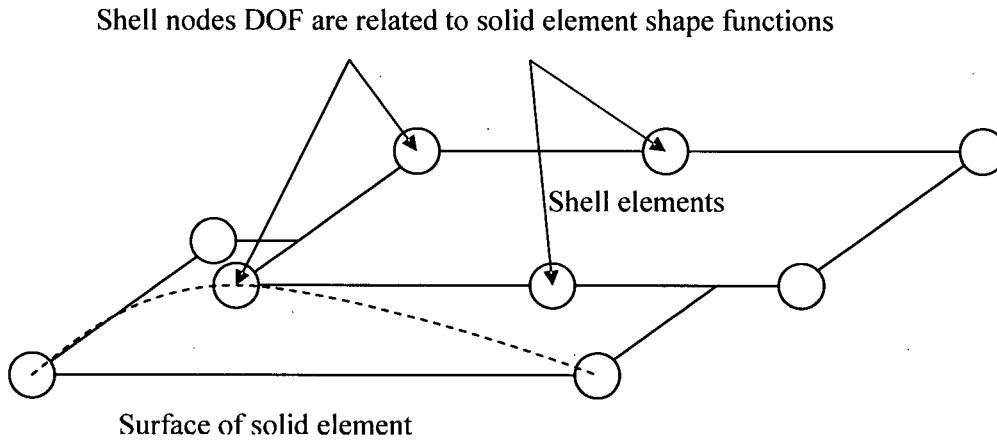


Figure 6a. Face-to-face shell to solid connection.

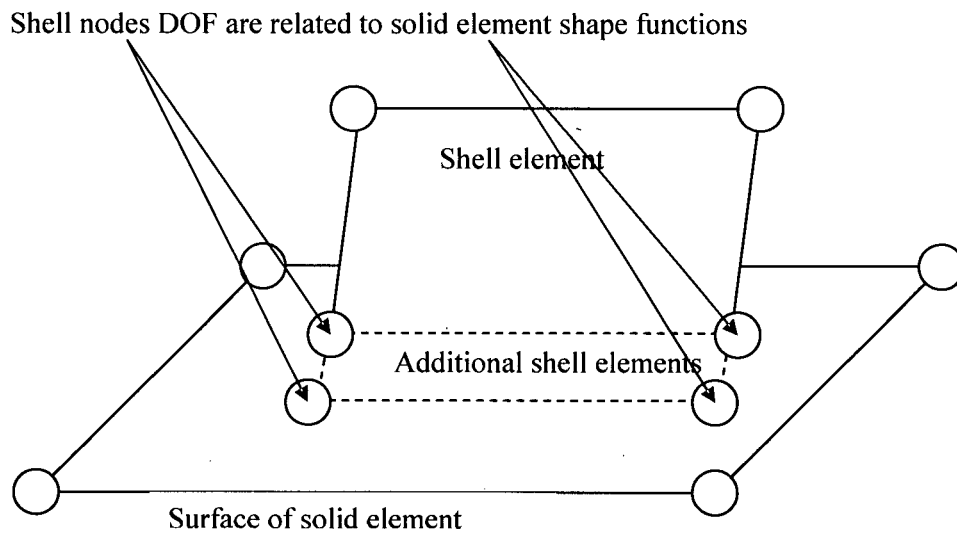


Figure 6b. Shell edge-to-solid face connection.

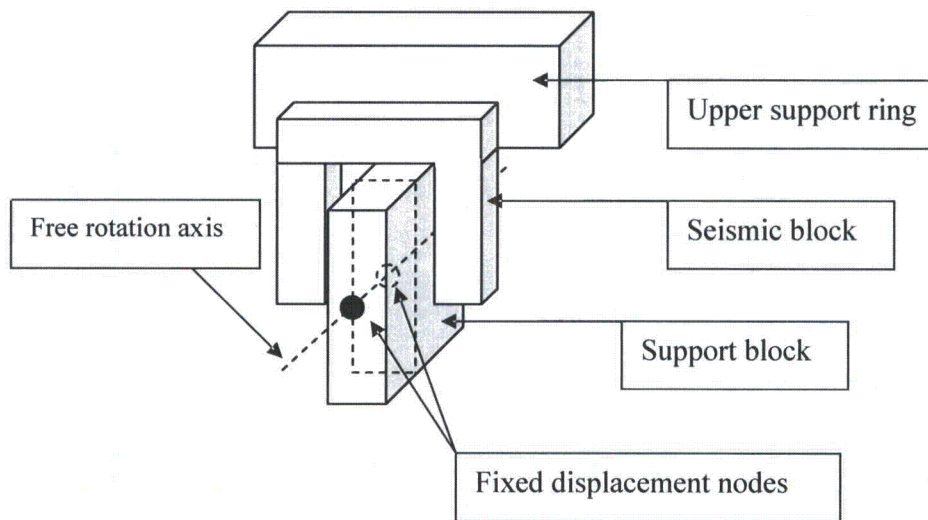


Figure 7. Boundary conditions. Inside node is half way between outer surface of support block and upper support ring.

### 3.10 Pressure Loading

The harmonic loads are produced by the pressures acting on the exposed surfaces of the steam dryer. At every frequency and for each MSL, the pressure distribution corresponding to a unit pressure at the MSL inlet is represented on a three-inch grid lattice grid (i.e., a mesh whose lines are aligned with the x-, y- and z-directions) that is superimposed over the steam dryer surface. This grid is compatible with the 'Table' format used by ANSYS to 'paint' general pressure distributions upon structural surfaces. The pressures are obtained from the Helmholtz solver routine in the acoustic analysis [2].

In general, the lattice nodes do not lie on the surface, so that to obtain the pressure differences at the surface it is necessary to interpolate the pressure differences stored at the lattice nodes. This is done using simple linear interpolation between the 8 forming nodes of the lattice cell containing the surface point of interest. Inspection of the resulting pressures at selected nodes shows that these pressures vary in a well-behaved manner between the nodes with prescribed pressures. Graphical depictions of the resulting pressures and comparisons between the peak pressures in the original nodal histories and those in the final surface load distributions produced in ANSYS, all confirm that the load data are interpolated accurately and transferred correctly to ANSYS.

The harmonic pressure loads are only applied to surfaces above the water level, as indicated in Figure 8. In addition to the pressure load, the static loading induced by the weight of the steam dryer is analyzed separately. The resulting static and harmonic stresses are linearly combined to obtain total values which are then processed to calculate maximum and alternating stress intensities for assessment in Section 5.

[[

<sup>(3)</sup>]] This is useful since revisions in the loads model do not necessitate recalculation of the unit stresses.



NODES  
PRES-NORM

ANSYS

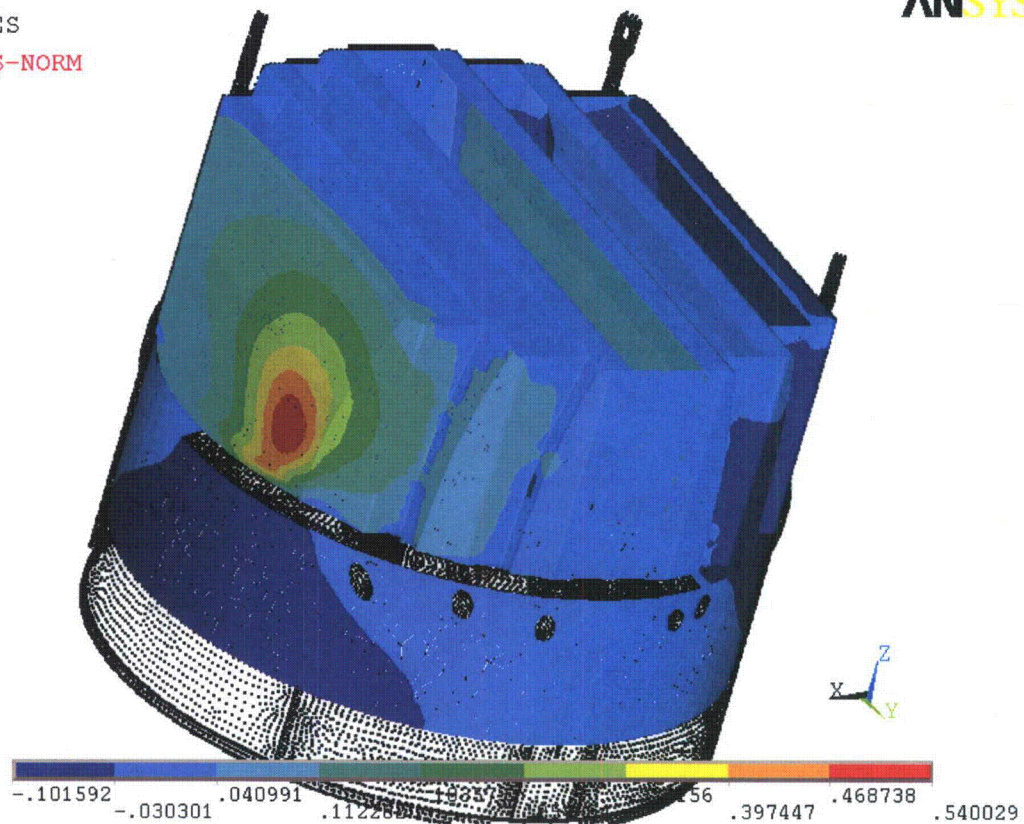


Figure 8a. Real part of unit pressure loading MSL A (in psid) on the steam dryer at 50.1 Hz. No loading is applied to the submerged surface and lifting rods.



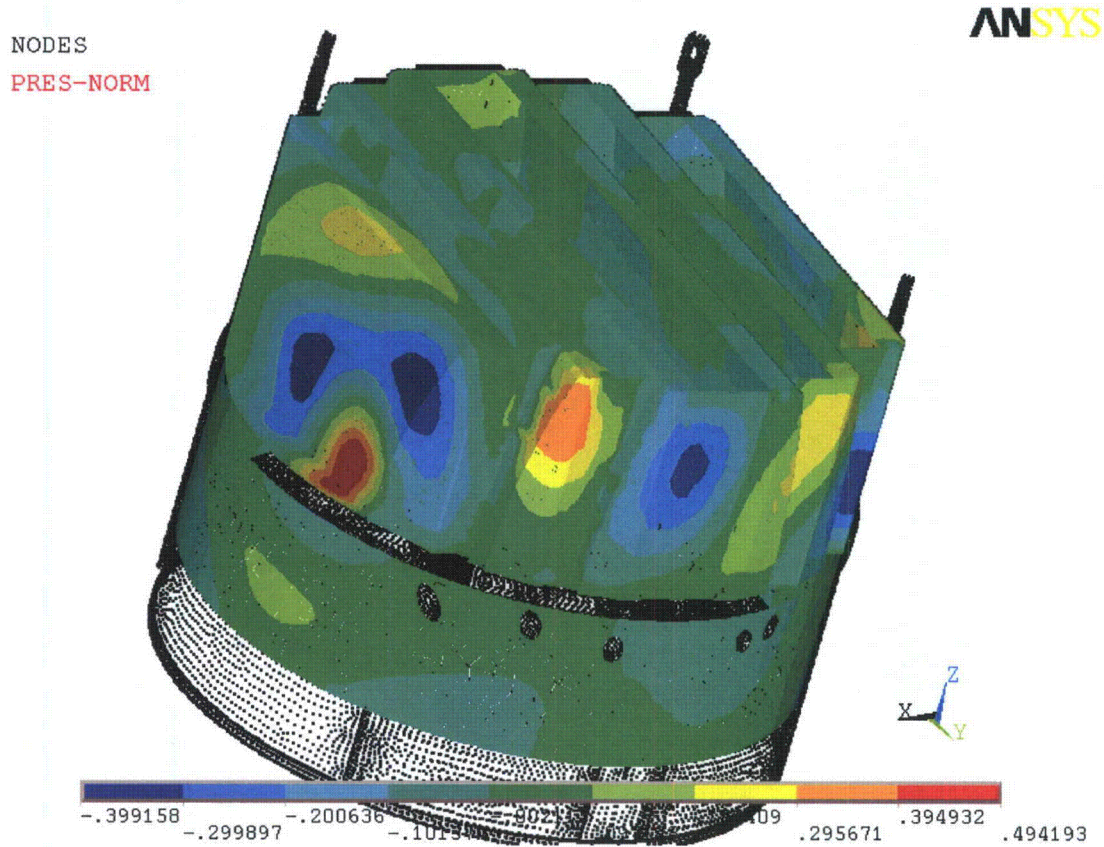


Figure 8b. Real part of unit pressure loading MSL A (in psid) on the steam dryer at 200.45 Hz. No loading is applied to the submerged surface and lifting rods.

## 4. Structural Analysis

The solution is decomposed into static and harmonic parts, where the static solution produces the stress field induced by the supported structure subjected to its own weight and the harmonic solution accounts for the harmonic stress field due to the unit pressure of given frequency in one of the main steam lines. All solutions are linearly combined, with amplitudes provided by signal measurements in each steam line, to obtain the final displacement and stress time histories. This decomposition facilitates the prescription of the added mass model accounting for hydrodynamic interaction and allows one to compare the stress contributions arising from static and harmonic loads separately. Proper evaluation of the maximum membrane and membrane+bending stresses requires that the static loads due to weight be accounted for. Hence both static and harmonic analyses are carried out.

### 4.1 Static Analysis

The results of the static analysis are shown in Figure 9. The locations with highest stress include the inner vane bank connection to inner base plate near support brackets with stress intensity 9,598 psi. There are four locations with artificial stress singularity, which are excluded from the analysis. The static stresses one node away are used at these locations as more realistic estimate of local stress. These locations are at the connections of the inner end plate to the inner base plate at the ends of the cut-out, as shown in Figure 9c.

### 4.2 Harmonic Analysis

The harmonic pressure loads were applied to the structural model at all surface nodes described in Section 3.10. Typical stress intensity distributions over the structure are shown in Figure 10. Stresses were calculated for each frequency, and results from static and harmonic calculations were combined.

To evaluate maximum stresses, the stress harmonics including the static component are transformed into a time history using FFT, and the maximum and alternating stress intensities for the response, evaluated. According to ASME B&PV Code, Section III, Subsection NG-3216.2 the following procedure was established to calculate alternating stresses. For every node, the stress difference tensors,  $\sigma'_{nm} = \sigma_n - \sigma_m$ , are considered for all possible pairs of the stresses  $\sigma_n$  and  $\sigma_m$  at different time levels,  $t_n$  and  $t_m$ . Note that all possible pairs require consideration since there are no "obvious" extrema in the stress responses. However, in order to contain computational cost, extensive screening of the pairs takes place (see Section 2.3) so that pairs known to produce alternating stress intensities less than 500 psi are rejected. For each remaining stress difference tensor, the principal stresses  $S_1, S_2, S_3$  are computed and the maximum absolute value among principal stress differences,  $S_{nm} = \max\{|S_1 - S_2|, |S_1 - S_3|, |S_2 - S_3|\}$ , obtained. The alternating stress at the node is then one-half the maximum value of  $S_{nm}$  taken over all combinations (n,m), i.e.,  $S_{alt} = \frac{1}{2} \max_{n,m} \{S_{nm}\}$ . This alternating stress is compared against allowable values, depending on the node location with respect to welds.

ANSYS

NODAL SOLUTION

STEP=1

SUB =1

TIME=1

USUM (AVG)

RSYS=0

DMX =.068847

SMN =.505E-03

SMX =.068847

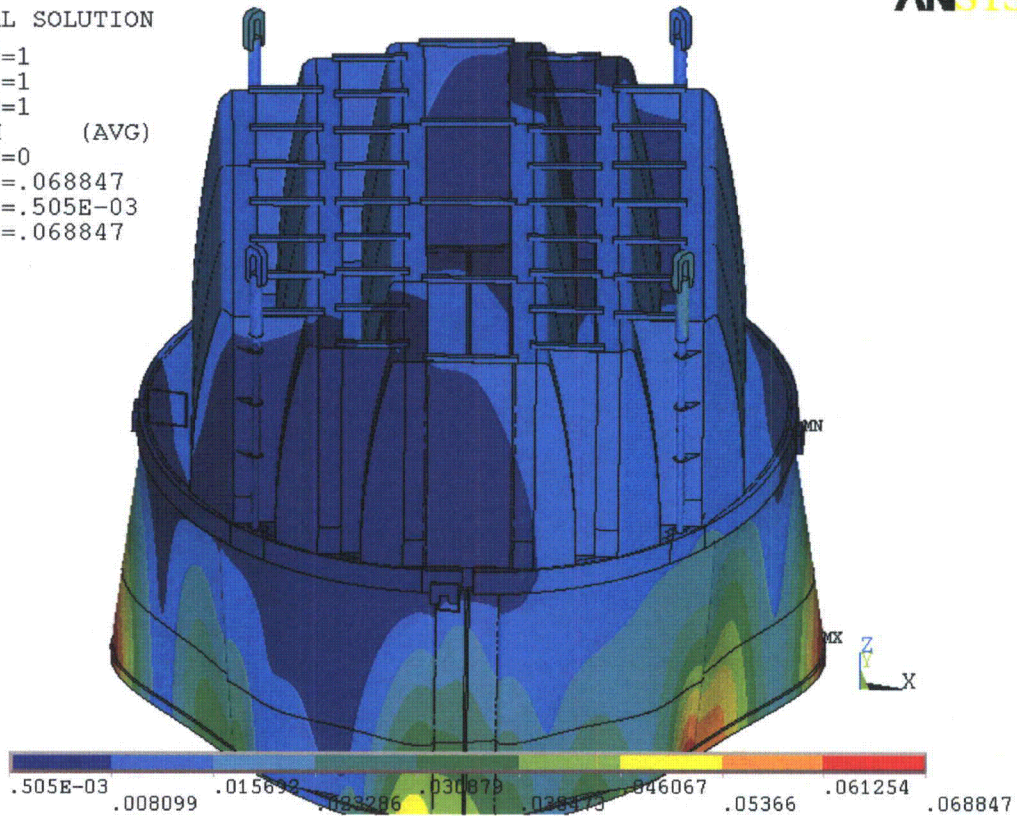


Figure 9a. Overview of static calculations showing displacements (in inches). Maximum displacement (DMX) is 0.069". Note that displacements are amplified for visualization.

ANSYS

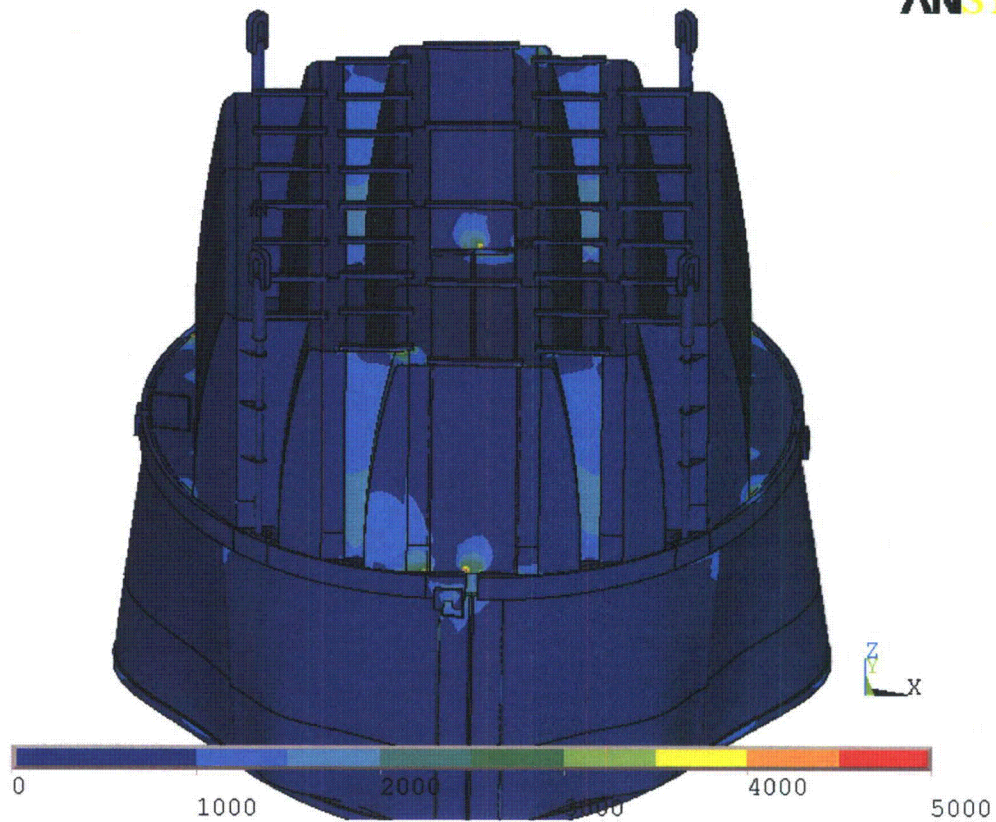


Figure 9b. Overview of static calculations showing stress intensities (in psi). Maximum stress intensity (SMX) is 9,598 psi. Note that displacements are amplified for visualization



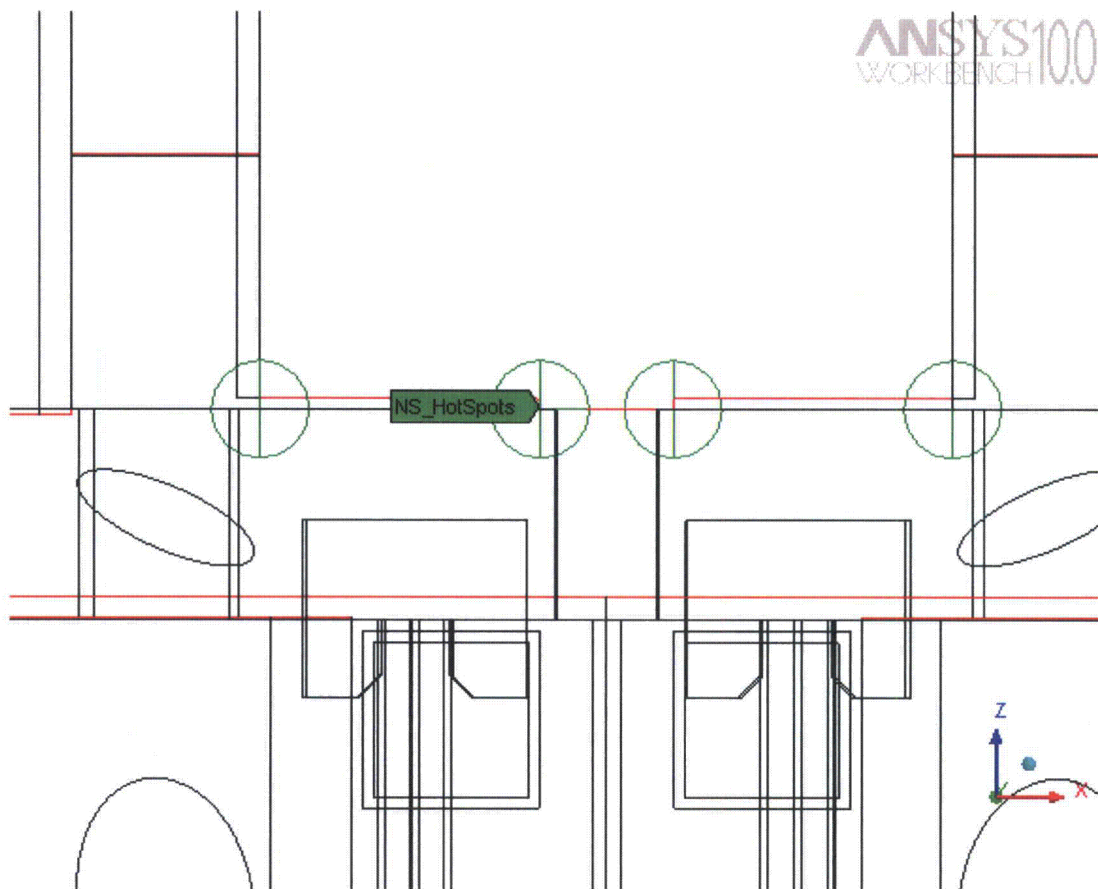


Figure 9c. Stress singularities. Model is shown in wireframe mode for clarity.

ANSYS

NODAL SOLUTION

STEP=1185

SUB =1

FREQ=50.418

REAL ONLY

SINT (AVG)

DMX =.195193

SMN =.081579

SMX =11642

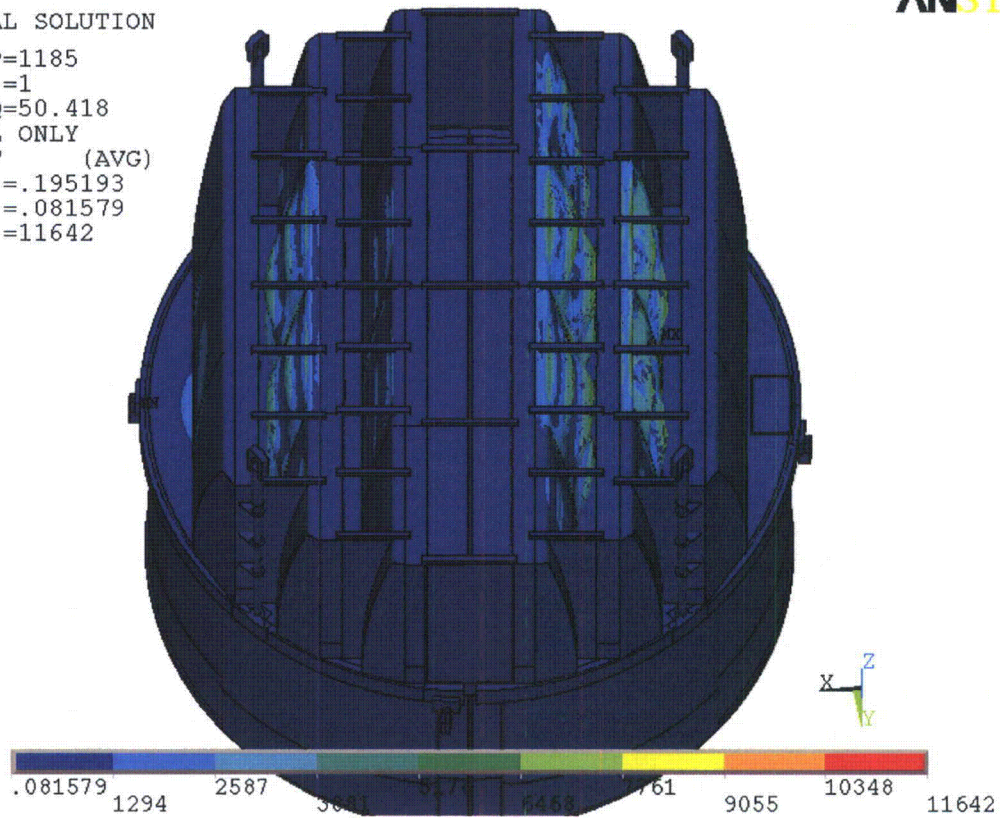


Figure 10a. Overview of harmonic calculations showing real part of stress intensities (in psi) along with displacements. Unit loading MSL A at 50.1 Hz (oriented to show high stress locations at the hoods).

ANSYS

NODAL SOLUTION

STEP=305

SUB =1

FREQ=200.446

REAL ONLY

SINT (AVG)

DMX =.021716

SMN =.177944

SMX =5801

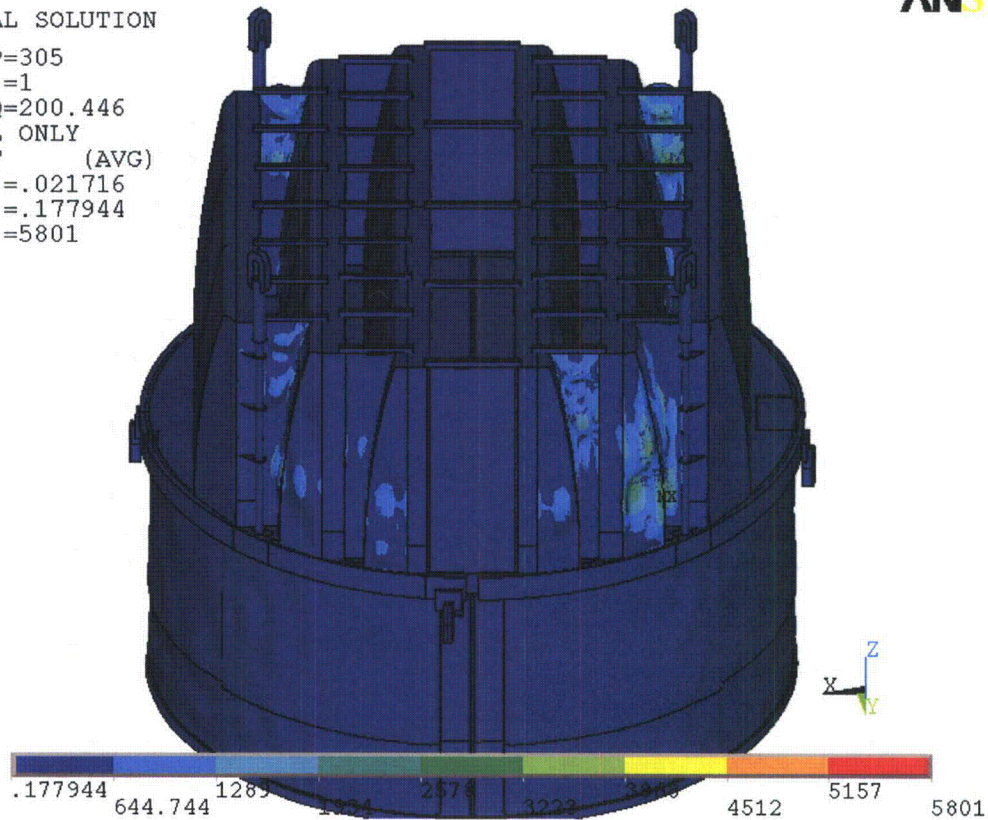


Figure 10b. Overview of harmonic calculations showing real part of stress intensities (in psi) along with displacements. Unit loading MSL A at 200.5 Hz.

#### 4.3 Post-Processing

The static and transient stresses computed at every node with ANSYS were exported into files for subsequent post-processing. These files were then read into separate customized software to compute the maximum and alternating stresses at every node. The maximum stress was defined for each node as the largest stress intensity occurring during the time history. Alternating stresses were calculated according to the ASME standard described above. For shell elements the maximum stresses were calculated separately at the mid-plane, where only membrane stress is present, and at top/bottom of the shell, where bending stresses are also present.

For nodes that are shared between several structural components or lie on junctions, the maximum and alternating stress intensities are calculated as follows. First, the nodal stress tensor is computed separately for each individual component by averaging over all finite elements meeting at the node and belonging to the same structural component. The time histories of these stress tensors are then processed to deduce the maximum and alternating stress intensities for each structural component. Finally for nodes shared across multiple components the highest of the component-wise maximum and alternating stresses is recorded as the "nodal" stress. This approach prevents averaging of stresses across components and thus yields conservative estimates for nodal stresses at the weld locations where several components are joined together.

The maximum stresses are compared against allowable values which depend upon the stress type (membrane, membrane+bending, alternating –  $P_m$ ,  $P_m+P_b$ ,  $S_{alt}$ ) and location (at a weld or away from welds). These allowables are specified in the following section. For solid elements the most conservative allowable for membrane stress,  $P_m$ , is used, although bending stresses are nearly always present also. The structure is then assessed in terms of stress ratios formed by dividing allowables by the computed stresses at every node. Stress ratios less than unity imply that the associated maximum and/or alternating stress intensities exceed the allowable levels. Post-processing tools calculate the stress ratios, identifying the nodes with low stress ratios and generating files formatted for input to the 3D graphics program, TecPlot, which provides more general and sophisticated plotting options than currently available in ANSYS.

#### 4.4 Computation of Stress Ratios for Structural Assessment

The ASME B&PV Code, Section III, subsection NG provides different allowable stresses for different load combinations and plant conditions. The stress levels of interest in this analysis are for the normal operating condition, which is the Level A service condition. The load combination for this condition is:

$$\text{Normal Operating Load Combination} = \text{Weight} + \text{Pressure} + \text{Thermal}$$

The weight and fluctuating pressure contributions have been calculated in this analysis and are included in the stress results. The static pressure differences and thermal expansion stresses are small, since the entire steam dryer is suspended inside the reactor vessel and all surfaces are exposed to the same conditions. Seismic loads only occur in Level B and C cases, and are not considered in this analysis.



### Allowable Stress Intensities

The ASME B&PV Code, Section III, subsection NG shows the following (Table 5) for the maximum allowable stress intensity ( $S_m$ ) and alternating stress intensity ( $S_a$ ) for the Level A service condition. The allowable stress intensity values for type 304 stainless steel at operating temperature 550°F are taken from Table I-1.2 and Fig. I-9.2.2 of Appendix I of Section III, in the ASME B&PV Code. The calculation for different stress categories is performed in accordance with Fig. NG-3221-1 of Division I, Section III, subsection NG.

Note that the allowable value for alternating stress corresponds to curve C of Fig. I-9.2.2 in Appendix I in Section III of the ASME B&PV Code. This is the conservative allowable when the stress range,  $(P_L + P_b + Q)_{\text{RANGE}}$ , exceeds 27.2 ksi. Here  $P_L$  is the primary local membrane stress (or average stress across any solid section) and considers discontinuities, but not stress concentrations;  $P_b$  is the primary bending stress excluding discontinuities or concentrations; and  $Q$  is the secondary membrane+bending stress or the self-equilibrating stress necessary to satisfy continuity of the structure and occurs at discontinuities, but excludes stress concentrations. For the steam dryer being considered here, this stress range is less than this value everywhere which, per the ASME code, permits comparison against curve B with allowable value 16.5 ksi. Since the stress ratios computed herein do not take credit for this higher allowable, the reported values implicitly carry an additional  $(16.5/13.6)-1$  or 21.3% margin.

Table 5. Maximum Allowable Stress Intensity and Alternating Stress Intensity for all areas other than welds. The notation  $P_m$  represents membrane stress;  $P_b$  represents stress due to bending;  $Q$  represents secondary stresses (from thermal effects and gross structural discontinuities, for example); and  $F$  represents additional stress increments (due to local structural discontinuities, for example).

Type	Notation	Service Limit	Allowable Value (ksi)
<i>Maximum Stress Allowables:</i>			
General Membrane	$P_m$	$S_m$	16.9
Membrane + Bending	$P_m + P_b$	$1.5 S_m$	25.35
Primary + Secondary	$P_m + P_b + Q$	$3.0 S_m$	50.7
<i>Alternating Stress Allowable:</i>			
Peak = Primary + Secondary + F	$S_{\text{alt}}$	$S_a$	13.6

When evaluating welds, either the calculated or allowable stress was adjusted, to account for stress concentration factor and weld quality. Specifically:

- For maximum allowable stress intensity, the allowable value is decreased by multiplying its value in Table 5 by 0.55.
- For alternating stress intensity, the calculated weld stress intensity is multiplied by a weld stress intensity (fatigue) factor of 1.8 for a fillet weld and 1.4 for a full penetration weld, before comparison to the  $S_a$  value given above.

The weld factors of 0.55 and 1.4 (full penetration weld) or 1.8 (fillet weld) were selected based on the observable quality of the shop welds and liquid penetrant NDE testing of all welds (excluding tack and intermittent welds, which were subject to 5X visual inspection) during fabrication. These factors are consistent with fatigue strength reduction factors recommended by the Welding Research Council, [23], and stress concentration factors at welds, provided in [24] and [25]. In addition, critical welds are subject to periodical visual inspections in accordance with the requirements of GE SIL 644 SIL and BWR VIP-139 [26]. Therefore, for weld stress intensities, the allowable values are shown in Table 6. As pointed out above, allowable value for alternating stress (13.6 ksi) corresponds to curve C of Fig. I-9.2.2 in Appendix I of Section III in the ASME B&PV Code whereas the flow chart in Figure I-9.2.3 of the ASME Code permits the use of curve B. No credit is taken for this higher allowable so that all reported alternating stress ratios are conservative by a 21.3% margin.

These factors (0.55 and 1.4 or 1.8) also conservatively presume that the structure is joined using fillet welds unless specified otherwise. Since fillet welds correspond to larger stress concentration factors than other types of welds, this assumption is a conservative one.

Table 6. Weld Stress Intensities.

Type	Notation	Service Limit	Allowable Value (ksi)
<i>Maximum Stress Allowables:</i>			
General Membrane	Pm	0.55 Sm	9.30
Membrane + Bending	Pm + Pb	0.825 Sm	13.94
Primary + Secondary	Pm + Pb + Q	1.65 Sm	27.89
<i>Alternating Stress Allowables:</i>			
Peak = Primary + Secondary + F	S <sub>alt</sub>	Sa	13.6

#### *Comparison of Calculated and Allowable Stress Intensities*

The classification of stresses into general membrane or membrane + bending types was made according to the exact location, where the stress intensity was calculated; namely, general membrane, Pm, for middle surface of shell element, and membrane + bending, Pm + Pb, for other locations. For solid elements the most conservative, general membrane, Pm, allowable is used.

The structural assessment is carried out by computing stress ratios between the computed maximum and alternating stress intensities, and the allowable levels. Locations where any of the stresses exceed allowable levels will have stress ratios less than unity. Since computation of stress ratios and related quantities within ANSYS is time-consuming and awkward, a separate FORTRAN code was developed to compute the necessary maximum and alternating stress intensities, Pm, Pm+Pb, and S<sub>alt</sub>, and then compare it to allowables. Specifically, the following quantities were computed at every node:

1. The maximum membrane stress intensity, Pm (evaluated at the mid-thickness location for shells),

2. The maximum membrane+bending stress intensity,  $P_m+P_b$ , (taken as the largest of the maximum stress intensity values at the bottom, top, and mid thickness locations, for shells),
3. The alternating stress,  $S_{alt}$ , (the maximum value over the three thickness locations is taken).
4. The stress ratio due to a maximum stress intensity assuming the node lies at a non-weld location (note that this is the minimum ratio obtained considering both membrane stresses and membrane+bending stresses):  
$$SR-P(nw) = \min \{ S_m/P_m, 1.5 * S_m/(P_m+P_b) \}.$$
5. The alternating stress ratio assuming the node lies at a non-weld location,  
$$SR-a(nw) = S_a / (1.1 * S_{alt}),$$
6. The same as 4, but assuming the node lies on a weld,  
$$SR-P(w) = SR-P(nw) * 0.55$$
7. The same as 5, but assuming the node lies on a weld,  
$$SR-a(w) = SR-a(nw) / f_{sw}.$$

Note that in steps 4 and 6, the minimum of the stress ratios based on  $P_m$  and  $P_m+P_b$ , is taken. The allowables listed in Table 6,  $S_m=16,900$  psi and  $S_a=13,600$  psi. The factors, 0.55 and  $f_{sw}$ , are the weld factors discussed above with  $f_{sw}=1.8$  being appropriate for a fillet weld and  $f_{sw}=1.4$  for a full penetration weld. The factor of 1.1 accounts for the differences in Young's moduli for the steel used in the steam dryer and the values assumed in alternating stress allowable. According to NG-3222.4 in subsection NG of Section III of the ASME Code [1], the effect of elastic modulus upon alternating stresses is taken into account by multiplying alternating stress  $S_{alt}$  at all locations by the ratio,  $E/E_{model}=1.1$ , where:

$$E = 28.3 \cdot 10^6 \text{ psi, as shown on Fig. I-9.2.2. ASME BP\&V Code}$$
$$E_{model} = 25.55 \cdot 10^6 \text{ psi (Table 1)}$$

The appropriate maximum and alternating stress ratios,  $SR-P$  and  $SR-a$ , are thus determined and a final listing of nodes having the smallest stress ratios is generated. The nodes with stress ratios lower than 4 are plotted in TecPlot (a 3D graphics plotting program widely used in engineering communities [27]). These nodes are tabulated and depicted in the following Results Section.

#### 4.5 Finite Element Sub-modeling

In order to meet target stress levels at EPU in the NMP2 steam dryer modifications are needed. These consist of stiffening the closure plates (see Appendix A) and reinforcing welds at three locations: (i) the top 18" of the welds connecting the closure plates to the hoods and vane banks (ii) the weld between the vane bank side plates and lifting rod support brace and (iii) the bottoms of the hood/hood support/base plate junctions (inner and middle hoods). These weld reinforcements are developed using high resolution solid element-based sub-models of these locations. The use of localized sub-models is motivated by the need to maintain computational costs at a feasible level. To this end the global steam dryer model is predominantly comprised of shell elements. These elements are well suited for structures such as the steam dryer consisting of shell-like components and tend to produce conservative estimates of the stresses. In some cases however, such as welded junctions involving multiple components, shell element models

can overestimate the nominal stress intensities in the vicinity of the junctions. In such cases a more refined analysis using solid elements to capture the complete 3D stress distribution, is warranted. Therefore, to efficiently analyze complex structures such as steam dryers, a standard engineering practice is to first analyze the structure using a shell-based model. Locations with high stresses are examined in greater detail using 3D solid elements to obtain a more definitive stress prediction.

The solid element-based sub-modeling follows the procedure outlined in Appendix A (also [29] and Appendix A of [30]) and validated in against both high resolution solid models of the full structure and sub-structuring results in [31] and [32]. Based on these models, the nominal stress intensities computed by the 3D solid element model are lower than those obtained with the shell-based FEA used to analyze the complete steam dryer by the stress reduction factors (SRFs) summarized in Table 7. Note that the SRFs vary according to location being dependent on the individual geometry and also the general loading characteristics. They are generally less than unity due to conservative stress estimates in the shell-based weld stresses. For example the discontinuity stresses computed in a shell model at a weld joint between two orthogonal members are often quite conservative because the shell element depiction does not provide any credit for the stress distribution associated with the specific weld geometry. Once the SRFs are obtained, the stress intensities predicted by the global shell element-based analysis at these locations are first multiplied by these SRFs to obtain more accurate estimates of the nominal stresses. These are then multiplied by the 1.8 weld factor before comparing against allowable stress limits to obtain the alternating stress ratios.

Detailed 3D solid element sub-models are applied at both the weld reinforcements and additional locations (see Table 7 for a complete list). For the closure plate the welds connecting the closure plate to the vane banks and hoods experience significant vibratory stresses due to a plate response in the 125-135 Hz frequency range. Though stresses remain well above allowable levels for all frequency shifts at both CLTP and EPU, the margin is below the target level (i.e., a stress ratio of  $SR-a=2.0$  at EPU). Therefore, the closure plate was reinforced and a sub-model developed for each of the locations on the closure plates where stresses exceeded target levels. On each closure plate there are four such locations. The first two are on the vertical weld joining the closure plate to the vane bank. The first node is at the top of this weld and the second one lies 13.5" below it. The other two locations are on the curved weld connecting the closure plate to the curved hood. Again the first location is at the top of this weld and the second one lies 14.5" below it. In both cases, the stresses at the top location result from a combination of membrane and bending stresses whereas the stresses at the lower locations are predominantly due to bending. The stresses are induced by a closure plate response dominated by a (1,2) mode (i.e., the mode shape resembles the first mode of a beam in the horizontal direction and the second mode in the vertical sense) which explains the high stress at the lower locations on the welds. Sub-model calculations at these locations show that to achieve the required target stress levels, an interior weld must be added along the top 18" of each weld thus effectively converting it from a single-sided to a double-sided fillet weld along this length. Additional details are given in Appendix A.

Sub-modeling is also applied to analyze the stresses in the lifting rod support brace where it connects to the vane bank side plate [33]. A sub-modeling analysis of the high stress location

shows that for the current ¼" double-sided fillet weld the stress reduction is minimal. Repeating the sub-model analysis with an increased weld of 1/2" resulted in a stress reduction factor of 0.60. To meet EPU target stress levels it is recommended to increase the weld to this size. Additional reinforcement of this weld is required when the loads processed with ACM Rev. 4.1 are applied. These reinforcements are not accounted for in Section 5, but are examined in Section 6 and shown to reduce stresses to below allowable levels.

The other locations where sub-modeling was performed are listed as locations 6-8 in Table 7 and involve the hood/hood support as well as two locations near tie bar ends involving large welds that are not accounted for in the shell model. The locations of all sub-models are depicted in Figure 11. Additional details of sub-models evaluated for locations away from the closure plate are given in [33]. These reinforcements and associated sub-models are the same as described in [5]. Note that the SRF for the hood/hood support weld (location 6 in Table 7) closely matches the value expected for this full penetration weld since the product of the SRF (0.77) and fillet weld factor (1.8),  $0.77 \times 1.80 = 1.39$ , agrees to within 1% with the weld factor for a full penetration weld (1.4). Therefore, rather than using the sub-model result, the weld factor (1.4) for a full penetration weld is used for this weld. This yields a slightly more conservative analysis.

Table 7. Summary of stress reduction factors obtained using sub-model analysis.

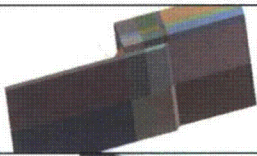
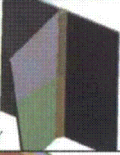
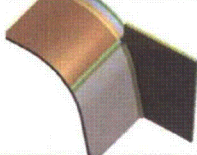

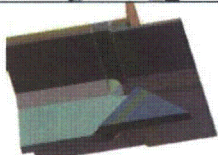
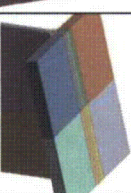
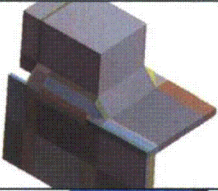
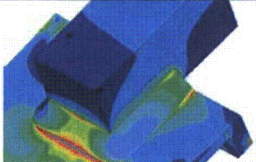
	Location	Stress Reduction Factor
	1. Top of vertical closure plate/vane bank weld	0.62 (Appendix A)
	2. 14.5" below location 3 on the same weld	0.71 (Appendix A)
	3. Top of closure plate/hood weld	0.86 (Appendix A)
	4. 13.5" below location 1 on the same weld	0.88 (Appendix A)
	5. Lifting rod support brace/vane side plate junction (assuming an increased 1/2" weld)	0.60 [33]
	6. Hood/hood support.	0.77 [30]

Table 7 (cont.). Summary of stress reduction factors obtained using sub-model analysis.

	Location	Stress Reduction Factor
	7. Side plate/top plate	0.70 [33]
	8. Tie bar/top vane bank plate.	0.71 [33]

Note: For locations 1-4 it is assumed that an inner weld has been to the top 18" of the welds joining the closure plate to the hoods or vane banks, thereby replacing the existing single-sided fillet weld by one that is double sided. Also, an increased ½" weld is assumed for location 5.



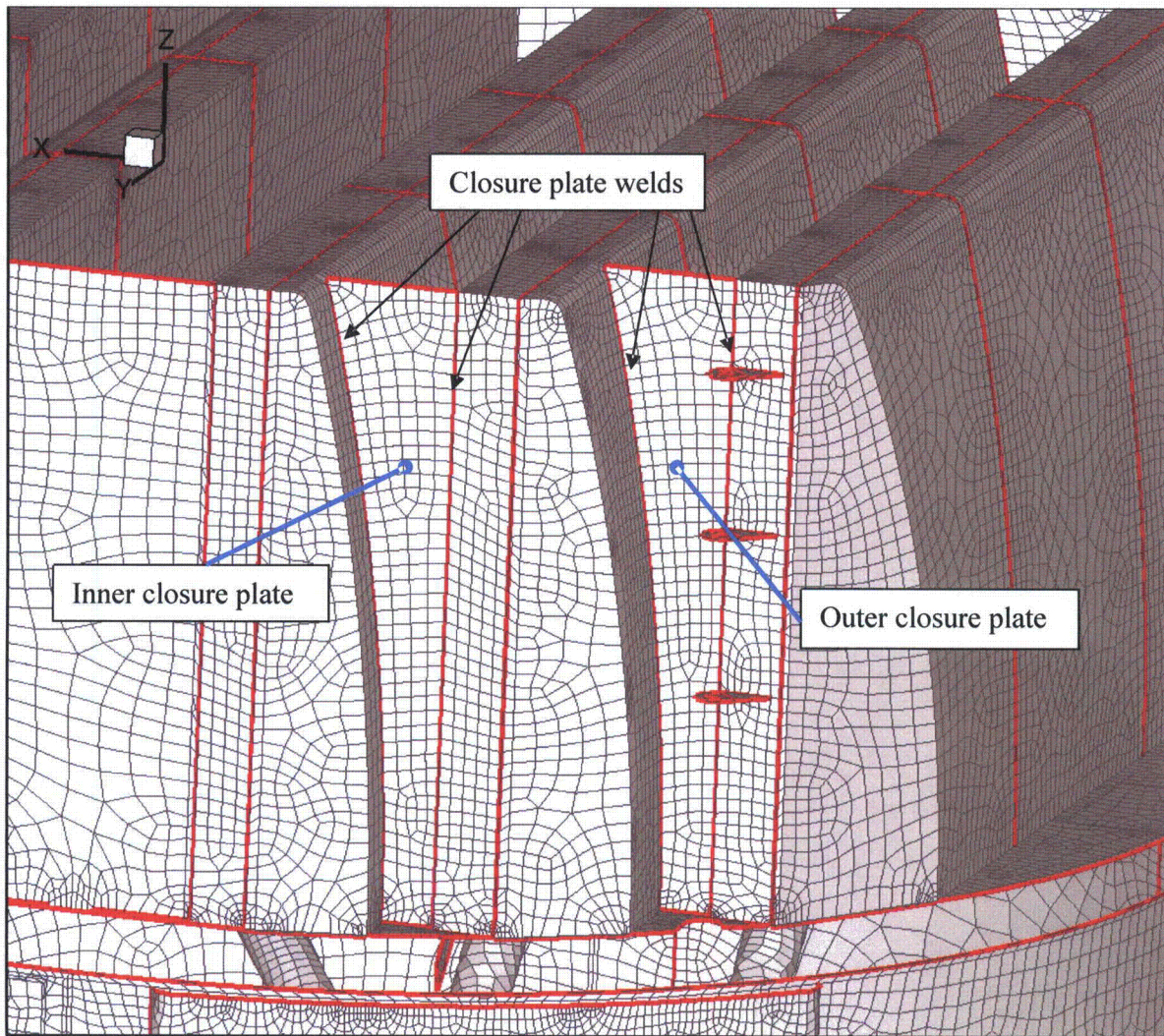


Figure 11a. Closure plates and associated attachment welds examined with sub-model in Appendix A (note lifting rods and other components modeled with solid elements are omitted for clarity). Sub-models on the perimeter are locations 1-4 in Table 7.



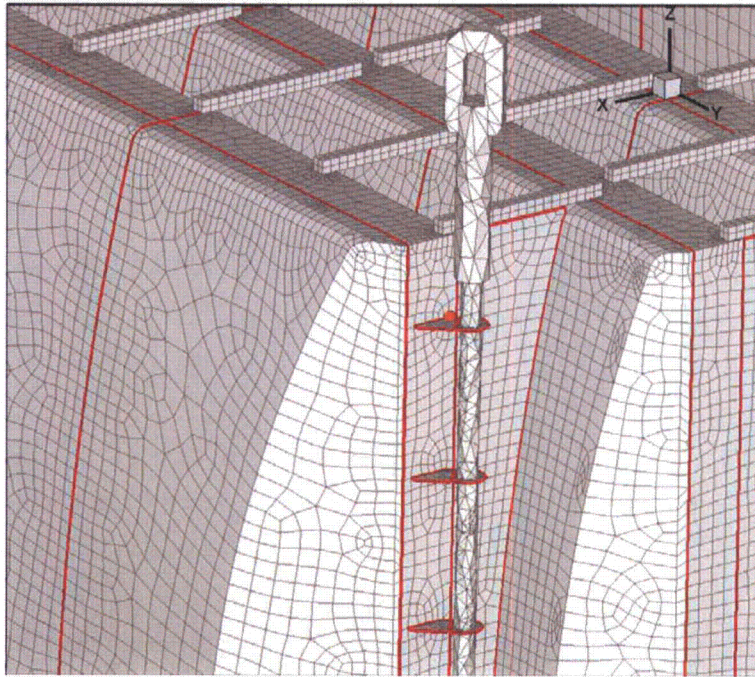


Figure 11b. Location of node on inner hood/hood support/middle base plate weld analyzed with sub-model in [33]. Sub-model corresponds to location 5 in Table 7.

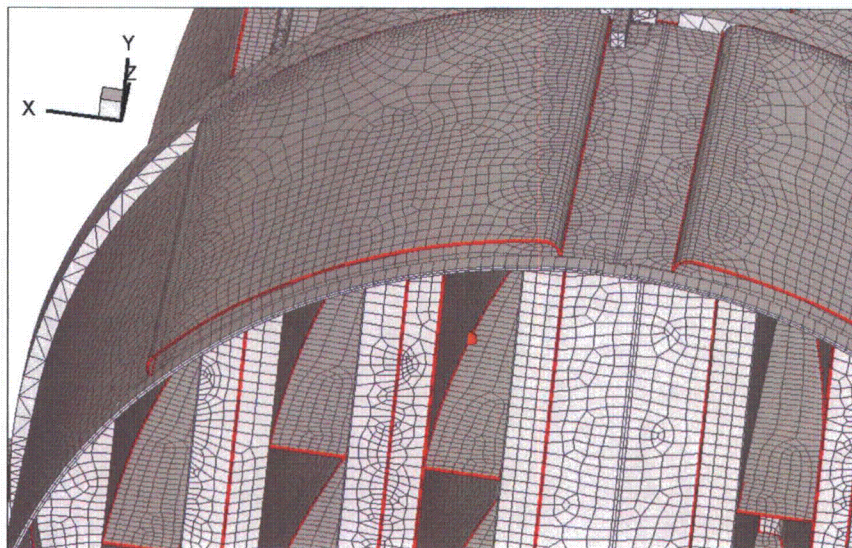


Figure 11c. Location of node on hood/hood support weld analyzed with sub-model analysis procedure in [30]. Sub-model corresponds to location 6 in Table 7.



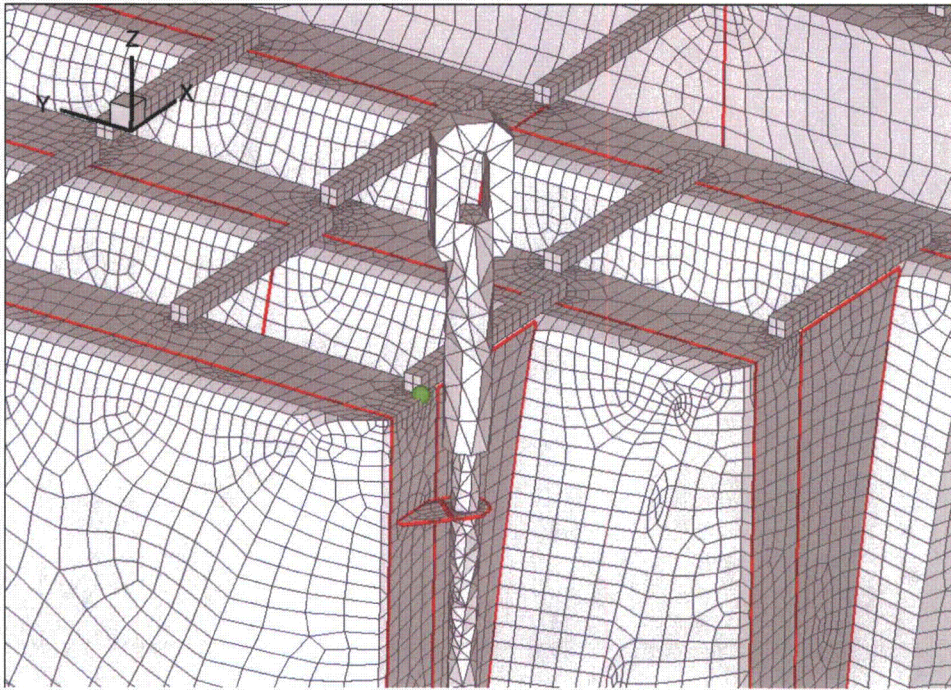


Figure 11d. Location of node on side plate/top plate weld analyzed with sub-model analysis procedure in [33]. Sub-model corresponds to location 7 in Table 7.

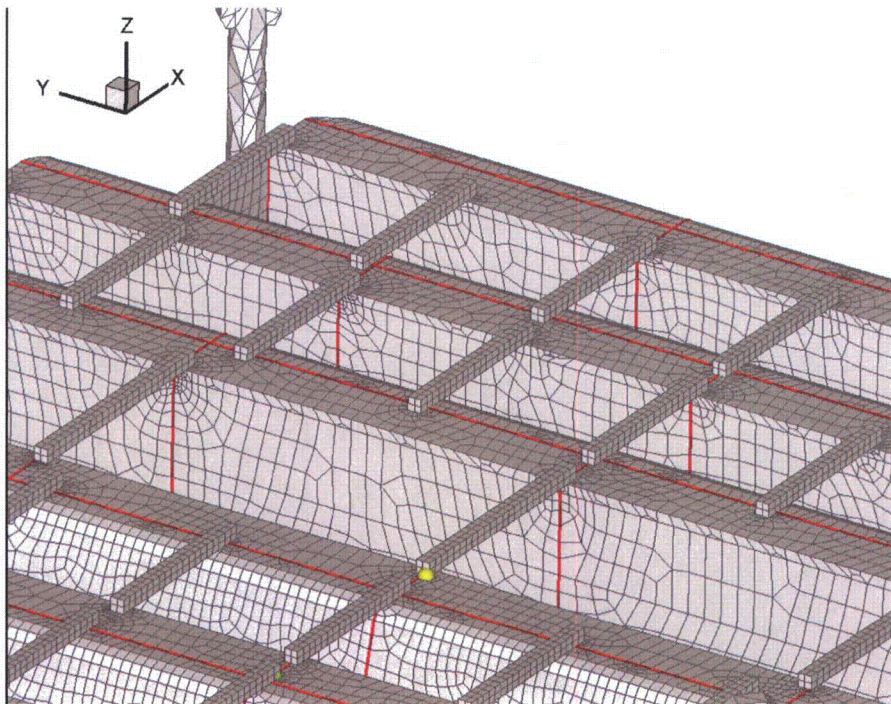


Figure 11e. Location of node on tie bar/top vane bank plate weld analyzed with sub-model analysis procedure in [33]. Sub-model corresponds to location 8 in Table 7.

## 5. Results

The stress intensities and associated stress ratios resulting from the Rev. 4 acoustic/hydrodynamic loads [11] with associated biases and uncertainties factored in, are presented below. The bias due to finite frequency discretization and uncertainty associated with the finite element model itself, are also factored in. In the following sections the highest maximum and alternating stress intensities are presented to indicate which points on the dryer experience significant stress concentration and/or modal response (Section 5.1). The lowest stress ratios obtained by comparing the stresses against allowable values, accounting for stress type (maximum and alternating) and location (on or away from a weld), are also reported (Section 5.2). Finally the frequency dependence of the stresses at nodes experiencing the lowest stress ratios is depicted in the form of accumulative PSDs (Section 5.3).

In each section results are presented both at nominal conditions (no frequency shift) and with frequency shift included. Unless specified otherwise, frequency shifts are generally performed at 2.5% increments. The tabulated stresses and stress ratios are obtained using a 'blanking' procedure that is designed to prevent reporting a large number of high stress nodes from essentially the same location on the structure. In the case of stress intensities this procedure is as follows. The relevant stress intensities are first computed at every node and then nodes sorted according to stress level. The highest stress node is noted and all neighboring nodes within 10 inches of the highest stress node and its symmetric images (i.e., reflections across the  $x=0$  and  $y=0$  planes) are "blanked" (i.e., excluded from the search for subsequent high stress locations). Of the remaining nodes, the next highest stress node is identified and its neighbors (closer than 10 inches) blanked. The third highest stress node is similarly located and the search continued in this fashion until all nodes are either blanked or have stresses less than half the highest value on the structure. For stress ratios, an analogous blanking procedure is applied. Thus the lowest stress ratio of a particular type in a 10" neighborhood and its symmetric images is identified and all other nodes in these regions excluded from listing in the table. Of the remaining nodes, the one with the lowest stress ratio is reported and its neighboring points similarly excluded, and so on until all nodes are either blanked or have a stress ratio higher than 4.

The applied load includes all biases and uncertainties for both the ACM (summarized in [11]) and the FEM. For the latter there are three main contributors to the bias and uncertainty. The first is an uncertainty (25.26%) that accounts for modeling idealizations (e.g., vane bank mass model), geometrical approximations and other discrepancies between the modeled and actual dryer such as neglecting of weld mass and stiffness in the FEA. The second contributor is a bias of 9.53% accounting for discretization errors associated with using a finite size mesh, upon computed stresses. The third contributor is also a bias and compensates for the use of a finite discretization schedule in the construction of the unit solutions. The frequencies are spaced such that at 1% damping the maximum (worst case) error in a resonance peak is 5%. The average error for this frequency schedule is 1.72%.

The acoustic loads applied to the steam dryer are obtained using the most recent and complete strain gage signals [4] and processed using the ACM Rev. 4.1 analysis with associated biases and uncertainties updated to reflect the new revision as described in [3].

### 5.1 General Stress Distribution and High Stress Locations

The maximum stress intensities obtained by post-processing the ANSYS stress histories for CLTP at nominal frequency and with frequency shift operating conditions are listed in Table 8. Contour plots of the stress intensities over the steam dryer structure are shown on Figure 12 (nominal frequency) and Figure 13 (maximum stress over all nine frequency shifts including nominal). The figures are oriented to emphasize the high stress regions. Note that these stress intensities *do not* account for weld factors but include end-to-end bias and uncertainty. Further, it should be noted that since the allowable stresses vary with location, stress intensities do not necessarily correspond to regions of primary structural concern. Instead, structural evaluation is more accurately made in terms of the stress ratios which compare the computed stresses to allowable levels with due account made for stress type and weld. Comparisons on the basis of stress ratios are made in Section 5.2.

The maximum stress intensities in most areas are low (less than 1000 psi). For the membrane stresses ( $P_m$ ) the high stress regions tend to occur at: (i) the bottom of the central vertical side plate that joins the innermost vane banks (stress concentrations occur where this plate is welded to the inner base plates resting on the upper support ring); (ii) the welds joining the tie bars to the top cover plates on the vane banks; (iii) the seismic blocks that rest on the steam dryer supports; (iv) the bottoms of the inner vane bank side plates where they connect to the USR; and (v) the closure plate welds. For these locations the stresses are dominated by the static contribution as can be inferred from the small alternating stress intensities ( $S_{alt}$ ) tabulated in Table 8 for the high  $P_m$  locations. From Figure 12a and Figure 13a higher  $P_m$  regions are seen to be in the vicinity of the supports where all of the dryer deadweight is transmitted, the closure plates connecting the inner hoods to the middle vane banks, and various localized concentrations such those along the bottom of the outer hood.

The membrane + bending stress ( $P_m + P_b$ ) distributions evidence a more pronounced modal response especially on the inner and middle hood structures. High stress concentrations are recorded on the bottom edge of the central vertical plate where it joins to the USR (immediately above the support blocks) and the inner vane bank. Other areas with high  $P_m + P_b$  stress concentrations include: (i) the tops of the closure plates where they are welded to a hood or vane bank end plates; (ii) the skirt/drain channel welds; (iii) the outer cover plates connecting to the upper support ring and bottom of the outer hoods; and (iv) the common junction between each hood, its hood support (or stiffener), and the adjoining base plate (see Figure 13c).

The alternating stress,  $S_{alt}$ , distributions are most pronounced on the outer hoods directly exposed to the MSL inlet acoustics, the thinner inner and middle hoods, the weld connecting the lifting rod restraint brace to the side plate and the welds involving the closure plates. The highest stress intensity at any frequency shift at a non-weld location occurs on the inner hood. Though not exposed directly to the MSL acoustic sources, the interior hoods are thinner and their response is driven mainly by structural coupling rather than direct forcing. The edge of the middle hood reinforcement strip also exhibits high stresses. This reinforcement strip was added following prior discovery of locations on the middle hoods. Numerous weld locations also show significant stress including the bottoms of drain channels and the junctions between the hoods, hood supports and base plates. These locations are characterized by localized stress concentrations as indicated in Figure 13e and have emerged as high stress locations in other

steam-dryers also. Other locations with high alternating stress intensities include the tie bar/top cover plate weld and welds involving the closure plate.

Comparing the nominal results (Table 8a) and results with frequency shifting it can be seen that maximum stress intensities,  $P_m$  and  $P_m + P_b$ , do not differ significantly. The highest alternating stress is approximately 5.1% higher when frequency shifts are considered. For other nodes however the variations are higher.

Table 8a. Locations with highest predicted stress intensities for CLTP conditions with no frequency shift.

Stress Category	Location	Weld	Location (in)			node(a)	Stress Intensities (psi)		
			x	y	z		Pm	Pm+Pb	S <sub>alt</sub>
Pm	Inner Side Plate	No	3.1	119	0.5	37229	7546	8993	650
"	Upper Support Ring (USR)/Support/Seismic Block	Yes	-6.9	-122.3	-9.5	113554	7346	7346	963
"	Side Plate Ext/Inner Base Plate	Yes	16.3	119	0	94143	7003	9918	585
"	Tie Bar	Yes	49.3	108.1	88	141275	6168	6168	1099
	Closure Plate/Backing Bar/Inner Hood	Yes	39.9	108.6	0.5	93062	5292	5307	953
Pm+Pb	Side Plate Ext/Inner Base Plate	Yes	16.3	119	0	94143	7003	9918	585
"	Inner Side Plate	No	3.1	119	0.5	37229	7546	8993	650
"	Side Plate/Top Plate	Yes	49.6	108.6	88	93256	2579	8884	1542
"	Side Plate/Top Plate	Yes	17.6	119	88	91215	992	7581	1821
"	Upper Support Ring/Support/Seismic Block	Yes	-6.9	-122.3	-9.5	113554	7346	7346	963
S <sub>alt</sub>	Side Plate/Brace	Yes	79.7	-85.2	31.2	87633	3612	4190	3538
"	Side Plate/Brace <sup>(5)</sup>	Yes	79.7	85.2	75.8	89649	3681	4309	3506
"	Brace	No	79.6	85.5	75.8	37811	3455	3573	3381
"	Hood Support/Inner Hood	Yes	-38.5	0	31	95636	1087	3148	3084
"	Inner hood	No	-38.6	-28	30	80557	946	2978	2890

Notes.

(a) Node numbers are retained for further reference.

(1-8) Appropriate stress reduction factor for the welds and modifications listed in Table 7 have been applied. The number refers to the particular location and corresponding stress reduction factor in Table 7.

(b) WF=1.4



Table 8b. Locations with highest predicted stress intensities taken over all frequency shifts CLTP conditions.

Stress Category	Location	Weld	Location (in)			node(a)	Stress Intensities (psi)			% Freq. Shift
			x	y	z		Pm	Pm+Pb	S <sub>alt</sub>	
Pm	Inner Side Plate	No	3.1	119	0.5	37229	7563	9033	680	2.5
"	USR/Support/Seismic Block	Yes	-6.9	-122.3	-9.5	113554	7422	7422	1082	10
"	Side Plate Ext/Inner Base Plate	Yes	16.3	119	0	94143	7024	9976	622	2.5
"	Tie Bar	Yes	-49.3	-108.1	88	143795	6354	6354	1114	2.5
"	Hood Support/Middle Base Plate/Inner Backing Bar/Inner Hood <sup>(b)</sup>	Yes	-39.9	0	0	85723	5716	6049	2444	-10
Pm+Pb	Side Plate Ext/Inner Base Plate	Yes	16.3	119	0	94143	7024	9976	622	2.5
"	Side Plate/Top Plate	Yes	49.6	108.6	88	93256	2609	9086	1716	2.5
"	Inner Side Plate	No	3.1	119	0.5	37229	7563	9033	680	2.5
"	Side Plate/Top Plate	Yes	17.6	119	88	91215	992	7803	2036	2.5
"	Middle Base Plate/Backing Bar/Inner Hood	Yes	-39.9	-108.6	0	84197	550	7572	1526	5
S <sub>alt</sub>	Side Plate/Brace <sup>(5)</sup>	Yes	79.7	85.2	75.8	89649	4022	5464	4413	-5
"	Hood Reinforcement/Middle Hood	Yes	-63.5	100.7	74.1	98275	414	4626	4229	10
"	Side Plate/Brace	Yes	79.7	85.2	31.2	89646	3460	4435	3947	5
"	Lifting Rod Restraint Brace	No	79.6	85.5	75.8	37811	3765	3875	3742	-5
"	Inner Hood	No	38.7	32	28.7	71783	970	3582	3544	-10

Notes.

(a) Node numbers are retained for further reference.

(1-8) Appropriate stress reduction factor for the welds and modifications listed in Table 7 have been applied. The number refers to the particular location and corresponding stress reduction factor in Table 7.

(b) WF=1.4

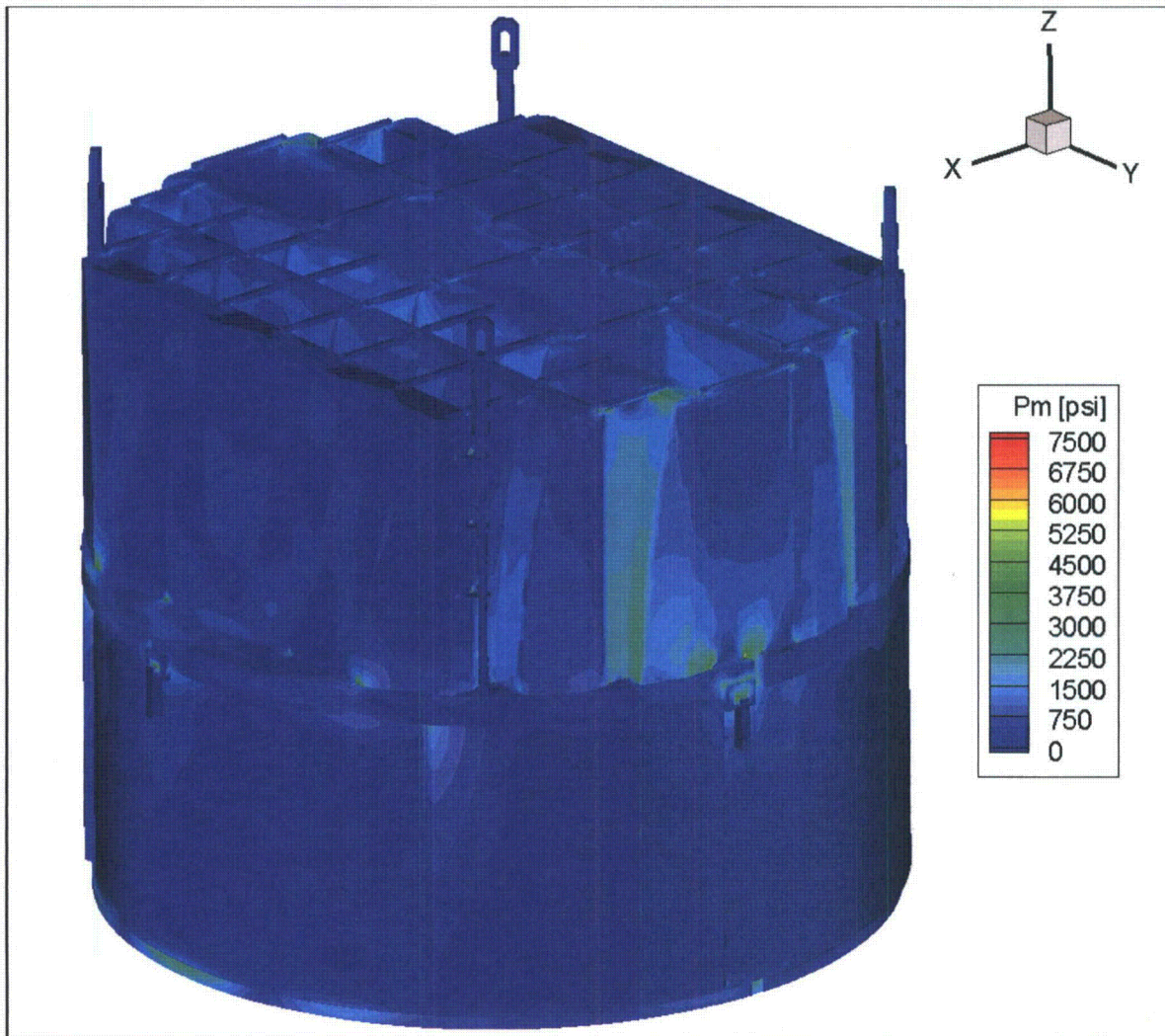


Figure 12a. Contour plot of maximum membrane stress intensity,  $P_m$ , for CLTP load. The maximum stress intensity is 7546 psi.

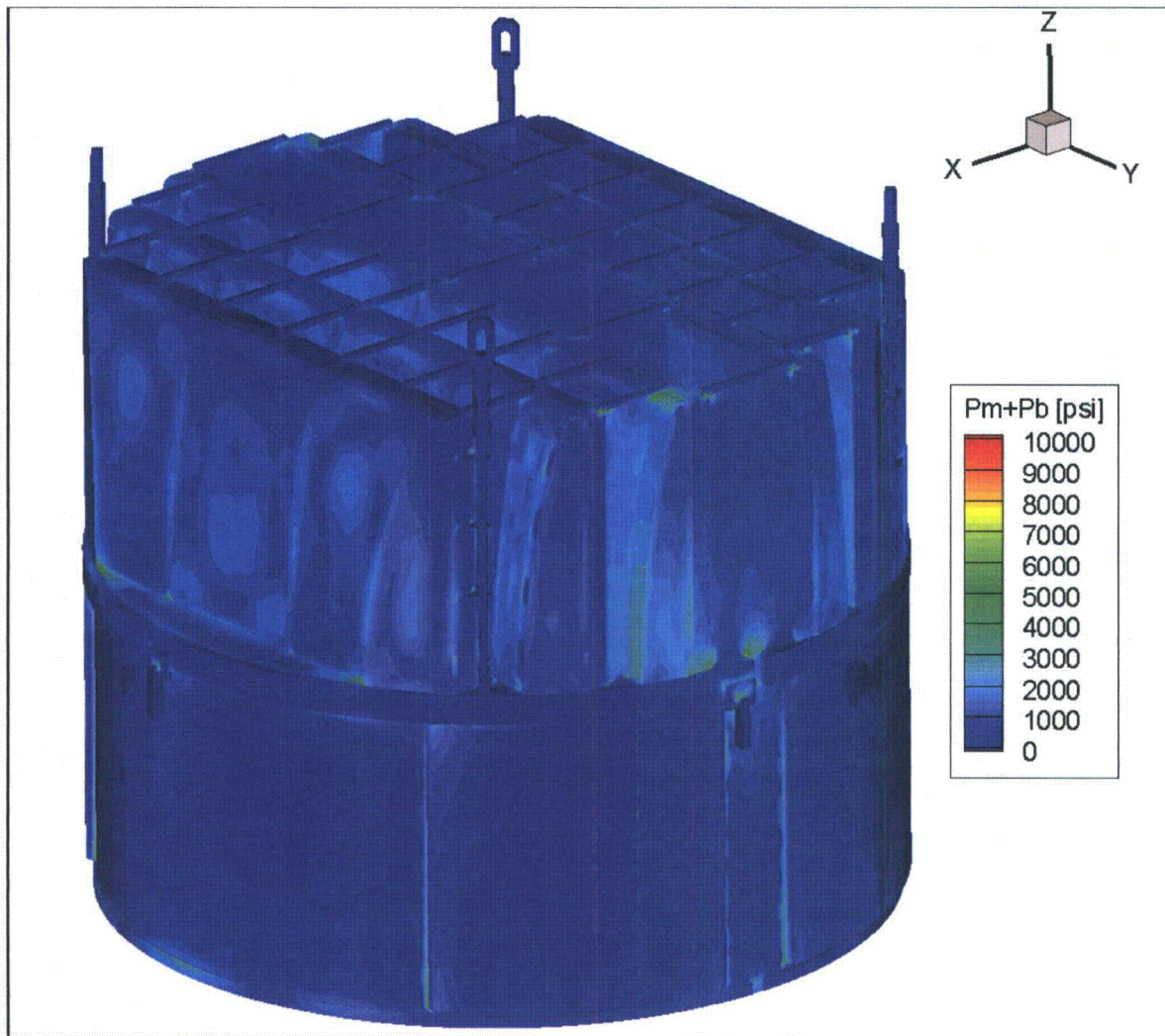


Figure 12b. Contour plot of maximum membrane+bending stress intensity,  $P_m+P_b$ , for CLTP load. The maximum stress intensity is 9918 psi. First view.



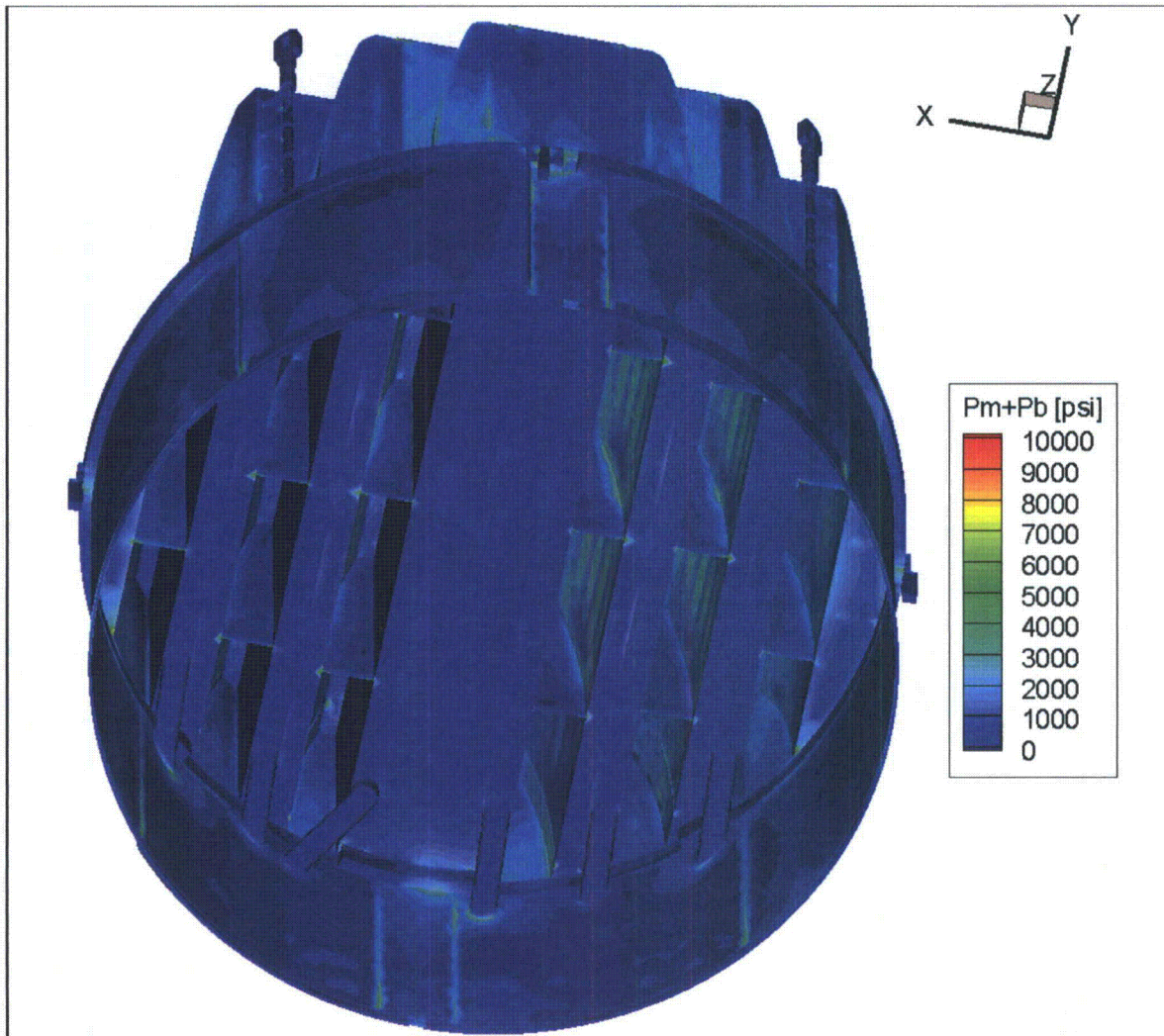


Figure 12c. Contour plot of maximum membrane+bending stress intensity,  $P_m + P_b$ , for CLTP load. This second view from below shows the high stress intensities at the hood/stiffener/base plate junctions and drain channel/skirt welds.

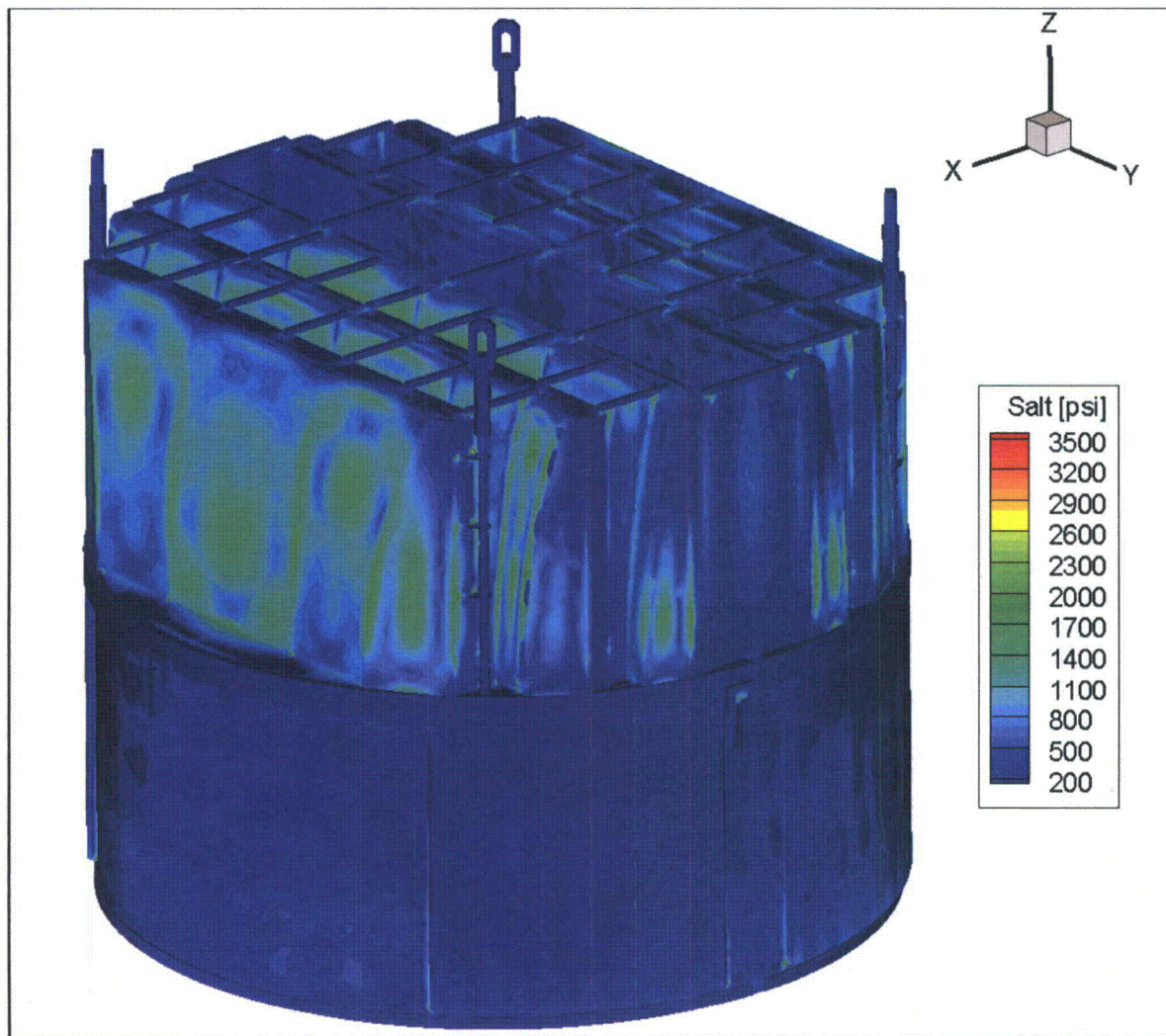


Figure 12d. Contour plot of alternating stress intensity,  $S_{alt}$ , for CLTP load. The maximum alternating stress intensity is 3538 psi. First view.



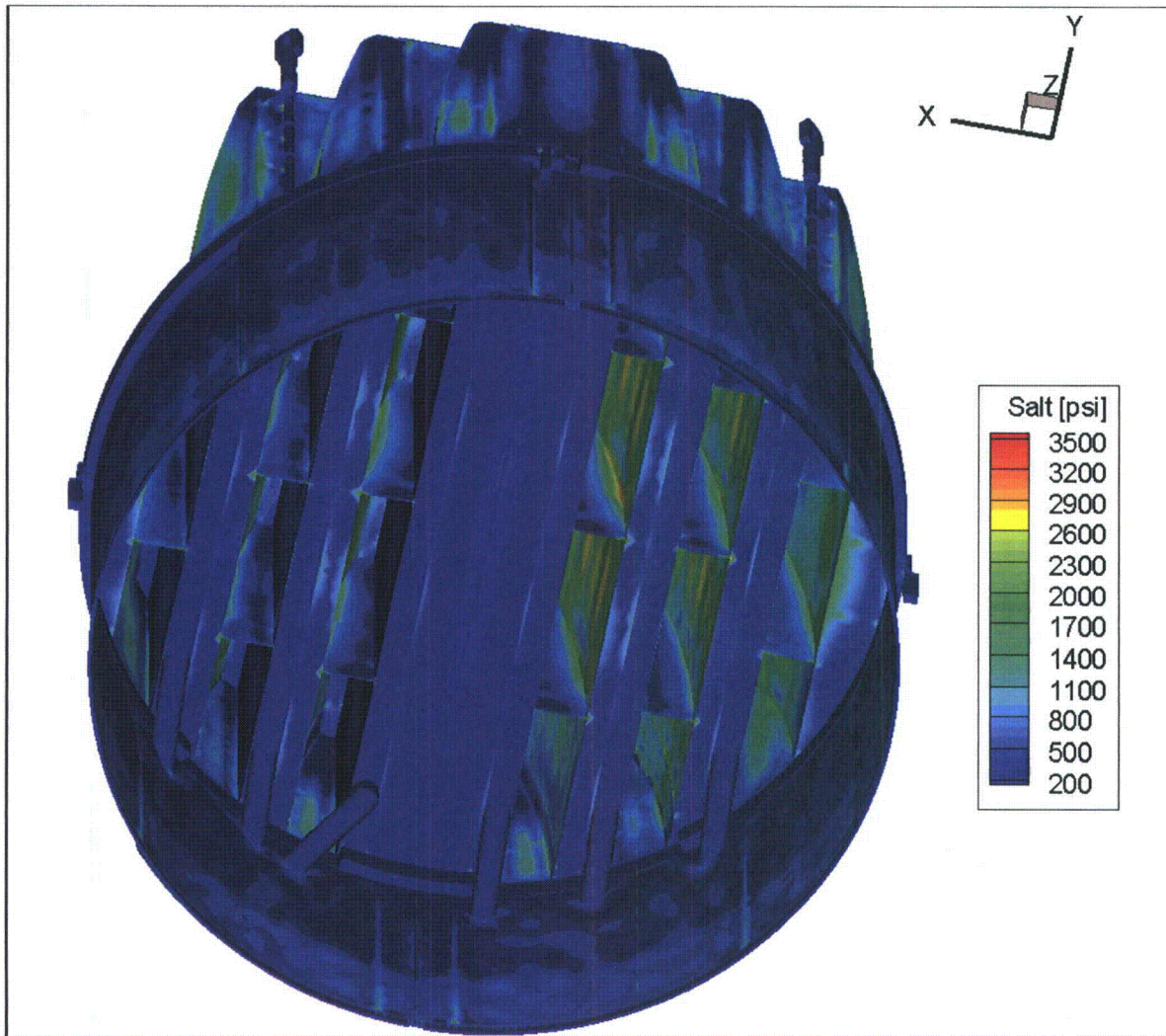


Figure 12e. Contour plot of alternating stress intensity,  $S_{alt}$ , for CLTP load. Second view showing details of the outer hood and closure plate.

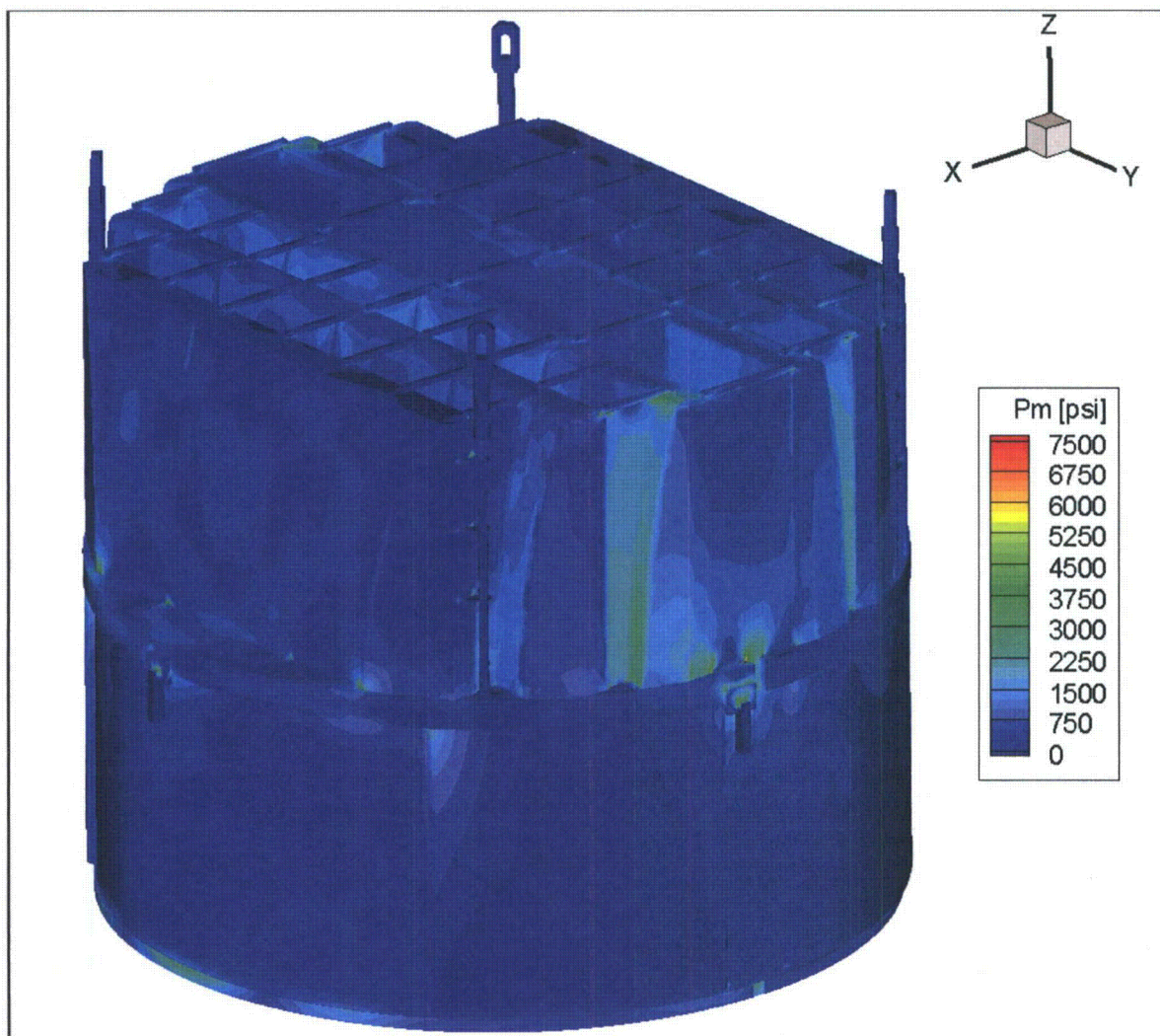


Figure 13a. Contour plot of maximum membrane stress intensity,  $P_m$ , for CLTP operation with frequency shifts. The recorded stress at a node is the maximum value taken over all frequency shifts. The maximum stress intensity is 7563 psi.



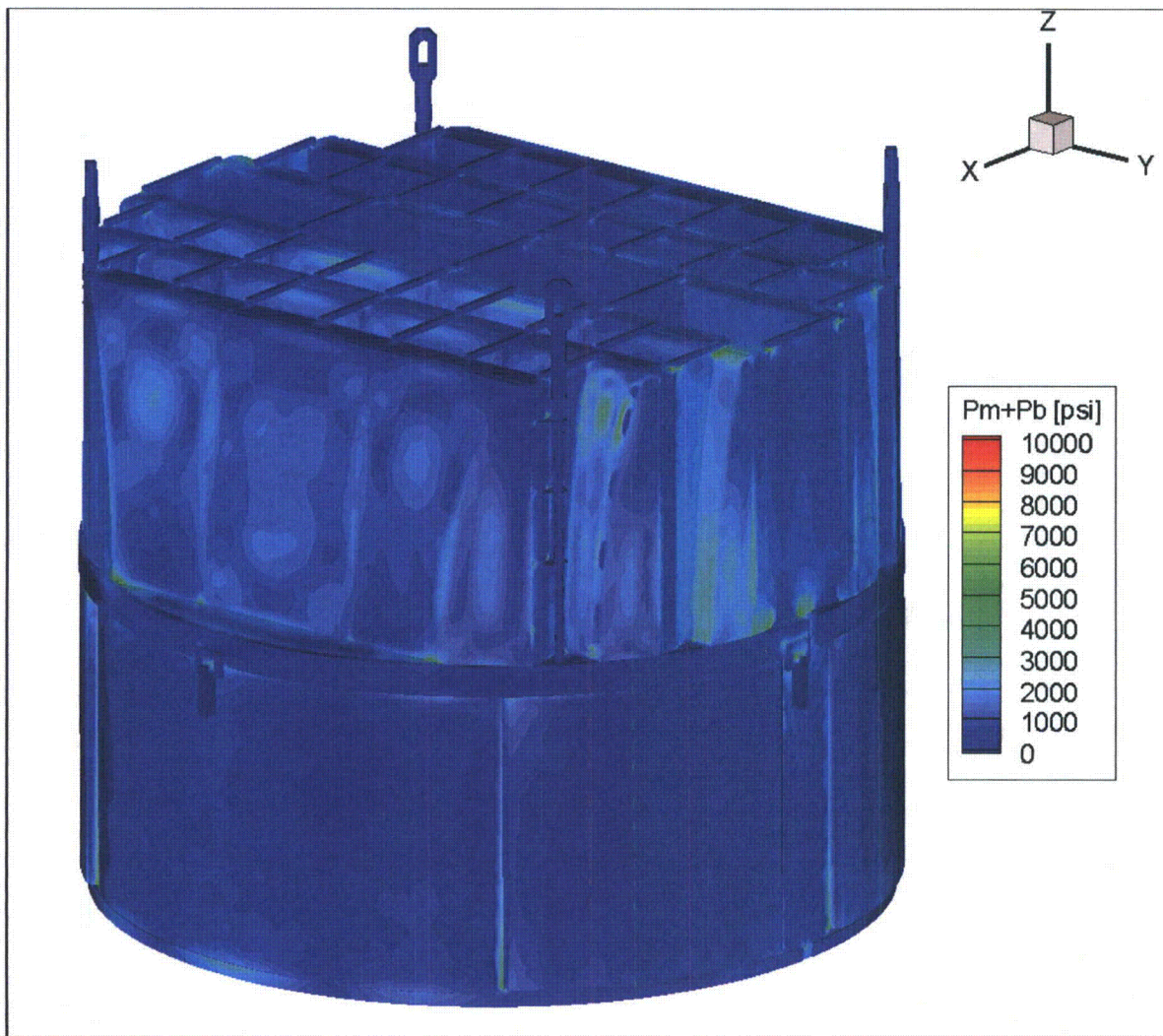


Figure 13b. Contour plot of maximum membrane+bending stress intensity,  $P_m + P_b$ , for CLTP operation with frequency shifts. The recorded stress at a node is the maximum value taken over all frequency shifts. The maximum stress intensity is 9976 psi. First view.

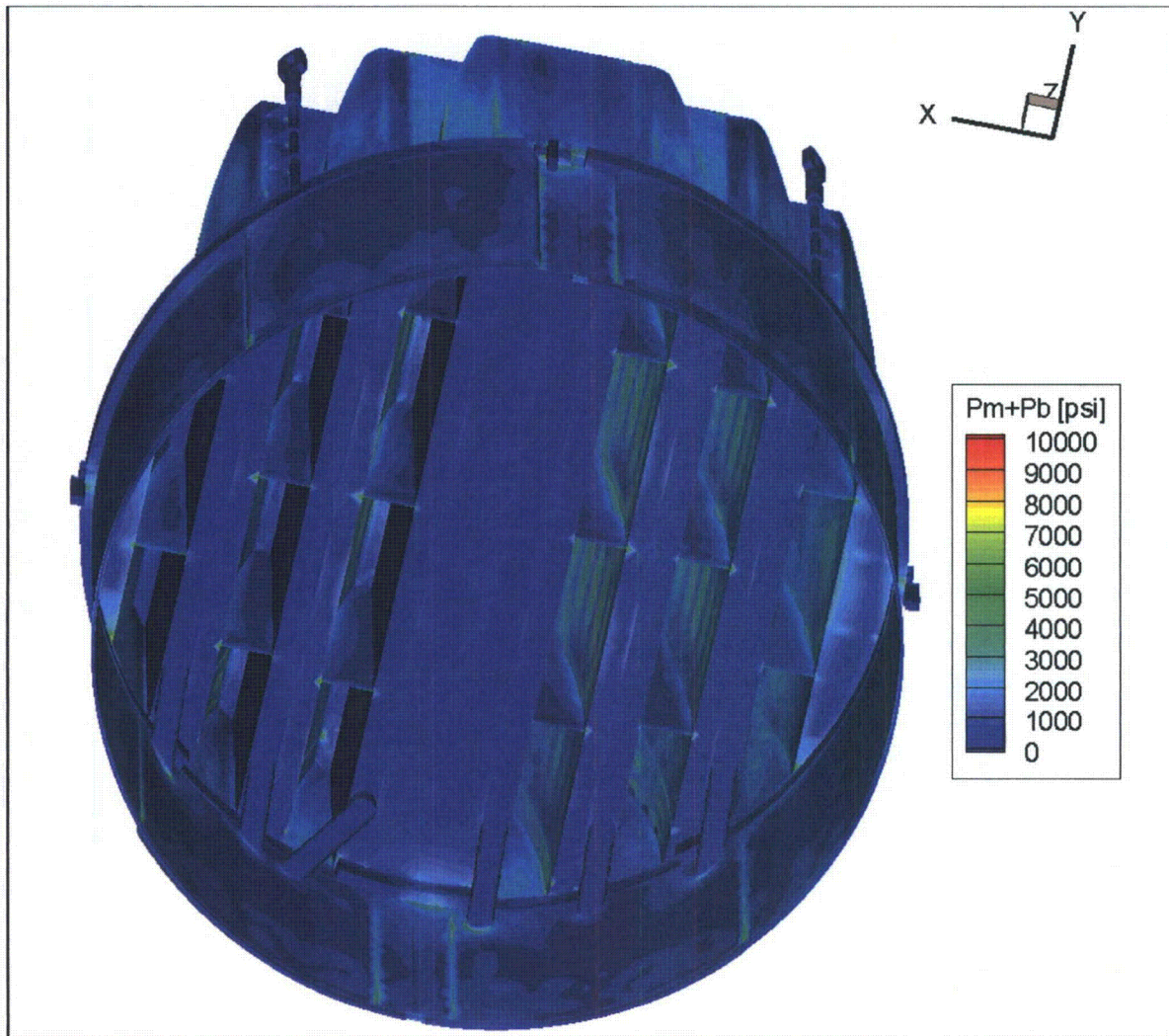


Figure 13c. Contour plot of maximum membrane+bending stress intensity,  $P_m+P_b$ , for CLTP operation with frequency shifts. This second view from beneath reveals stresses on the hood support/base plate junctions, outer cover plate and drain channel/skirt welds.



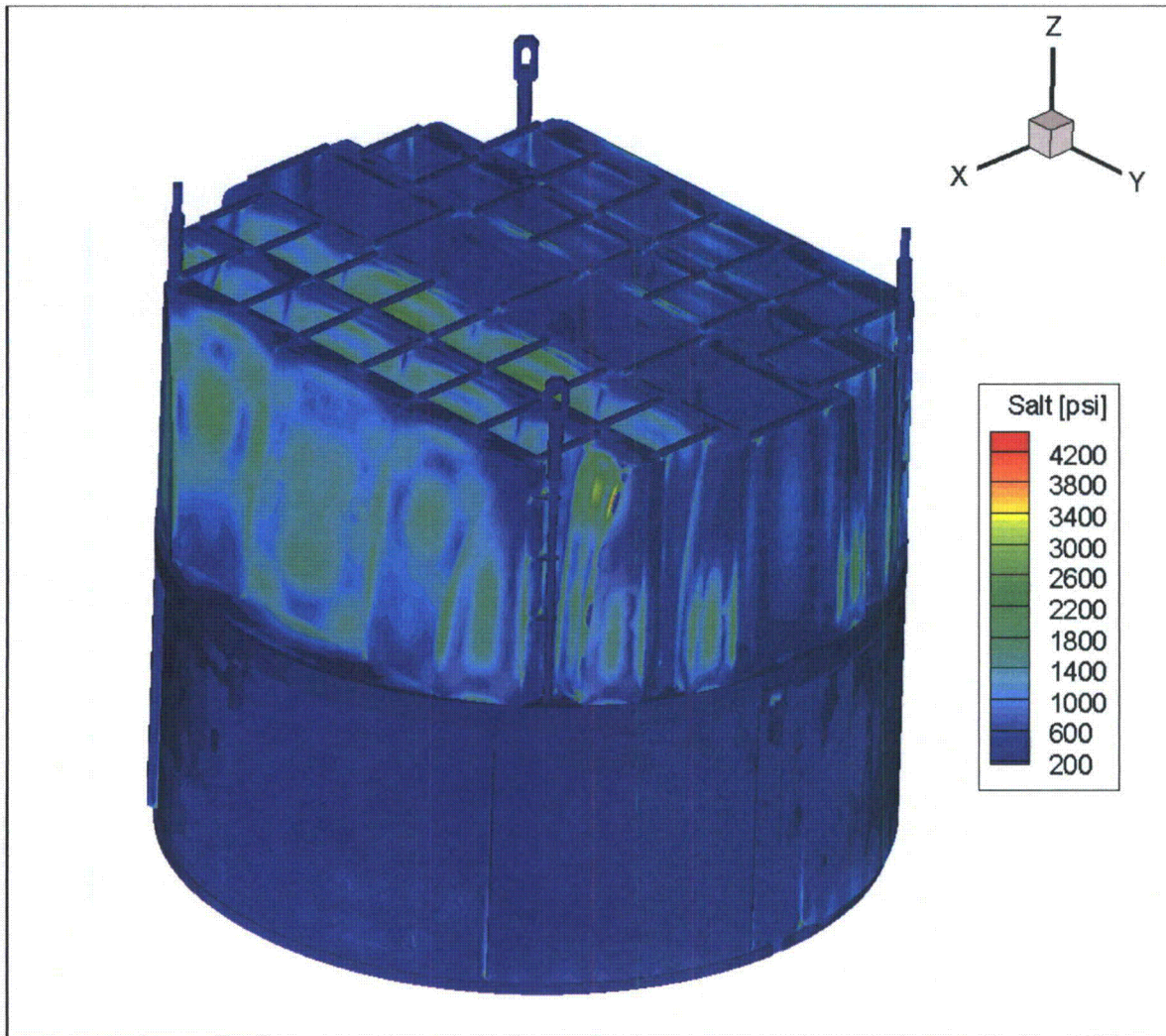


Figure 13d. Contour plot of alternating stress intensity,  $S_{alt}$ , for CLTP operation with frequency shifts. The recorded stress at a node is the maximum value taken over all frequency shifts. The maximum alternating stress intensity is 4413 psi. First view.

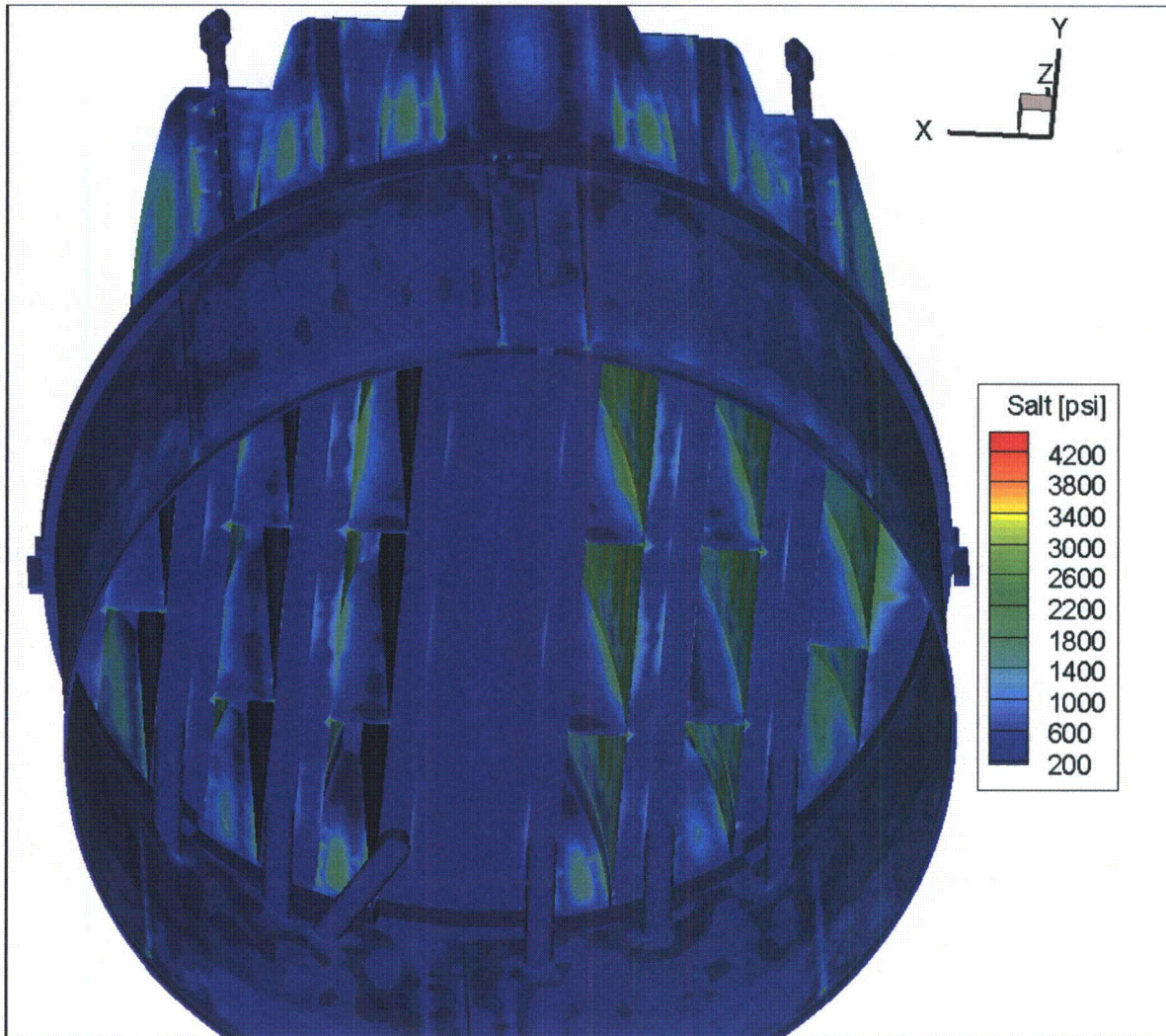


Figure 13e. Contour plot of alternating stress intensity,  $S_{alt}$ , for CLTP operation with frequency shifts. The recorded stress at a node is the maximum value taken over all frequency shifts. Second view from below.



## 5.2 Load Combinations and Allowable Stress Intensities

The stress ratios computed for CLTP at nominal frequency and with frequency shifting are listed in Table 9. The stress ratios are grouped according to type (SR-P for maximum membrane and membrane+bending stress, SR-a for alternating stress) and location (away from welds or on a weld). The tabulated nodes are also depicted in Figure 14 (no frequency shift) and Figure 15 (all frequency shifts included). The plots corresponding to maximum stress intensities depict all nodes with stress ratios less than 4 or 5 as indicated, and the plots of alternating stress ratios display all nodes with  $SR-a \leq 5$ .

For CLTP operation at nominal frequency the minimum stress ratio is identified as a maximum stress,  $SR-P=1.27$ , and is recorded on upper support ring where it rests on the support block. This stress at this location is dominated by the static stress due to deadweight and is only weakly responsive to acoustic loads as can be seen from the high alternating stress ratio at this location ( $SR-a > 6.35$  at all frequency shifts). This is true for all three nodes having the lowest values of  $SR-P$ , all having  $SR-a > 6.17$  at all frequency shifts. The minimum alternating stress ratio at zero frequency shift,  $SR-a=1.94$ , occurs on the weld connecting the lifting rod brace to the side plate. At zero shift the lower lifting rod brace has the lowest alternating stress ratio. This is because, unlike the middle and upper braces which experience higher alternating lateral loads, the lower brace weld is not reinforced.

The effects of frequency shifts can be conservatively accounted for by identifying the minimum stress ratio at every node, where the minimum is taken over all the frequency shifts considered (including the nominal or 0% shift case). The resulting stress ratios are then processed as before to identify the smallest stress ratios anywhere on the structure, categorized by stress type (maximum or alternating) and location (on or away from a weld). The results are summarized in Table 9b and show that the lowest stress ratio,  $SR-P=1.25$ , occurs at the same location as in the nominal case and retains virtually the same value. Moreover, the next three lowest  $SR-P$  locations are the same as in Table 9a, taking into account rotational symmetry of the nodes. The lowest alternating stress ratio,  $SR-a=1.56$  occurs on the weld connecting the lifting rod brace (here the upper one) to the side plate (see Figure 15g). The high stresses on these braces occur on a re-entrant corner coinciding with the end of the brace/side plate weld and are induced by vibrations of the lifting rods. The next highest location occurs on the edge of the reinforcement strip added to the middle hood. The high stress occurs in the thinner member (i.e., the non-reinforced part of the middle hood) and is caused by vibration of the section of the middle hood lying outboard of the closure plate. The next collection of locations involves the weld connecting the inner hood and underlying central hood support. The high stress is associated with hood vibration. A similar, but weaker response is observed in the middle hood/hood support weld. Other points with low alternating stress ratios include the submerged drain channel/skirt welds and some locations on the welds on the perimeter of the closure plates.

The estimated alternating stress ratio at EPU operation is obtained by scaling the corresponding value at CLTP by the square of the ratio of the steam flow velocities at EPU and CLTP conditions. Since this ratio,  $(U_{EPU}/U_{CLTP})^2 = 1.1756^2 = 1.382$ , the limiting alternating stress ratio at any frequency shift for EPU is estimated as  $SR-a = 1.56/1.382 = 1.13$  which does not meet the EPU target of 2.0. This location and others that do not meet the EPU target are all accessible and can be modified. Section 6 addresses the additional modifications needed to meet the EPU

target stress ratio. The lowest stress ratio associated with a maximum stress is  $SR-P=1.25$  at CLTP. This value is dominated by the static component and is only weakly altered by acoustic loads and reduces to 1.19 at EPU.

Table 9a. Locations with minimum stress ratios for CLTP conditions with no frequency shift. Stress ratios are grouped according to stress type (maximum – SR-P; or alternating – SR-a) and location (away from a weld or at a weld). Bold text indicates minimum stress ratio of any type on the structure. Locations are depicted in Figure 14.

Stress Ratio	Weld	Location	Location (in.)			node(a)	Stress Intensity (psi)			Stress Ratio	
			x	y	z		Pm	Pm+Pb	Salt	SR-P	SR-a
SR-P	No	1. Inner Side Plate	3.1	119	0.5	37229	7546	8993	650	2.24	19.02
"	"	2. Thin Vane Bank Plate	-15.6	-118.4	0.6	2558	4829	5245	261	3.50	47.39
"	"	3. Support/Seismic Block	10.2	123.8	-9.5	113286	4438	4438	1476	3.81	8.38
SR-a	No	1. Brace	79.6	85.5	75.8	37811	3455	3573	3381	4.89	3.66
"	"	2. Inner Hood	-38.6	-28	30	80557	946	2978	2890	8.51	4.28
SR-P	Yes	<b>1. USR/Support/Seismic Block</b>	<b>-6.9</b>	<b>-122.3</b>	<b>-9.5</b>	<b>113554</b>	<b>7346</b>	<b>7346</b>	<b>963</b>	<b>1.27</b>	<b>7.13</b>
"	"	2. Side Plate Ext/Inner Base Plate	16.3	119	0	94143	7003	9918	585	1.33	11.74
"	"	3. Tie Bar	49.3	108.1	88	141275	6168	6168	1099	1.51	6.25
"	"	4. Inner Side Plate/Inner Base Plate	2.3	119	0	98446	4635	8029	754	1.74	9.10
"	"	5. Closure Plate Backing Bar/Inner Hood	39.9	108.6	0.5	93062	5292	5307	953	1.76	7.21
"	"	6. Hood Support/Middle Base Plate/Inner Backing Bar/Inner Hood(b)	39.9	0	0	88639	5247	5442	2142	1.77	3.21
"	"	7. Side Plate/Top Plate	17.6	119	88	91215	992	7581	1821	1.84	3.77
"	"	8. Thin Vane Bank Plate/Hood Support/Inner Base Plate	24.1	-59.5	0	85191	4960	5103	1472	1.87	4.67
"	"	9. Outer Cover Plate/Outer Hood	102.8	-58.1	0	94498	1033	7264	1044	1.92	6.58
"	"	10. Hood Support/Middle Base Plate/Inner Backing Bar/Inner Hood(b)	39.9	-59.5	0	101435	4802	4916	1695	1.94	4.05
"	"	11. Hood Support/Outer Cover Plate/Outer Hood(b)	-102.8	28.4	0	95267	4772	5206	2329	1.95	2.95
"	"	12. Hood Support/Outer Base Plate/Middle Backing Bar(b)	-71.3	0	0	95428	4516	4807	2588	2.06	2.65

Notes.

(a) Node numbers are retained for further reference.

(1-8) Appropriate stress reduction factor for the welds and modifications listed in Table 7 have been applied. The number refers to the particular location and corresponding stress reduction factor in Table 7.

(b) WF=1.4

Table 9a (cont.). Locations with minimum stress ratios for CLTP conditions with no frequency shift. Stress ratios are grouped according to stress type (maximum – SR-P; or alternating – SR-a) and location (away from a weld or at a weld). Bold text indicates minimum alternating stress ratio on the structure. Locations are depicted in Figure 14.

Stress Ratio	Weld	Location	Location (in.)			node(a)	Stress Intensity (psi)			Stress Ratio	
			x	y	z		Pm	Pm+Pb	S <sub>alt</sub>	SR-P	SR-a
SR-a	Yes	1. Side Plate/Brace	79.7	-85.2	31.2	87633	3612	4190	3538	2.57	1.94
"	"	2. Side Plate/Brace <sup>(5)</sup>	79.7	85.2	75.8	89649	3681	4309	3506	2.53	1.96
"	"	3. Hood Support/Inner Hood <sup>(b)</sup>	-38.5	0	31	95636	1087	3148	3084	4.43	2.23
"	"	4. Hood Support/Inner Hood <sup>(b)</sup>	-35	0	58.7	95650	1046	3186	2888	4.38	2.38
"	"	5. Hood Support/Inner Hood <sup>(b)</sup>	37.3	0	42.9	99525	1139	2808	2707	4.96	2.54
		6. Hood Support/Outer Base Plate/Middle Backing Bar <sup>(b)</sup>	-71.3	0	0	95428	4516	4807	2588	2.06	2.65
"	"	7. Side Plate/Brace <sup>(5)</sup>	79.7	-85.2	53.5	87630	2374	3500	2579	3.91	2.66
"	"	8. Hood Reinforcement/Middle Hood	-66.4	98.6	58.5	98267	531	2977	2536	4.68	2.71
"	"	9. Hood Reinforcement/Middle Hood	-62.6	101.2	77.9	98277	447	2604	2518	5.35	2.73
"	"	10. Hood Reinforcement/Middle Hood	-69.6	-96.5	34.9	90949	1060	2731	2492	5.11	2.76
"	"	11. Hood Support/Middle Hood <sup>(b)</sup>	-68.7	0	42.9	96022	905	2710	2476	5.14	2.77
"	"	12. Hood Support/Outer Cover Plate/Outer Hood <sup>(b)</sup>	-102.8	28.4	0	95267	4772	5206	2329	1.95	2.95
"	"	13. Submerged Drain Channel/Submerged Skirt	11.5	-118.4	-101.5	84597	1125	4267	2205	3.27	3.12
"	"	14. Hood Support/Middle Base Plate/Inner Backing Bar/Inner Hood <sup>(b)</sup>	-39.9	0	0	85723	5194	5486	2191	1.79	3.13
"	"	15. Submerged Drain Channel/Submerged Skirt	-91	76.7	-101.5	93430	731	5955	2189	2.34	3.14

Notes.

- (a) Node numbers are retained for further reference.
- (1-8) Appropriate stress reduction factor for the welds and modifications listed in Table 7 have been applied. The number refers to the particular location and corresponding stress reduction factor in Table 7.
- (b) WF=1.4

Table 9b. Locations with minimum stress ratios for CLTP conditions with frequency shifts. Stress ratios at every node are recorded as the lowest stress ratio identified during the frequency shifts. Stress ratios are grouped according to stress type (maximum – SR-P; or alternating – SR-a) and location (away from a weld or at a weld). Bold text indicates minimum stress ratio of any type on the structure. Locations are depicted in Figure 15.

Stress Ratio	Weld	Location	Location (in.)			node(a)	Stress Intensity (psi)			Stress Ratio		% Freq. Shift
			x	y	z		Pm	Pm+Pb	S <sub>alt</sub>	SR-P	SR-a	
SR-P	No	1. Inner Side Plate	3.1	119	0.5	37229	7563	9033	680	2.23	18.17	2.5
"	"	2. Thin Vane Bank Plate	-15.6	-118.4	0.6	2558	4871	5284	315	3.47	39.31	2.5
"	"	3. Support/Seismic Block	10.2	123.8	-9.5	113286	4576	4576	1748	3.69	7.07	10
SR-a	No	1. Brace	79.6	85.5	75.8	37811	3765	3875	3742	4.49	3.30	-5
"	"	2. Inner Hood	38.7	32	28.7	71783	970	3582	3544	7.08	3.49	-10
"	"	3. Inner Hood	34.8	31.5	59.6	71778	955	3516	3482	7.21	3.55	-10
SR-P	Yes	<b>1. USR/Support/Seismic Block</b>	<b>-6.9</b>	<b>-122.3</b>	<b>-9.5</b>	<b>113554</b>	<b>7422</b>	<b>7422</b>	<b>1082</b>	<b>1.25</b>	<b>6.35</b>	<b>10</b>
"	"	2. Side Plate Ext/Inner Base Plate	16.3	119	0	94143	7024	9976	622	1.32	11.05	2.5
"	"	3. Tie Bar	-49.3	-108.1	88	143795	6354	6354	1114	1.46	6.17	2.5
"	"	4. Hood Support/Middle Base Plate/Inner Backing Bar/Inner Hood(b)	-39.9	0	0	85723	5716	6049	2444	1.63	2.81	-10
"	"	5. Inner Side Plate/Inner Base Plate	-2.3	-119	0	99200	4510	8239	817	1.69	8.41	7.5
"	"	6. Closure Plate/Backing Bar/Inner Hood	-39.9	-108.6	0.5	84198	5398	5401	1024	1.72	6.7	5
"	"	7. Thin Vane Bank Plate/Hood Support/Inner Base Plate	24.1	-59.5	0	85191	5281	5315	1652	1.76	4.16	10
"	"	8. Side Plate/Top Plate	17.6	119	88	91215	992	7803	2036	1.79	3.37	2.5
"	"	9. Hood Support/Outer Cover Plate/Outer Hood(b)	-102.8	28.4	0	95267	4892	5223	2538	1.90	2.71	2.5
"	"	10. Outer Cover Plate/Outer Hood	102.8	-58.1	0	94498	1063	7280	1044	1.92	6.58	10
"	"	11. Hood Support/Middle Base Plate/Inner Backing Bar/Inner Hood(b)	39.9	-59.5	0	101435	4802	5147	1808	1.94	3.8	0
"	"	12. Hood Support/Outer Base Plate/Middle Backing Bar(b)	-71.3	0	0	95428	4516	4994	2593	2.06	2.65	0

Notes.

(a) Node numbers are retained for further reference.

(1-8) Appropriate stress reduction factor for the welds and modifications listed in Table 7 have been applied. The number refers to the particular location and corresponding stress reduction factor in Table 7.

(b) WF=1.4



Table 9b (cont.). Locations with minimum stress ratios for CLTP conditions with frequency shifts. Stress ratios at every node are recorded as the lowest stress ratio identified during the frequency shifts. Stress ratios are grouped according to stress type (maximum – SR-P; or alternating – SR-a) and location (away from a weld or at a weld). Locations are depicted in Figure 15.

0

Stress Ratio	Weld	Location	Location (in.)			node(a)	Stress Intensity (psi)			Stress Ratio		% Freq. Shift
			x	y	z		Pm	Pm+Pb	S <sub>alt</sub>	SR-P	SR-a	
SR-a	Yes	1. Side Plate/Brace(5)	79.7	85.2	75.8	89649	4022	5464	4413	2.31	1.56	-5
"	"	2. Hood Reinforcement/Middle Hood	-63.5	100.7	74.1	98275	414	4626	4229	3.01	1.62	10
"	"	3. Side Plate/Brace	79.7	85.2	31.2	89646	3460	4435	3947	2.69	1.74	5
"	"	4. Hood Support/Inner Hood(b)	-38.5	0	31	95636	1160	3228	3172	4.32	2.17	-10
"	"	5. Hood Support/Inner Hood(b)	-35	0	58.7	95650	1126	3277	3027	4.25	2.27	-10
"	"	6. Hood Support/Inner Hood(b)	-37.3	0	42.9	95642	1270	3023	3017	4.61	2.28	2.5
"	"	7. Side Plate/Brace(5)	79.7	85.2	53.5	89652	2656	3752	2924	3.50	2.35	-5
"	"	8. Hood Reinforcement/Middle Hood	71.3	95.3	3	90126	1090	3925	2918	3.55	2.35	10
"	"	9. Hood Reinforcement/Middle Hood	-66.1	98.9	60.5	98268	665	2992	2889	4.66	2.38	-7.5
"	"	10. Hood Reinforcement/Middle Hood	-69.6	-96.5	34.9	90949	1071	2776	2673	5.02	2.57	2.5
"	"	11. Hood Support/Outer Base Plate/Middle Backing Bar(b)	-71.3	0	0	95428	4516	4994	2593	2.06	2.65	5
"	"	12. Submerged Drain Channel/Submerged Skirt	-91	76.7	-101.5	93430	820	6224	2591	2.24	2.65	5
"	"	13. Hood Support/Middle Hood(b)	-68.7	0	42.9	96022	905	2750	2562	5.07	2.68	-5
"	"	14. Hood Support/Outer Cover Plate/Outer Hood(b)	-102.8	28.4	0	95267	4892	5223	2538	1.90	2.71	-10
"	"	15. Submerged Drain Channel/Submerged Skirt	11.5	-118.4	-101.5	84597	1167	4640	2527	3.00	2.72	2.5

Notes

- (a) Node numbers are retained for further reference.
- (1-8) Appropriate stress reduction factor for the welds and modifications listed in Table 7 have been applied. The number refers to the particular location and corresponding stress reduction factor in Table 7.
- (b) WF=1.4

Table 9b (cont.). Locations with minimum stress ratios for CLTP conditions with frequency shifts. Stress ratios at every node are recorded as the lowest stress ratio identified during the frequency shifts. Stress ratios are grouped according to stress type (maximum – SR-P; or alternating – SR-a) and location (away from a weld or at a weld). Locations are depicted in Figure 15.

Stress Ratio	Weld	Location	Location (in.)			node(a)	Stress Intensity (psi)			Stress Ratio		% Freq. Shift
			x	y	z		Pm	Pm+Pb	S <sub>alt</sub>	SR-P	SR-a	
SR-a	Yes	16. Closure Plate/Middle Hood	-62.5	85.2	78.3	91608	745	2773	2473	5.03	2.78	10
"	"	17. Outer Cover Plate/Outer Hood	-102.8	-1	0	95236	1339	2766	2454	5.04	2.80	5
"	"	18. Hood Support/Middle Base Plate/Inner Backing Bar/Inner Hood <sup>(b)</sup>	-39.9	0	0	85723	5716	6049	2444	1.63	2.81	-10
"	"	19. Thick Vane Bank Plate/Thin Vane Bank Plate/Side Plate/End Plate	24.1	-119	11.6	90582	842	2713	2441	5.14	2.81	-5
"	"	20. Closure Plate/Middle Hood <sup>(3)</sup>	60.2	-85.2	87	89317	1160	4740	2397	2.94	2.87	2.5
"	"	21. Inner Backing Bar/Inner Hood	39.9	-29.8	1	92414	537	2501	2345	5.57	2.93	-7.5
"	"	22. Hood Reinforcement/Middle Hood	60.9	103	85.1	90129	356	2617	2290	5.33	3.00	10

Notes

- (a) Node numbers are retained for further reference.
- (1-8) Appropriate stress reduction factor for the welds and modifications listed in Table 7 have been applied. The number refers to the particular location and corresponding stress reduction factor in Table 7.
- (b) WF=1.4

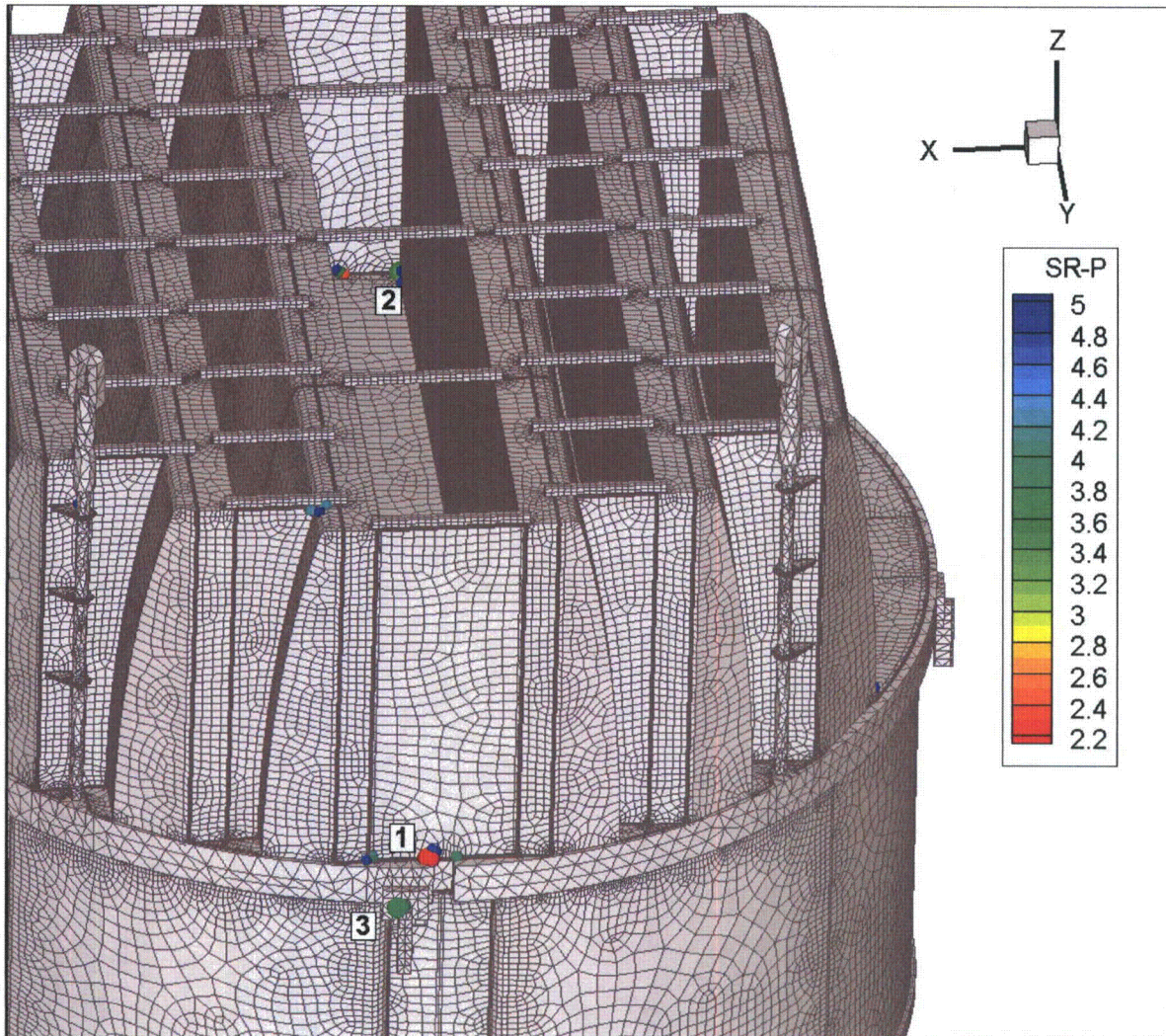


Figure 14a. Locations of nodes with stress ratios,  $SR-P \leq 5$ , associated with a maximum stress at non-welds for nominal CLTP operation. Numbers refers to the enumerated locations for SR-P values at non-welds in Table 9a.



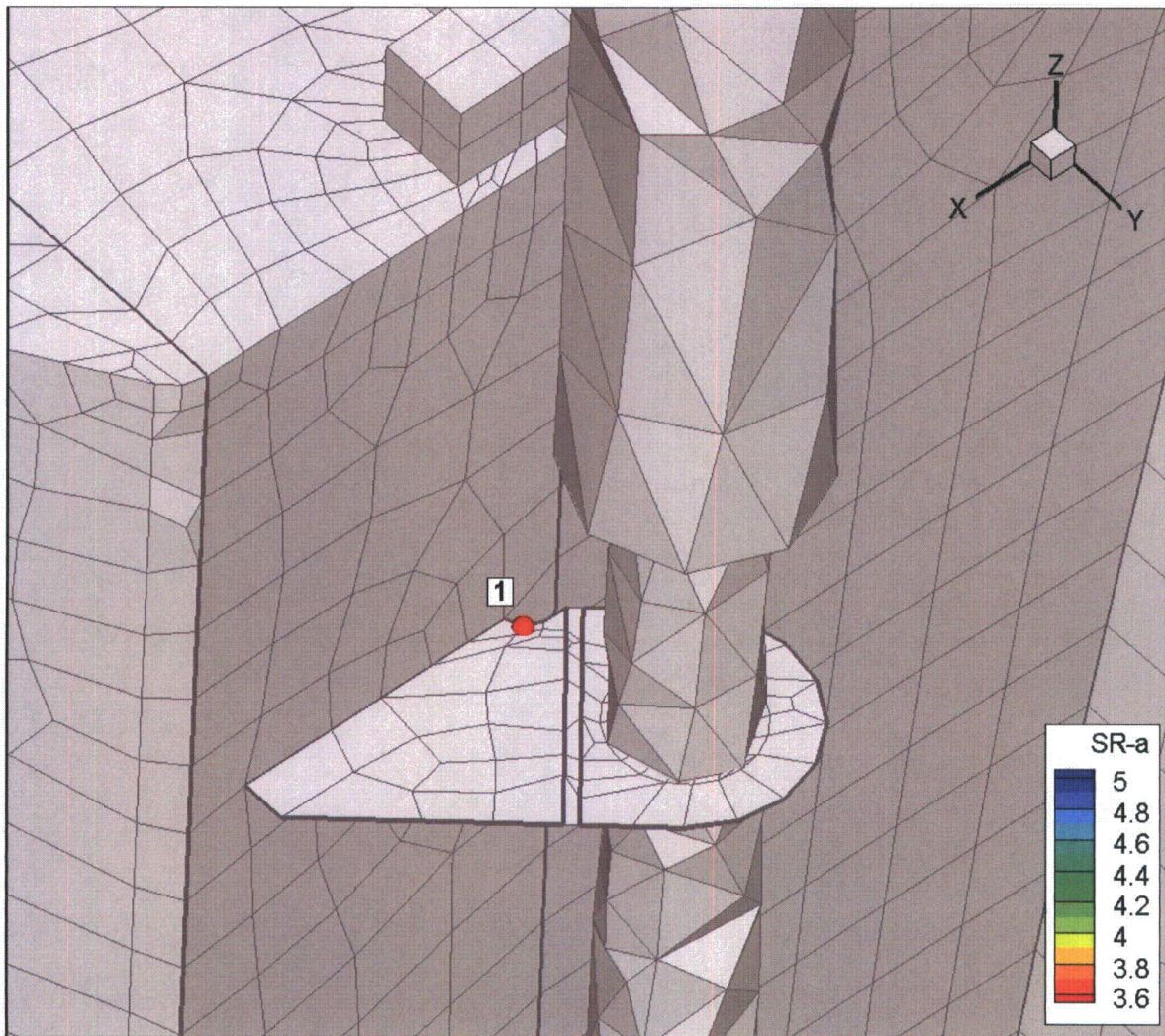


Figure 14b. Locations of smallest alternating stress ratios,  $SR-a \leq 5$ , at non-welds for nominal CLTP operation. Numbers refer to the enumerated locations for SR-a values at non-welds in Table 9a. View showing location 1 on lifting rod brace.



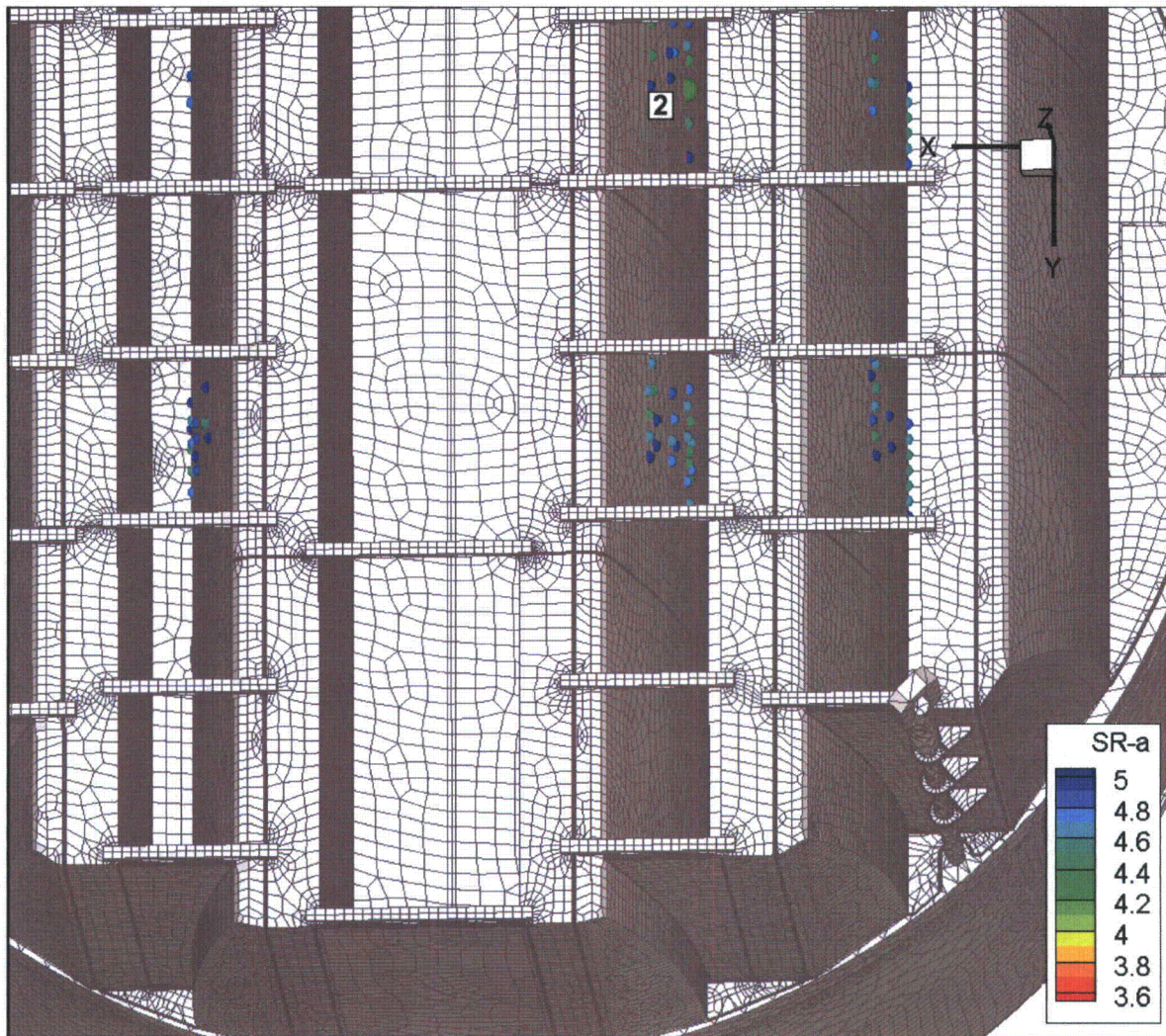


Figure 14c. Locations of smallest alternating stress ratios,  $SR-a \leq 5$ , at non-welds for nominal CLTP operation. Numbers refer to the enumerated locations for  $SR-a$  values at non-welds in Table 9a. View showing location 2.



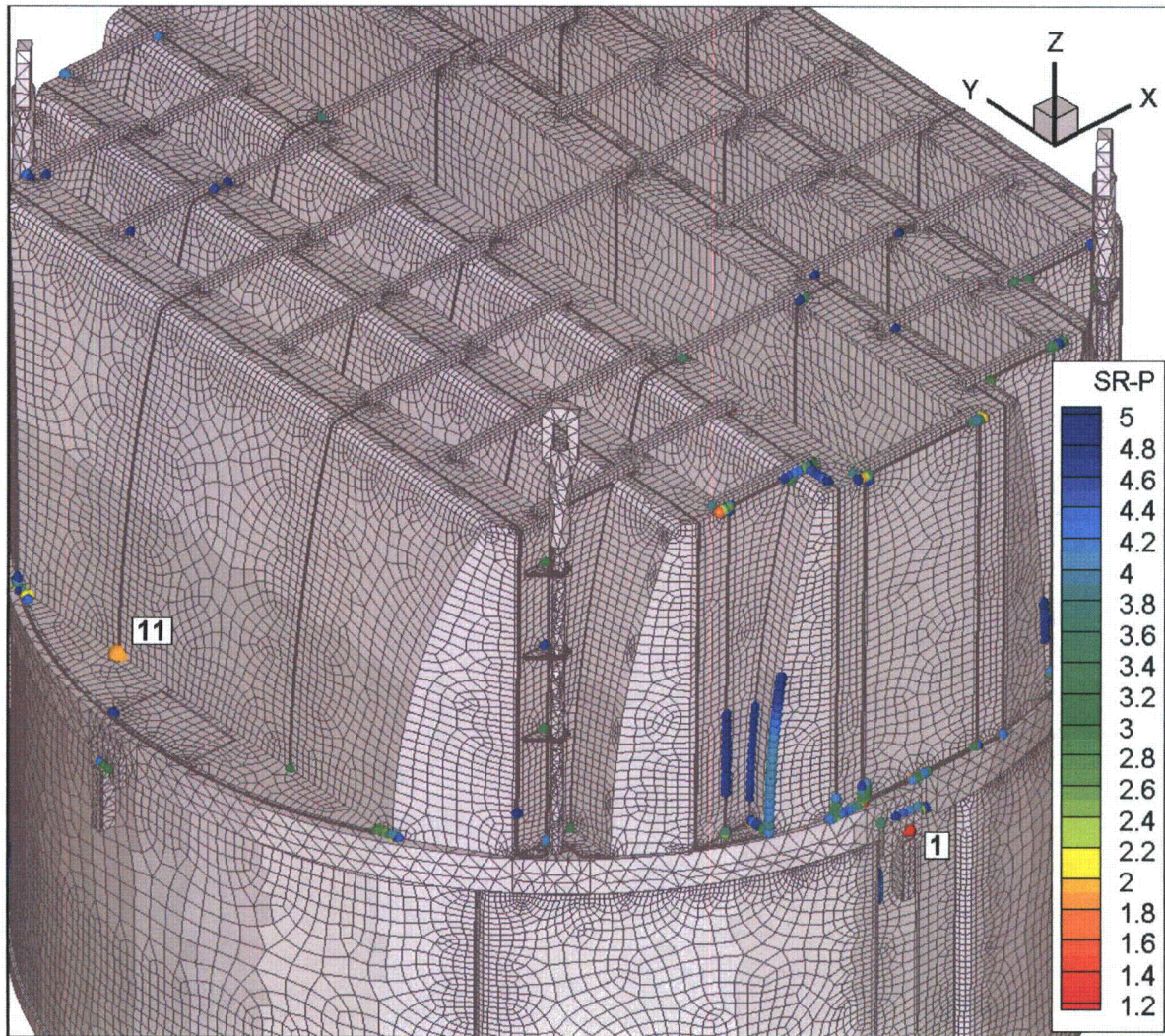


Figure 14d. Locations of smallest stress ratios,  $SR-P \leq 5$ , associated with maximum stresses at welds for nominal CLTP operation. Numbers refer to the enumerated locations for SR-P values at welds in Table 9a. This view shows locations 1 and 11.



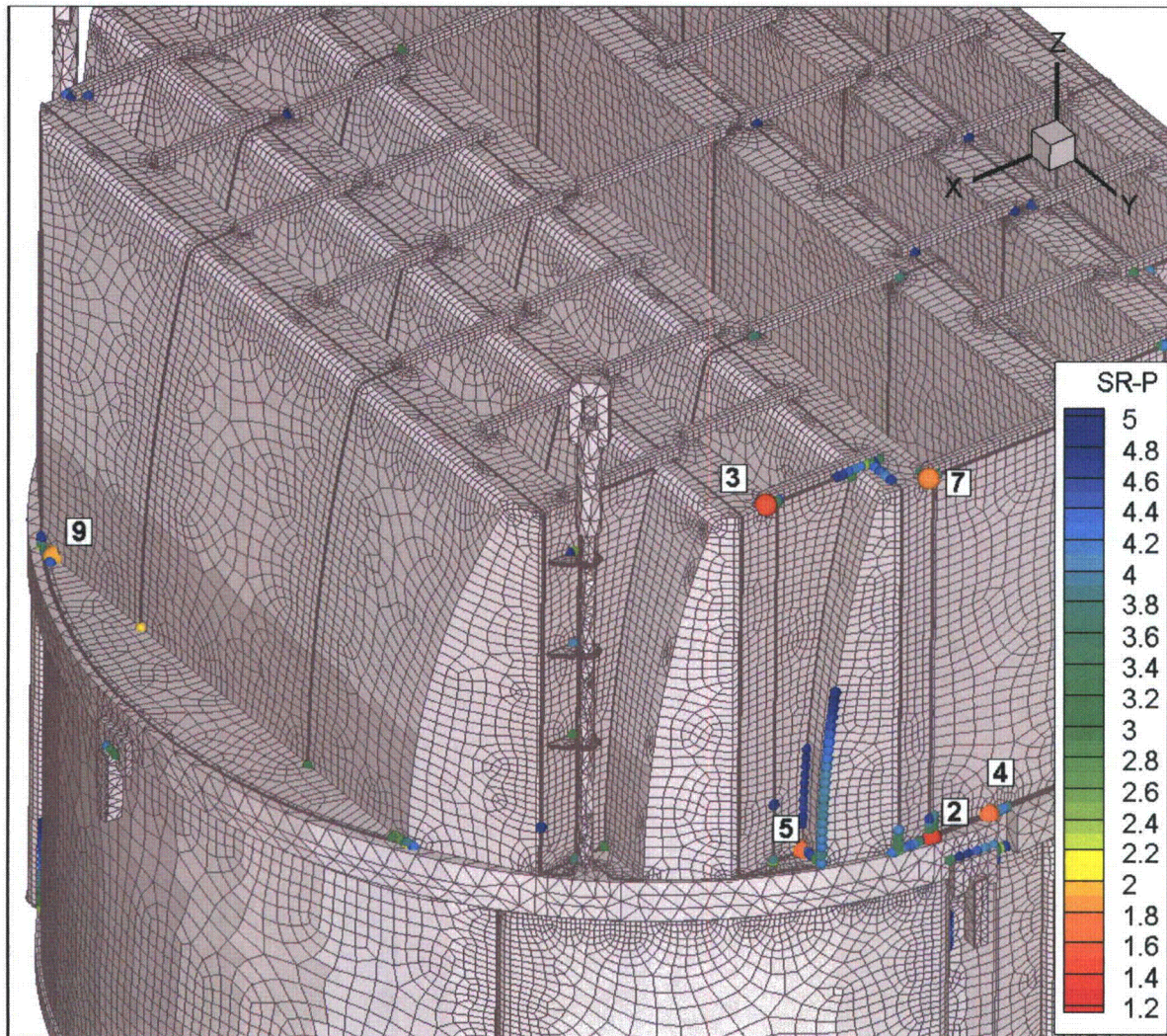


Figure 14e. Locations of minimum stress ratios,  $SR-P \leq 5$ , associated with maximum stresses at welds for nominal CLTP operation. Numbers refer to the enumerated locations for SR-P values at welds in Table 9a. This view shows locations 2-5, 7 and 9.



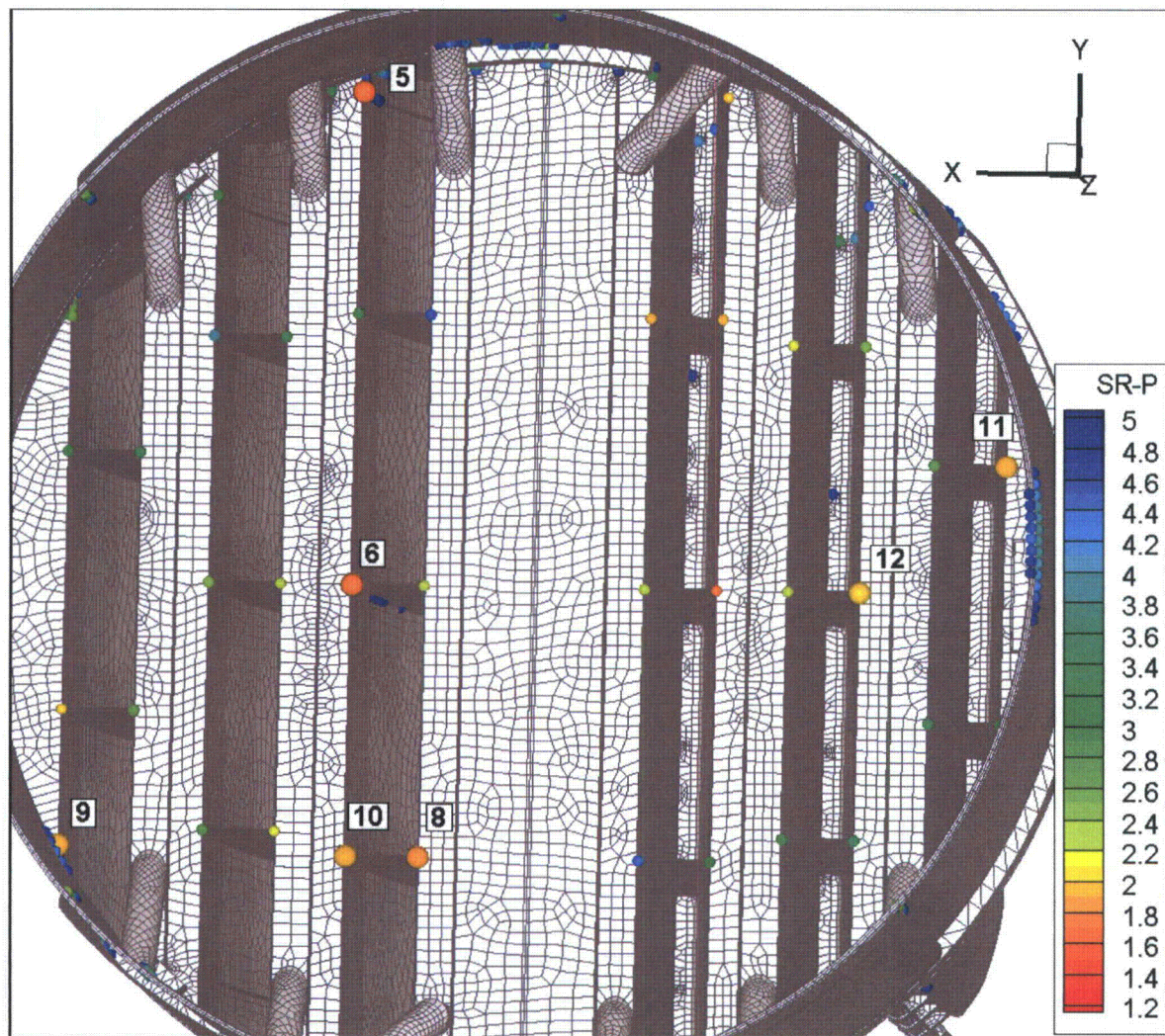


Figure 14f. Locations of minimum stress ratios,  $SR-P \leq 5$ , associated with maximum stresses at welds for nominal CLTP operation. Numbers refer to the enumerated locations for SR-P values at welds in Table 9a. This view shows locations 5, 6 and 8-12



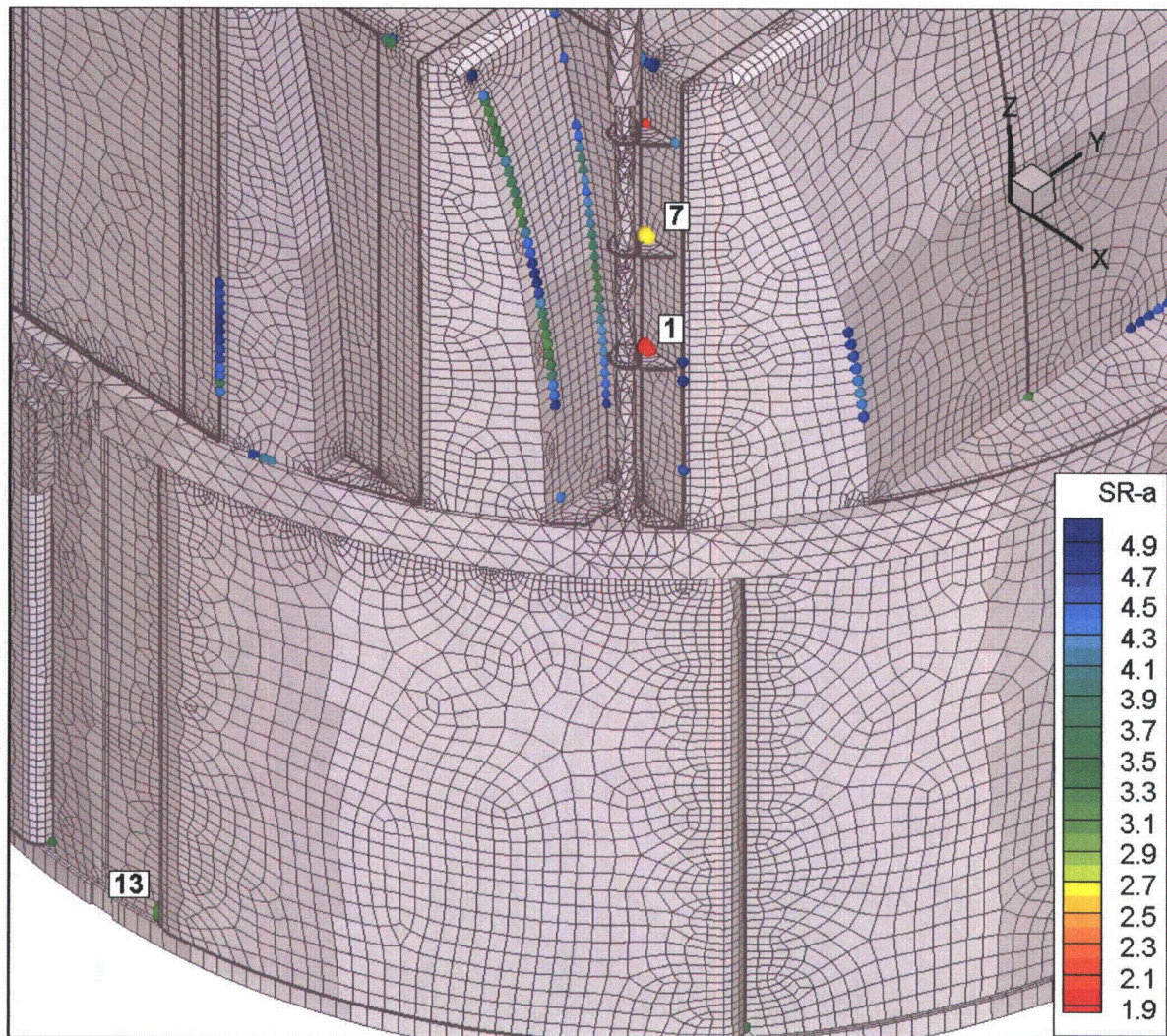


Figure 14g. Locations of minimum alternating stress ratios,  $SR-a \leq 5$ , at welds for nominal CLTP operation. Numbers refer to the enumerated locations for  $SR-a$  values at welds in Table 9a. Locations 1, 7 and 13 are shown.



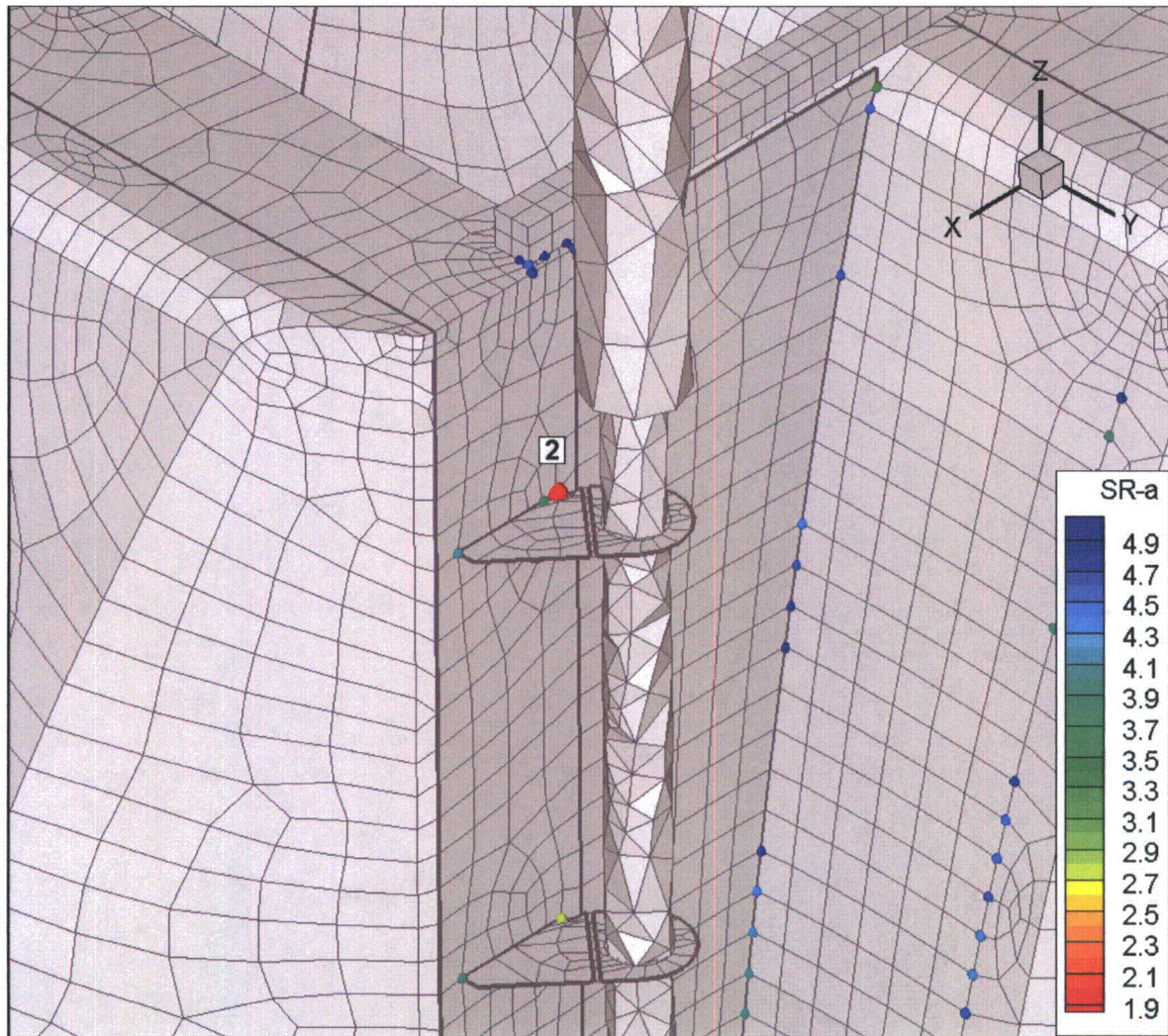


Figure 14h. Locations of minimum alternating stress ratios,  $SR-a \leq 5$ , at welds for nominal CLTP operation. Numbers refer to the enumerated locations for  $SR-a$  values at welds in Table 9a. Location 2 on the lifting rod brace is shown.



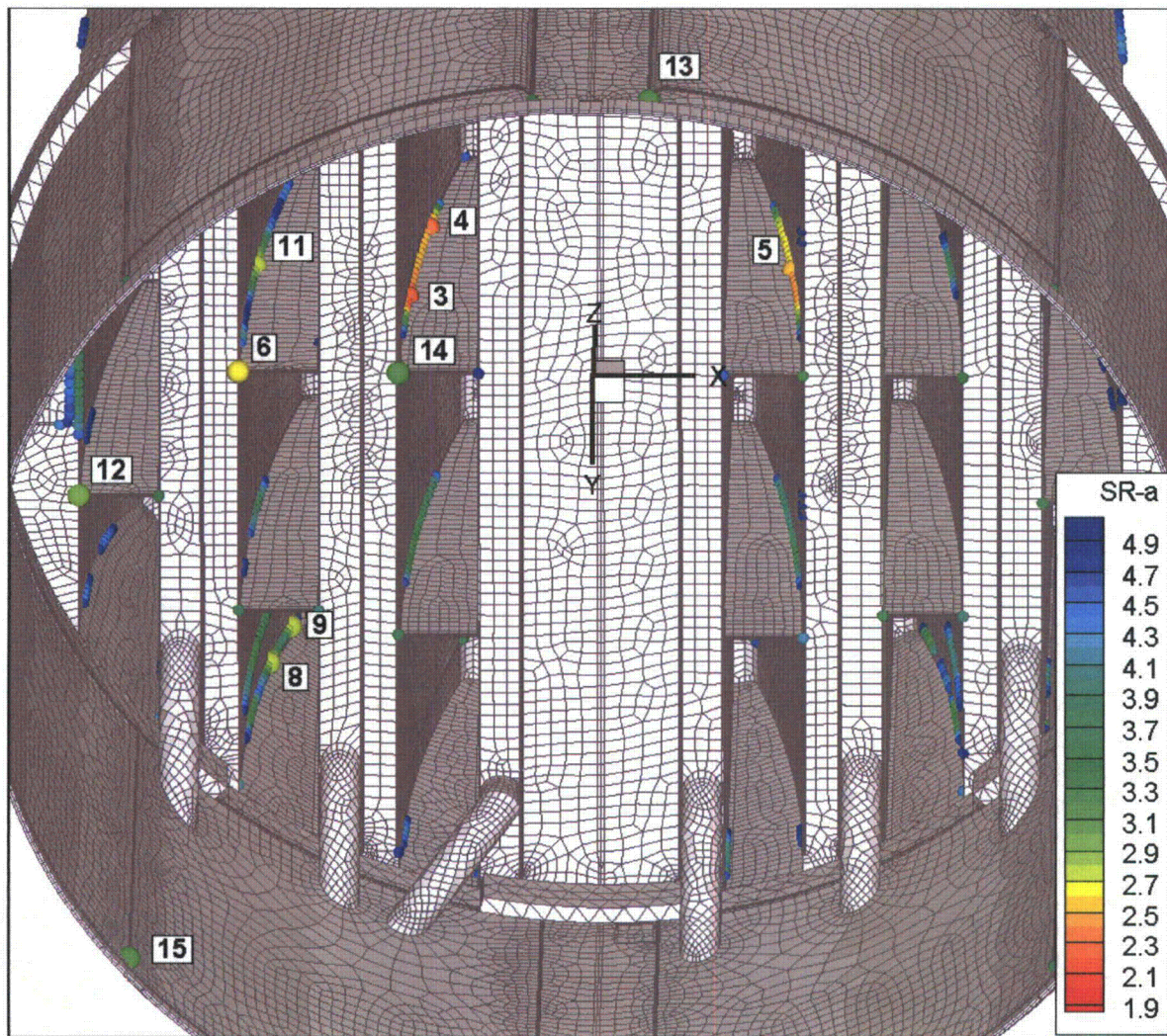


Figure 14i. Locations of minimum alternating stress ratios,  $SR-a \leq 5$ , at welds for nominal CLTP operation. Numbers refer to the enumerated locations for SR-a values at welds in Table 9a. View from below showing locations 3-6, 8, 9 and 11-15.



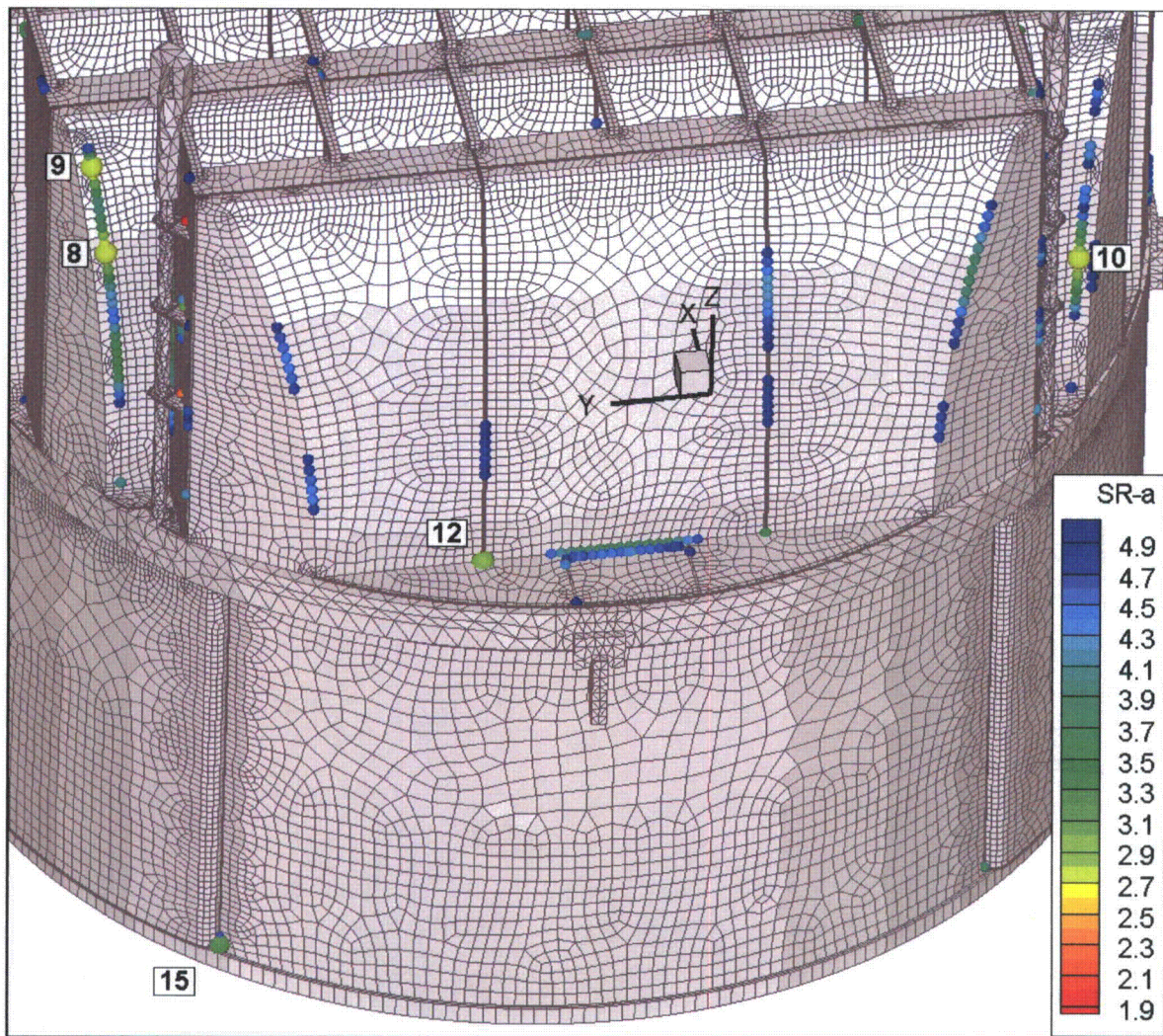


Figure 14j. Locations of minimum alternating stress ratios,  $SR-a \leq 5$ , at welds for nominal CLTP operation. Numbers refer to the enumerated locations for  $SR-a$  values at welds in Table 9a. Locations 8-10, 12 and 15 are shown.



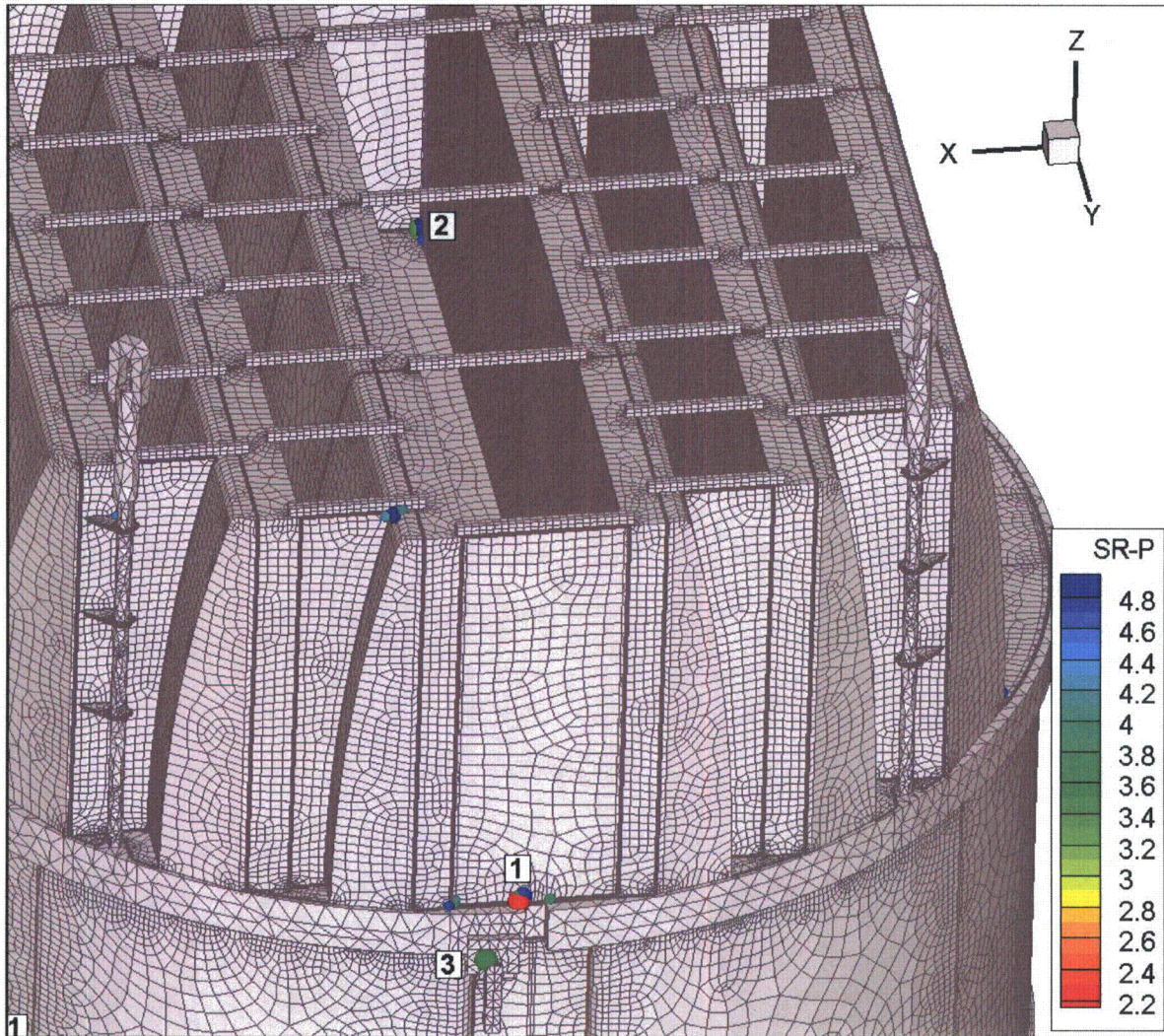


Figure 15a. Locations of minimum stress ratios,  $SR-P \leq 5$ , associated with maximum stresses at non-welds for CLTP operation with frequency shifts. The recorded stress ratio is the minimum value taken over all frequency shifts. The numbers refers to the enumerated location for SR-P values at non-welds in Table 9b.



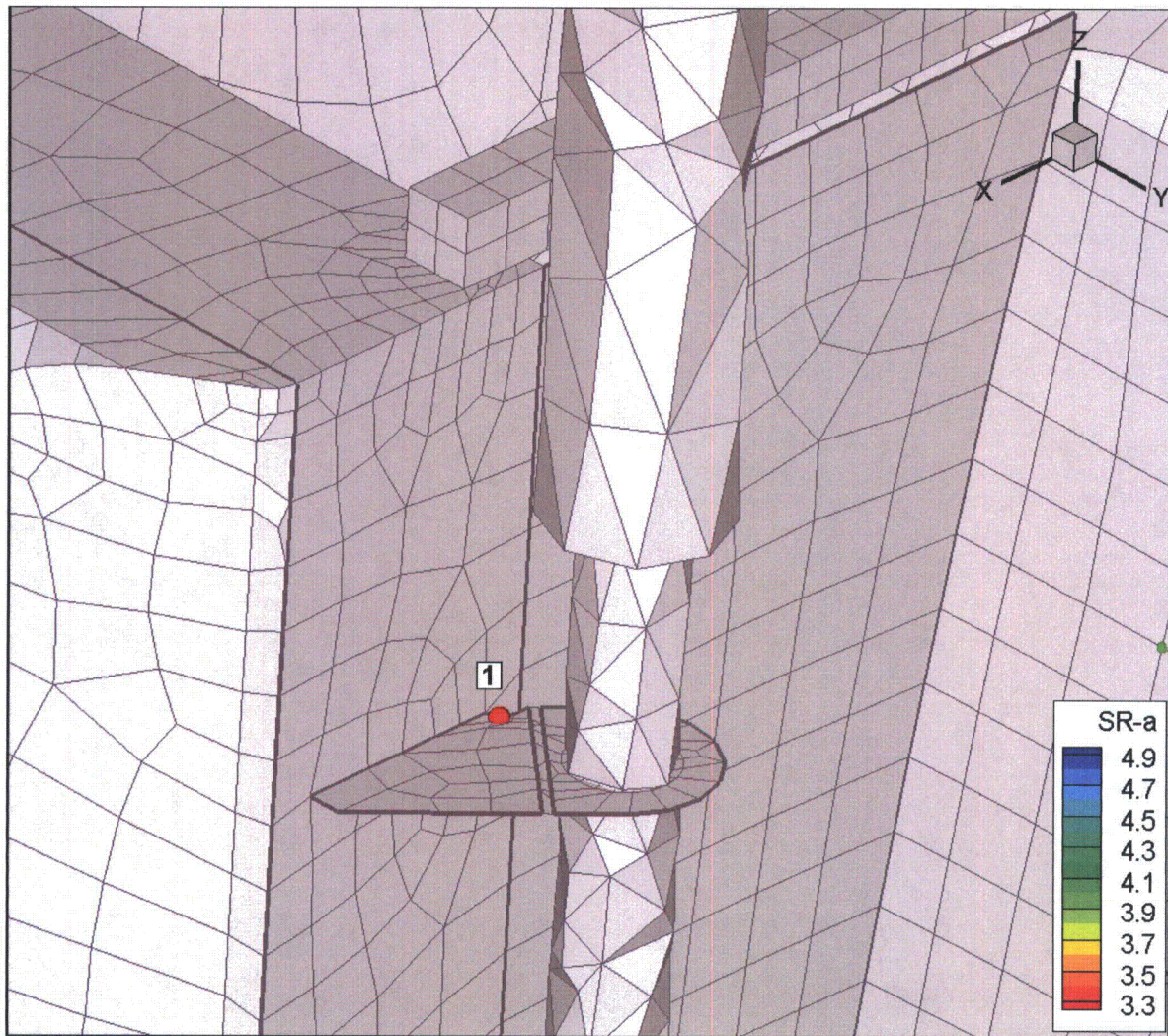


Figure 15b. Locations of minimum alternating stress ratios,  $SR-a \leq 5$ , at non-welds for CLTP operation with frequency shifts. The recorded stress ratio at a node is the minimum value taken over all frequency shifts. Numbers refer to the enumerated locations for  $SR-a$  values at non-welds in Table 9b. View showing location 1.



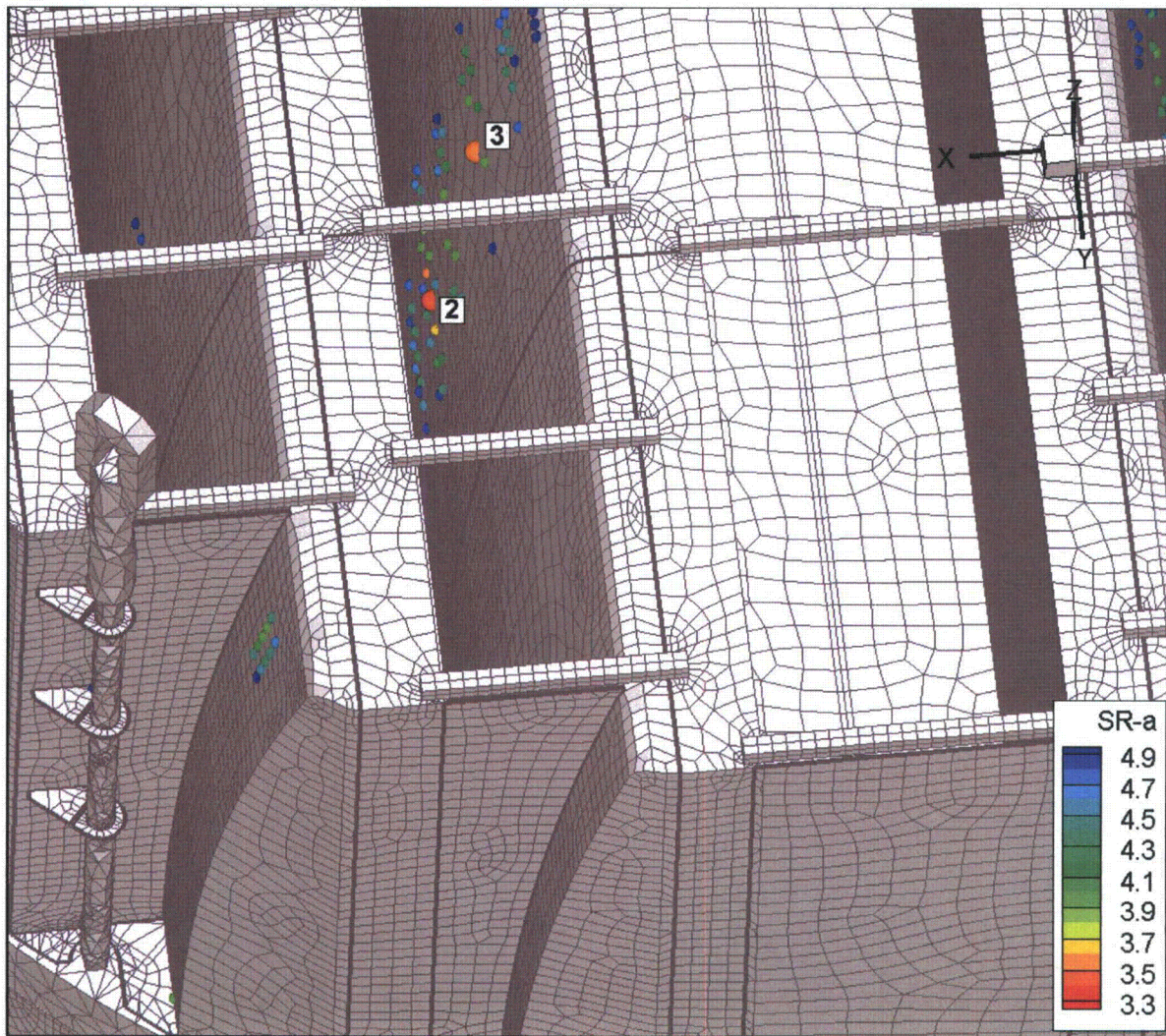


Figure 15c. Locations of minimum alternating stress ratios,  $SR-a \leq 5$ , at non-welds for CLTP operation with frequency shifts. The recorded stress ratio at a node is the minimum value taken over all frequency shifts. Numbers refer to the enumerated locations for  $SR-a$  values at non-welds in Table 9b. View showing locations 2 and 3.



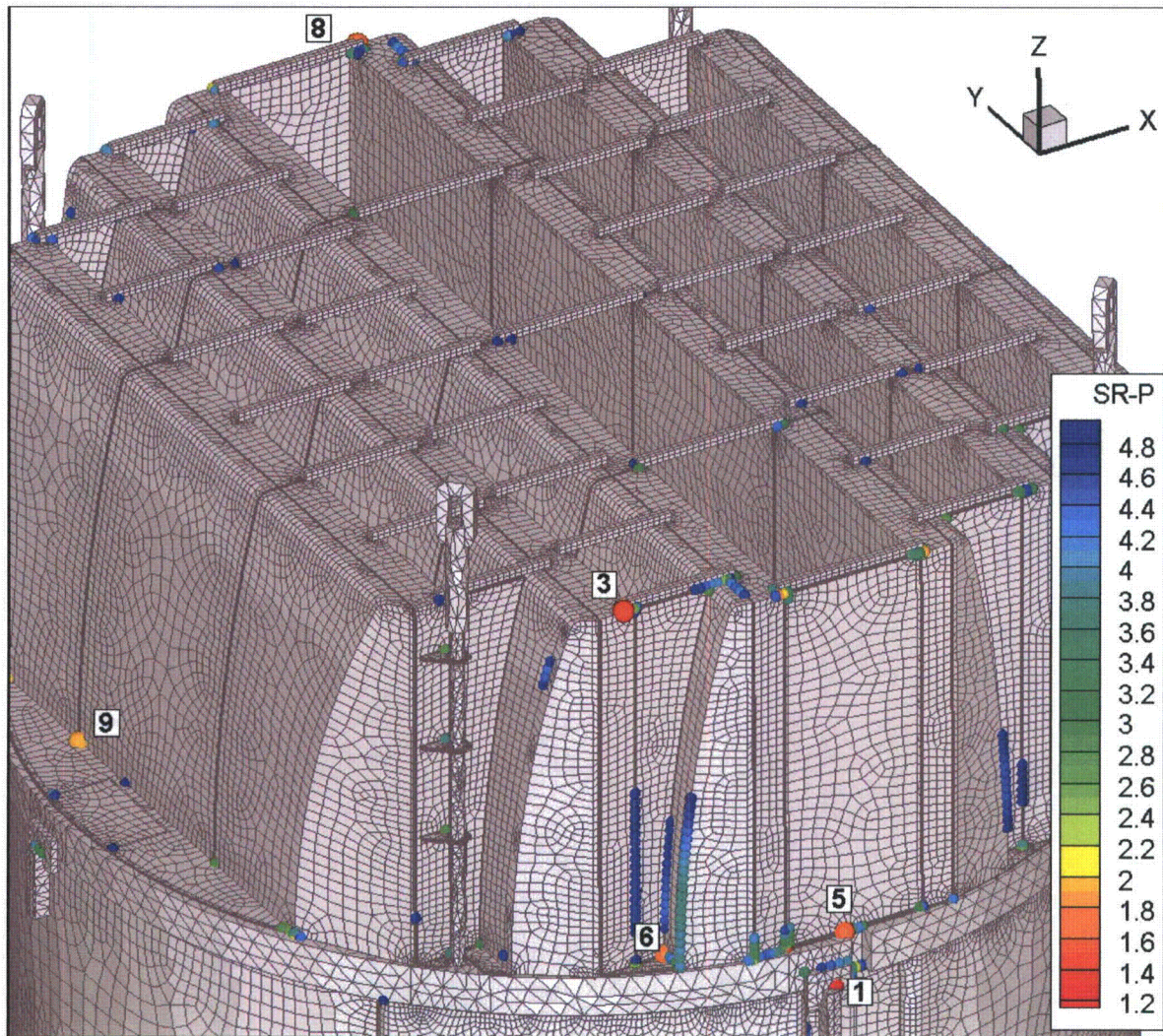


Figure 15d. Locations of minimum stress ratios,  $SR-P \leq 5$ , associated with maximum stresses at welds for CLTP operation with frequency shifts. The recorded stress ratio at a node is the minimum value taken over all frequency shifts. Numbers refer to the enumerated locations for SR-P values at welds in Table 9b. This view shows locations 1, 3, 5, 6, 8 and 9.



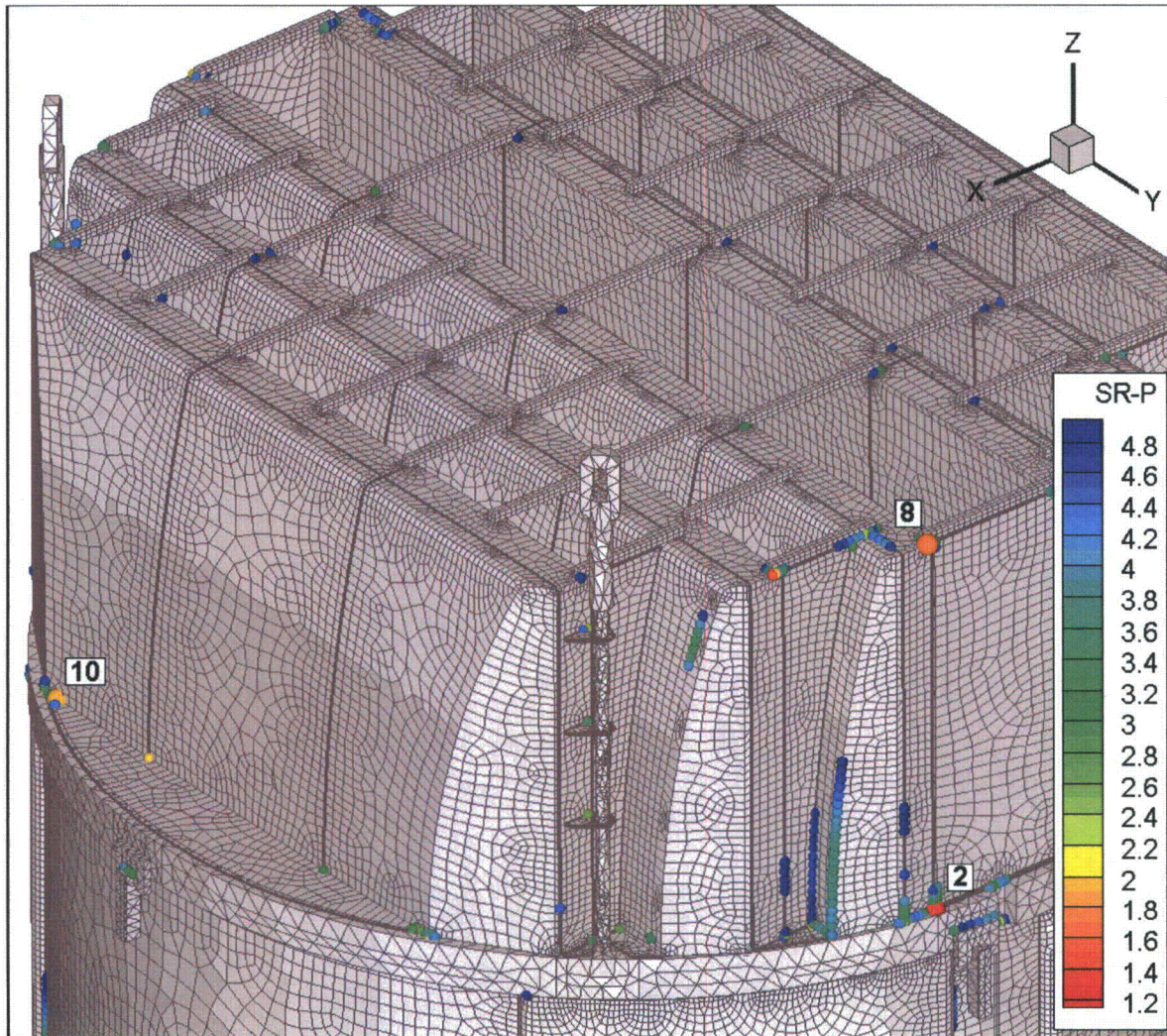


Figure 15e. Locations of minimum stress ratios,  $SR-P \leq 5$ , associated with maximum stresses at welds for CLTP operation with frequency shifts. The recorded stress ratio at a node is the minimum value taken over all frequency shifts. Numbers refer to the enumerated locations for SR-P values at welds in Table 9b. This view shows locations 2, 8 and 10.



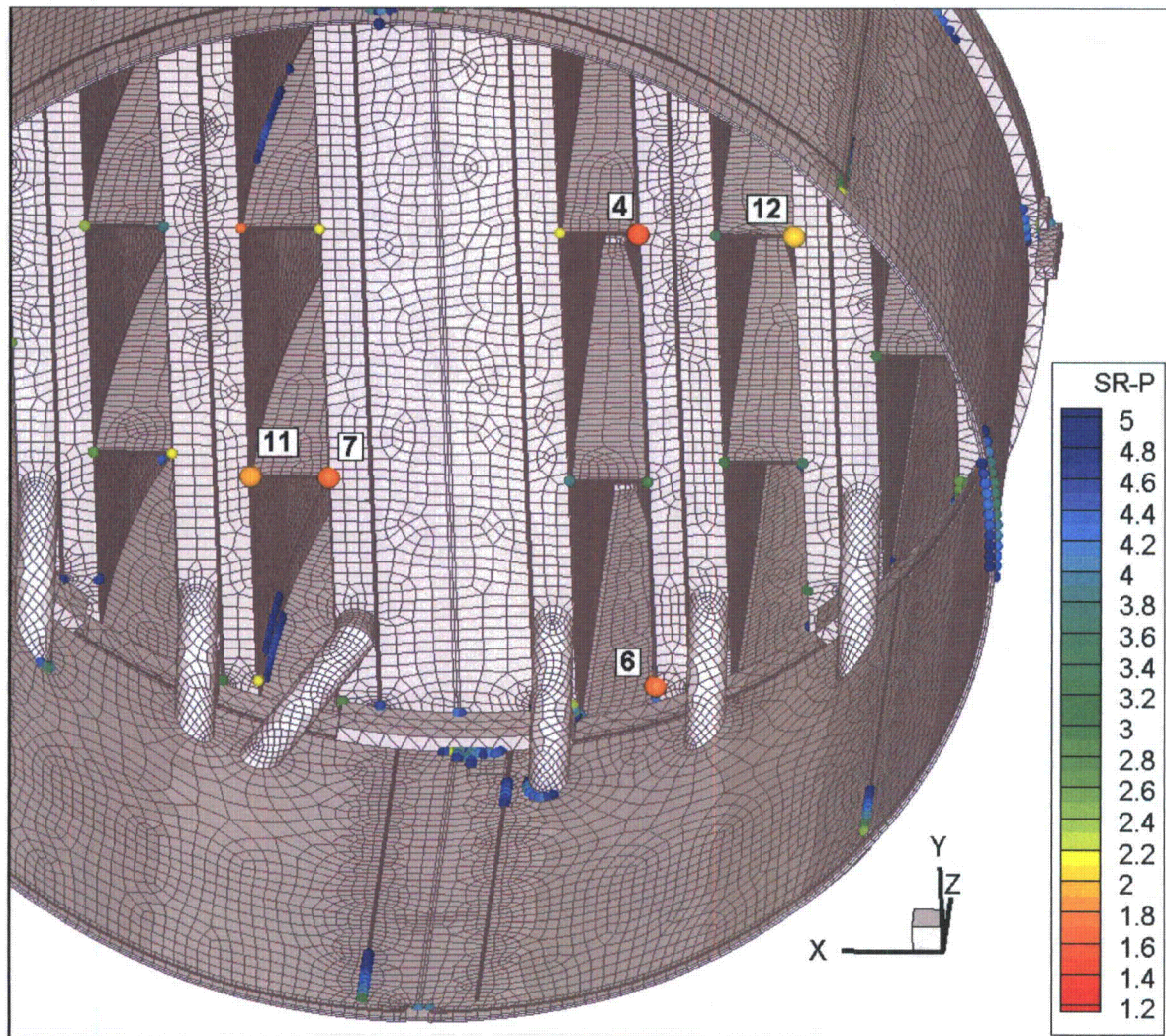


Figure 15f. Locations of minimum stress ratios,  $SR-P \leq 5$ , at welds for CLTP operation with frequency shifts. The recorded stress ratio at a node is the minimum value taken over all frequency shifts. Numbers refer to the enumerated locations for SR-P values at welds in Table 9b. This view from below shows locations 4, 6, 7, 11 and 12.



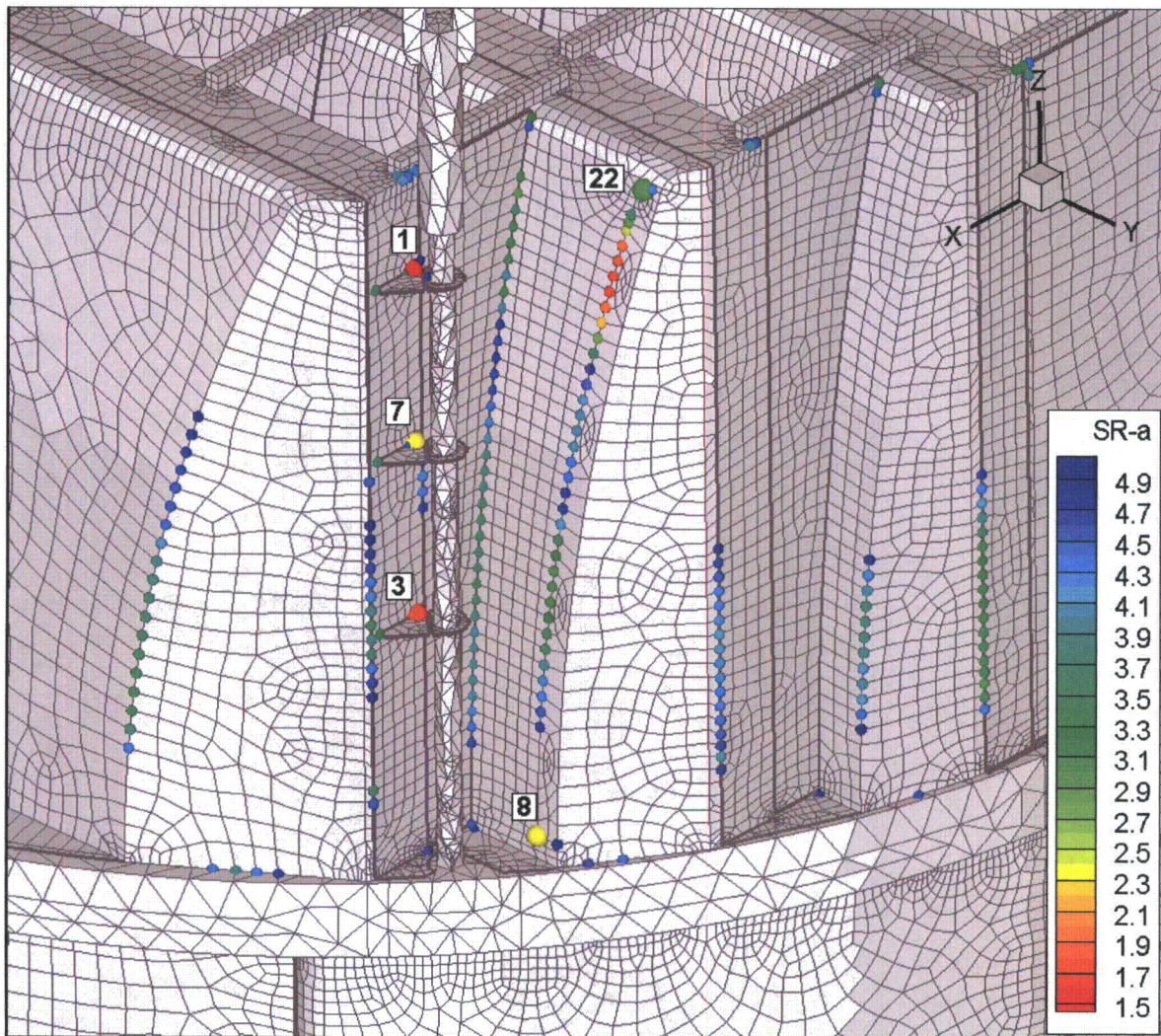


Figure 15g. Locations of minimum alternating stress ratios,  $SR-a \leq 5$ , at welds for CLTP operation with frequency shifts. The recorded stress ratio at a node is the minimum value taken over all frequency shifts. Numbers refer to the enumerated locations for SR-a values at welds in Table 9b. This view shows locations 1, 3, 7, 8 and 22.



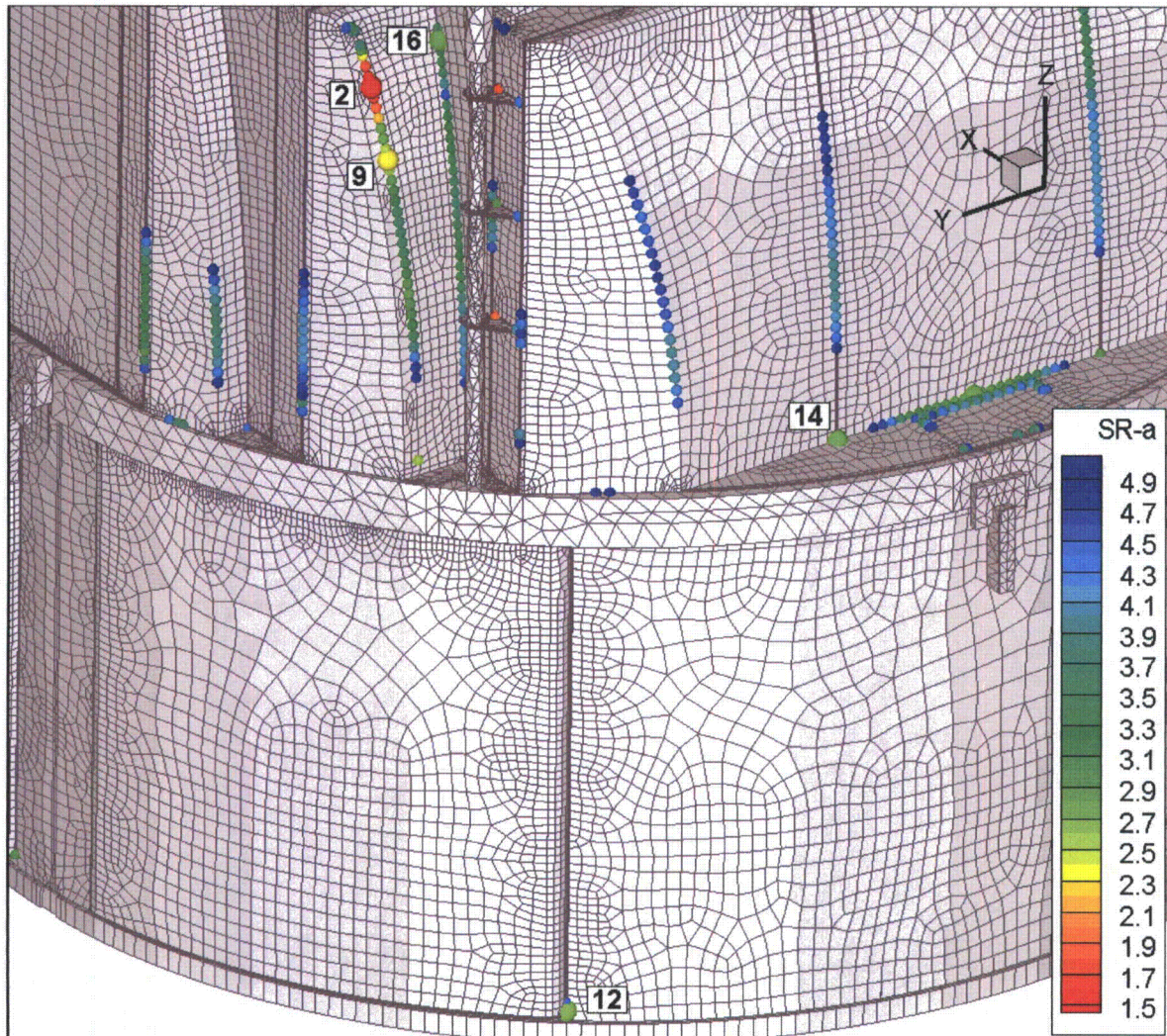


Figure 15h. Locations of minimum alternating stress ratios,  $SR-a \leq 5$ , at welds for CLTP operation with frequency shifts. The recorded stress ratio at a node is the minimum value taken over all frequency shifts. Numbers refer to the enumerated locations for  $SR-a$  values at welds in Table 9b. View showing locations 2, 9, 12, 14 and 16.



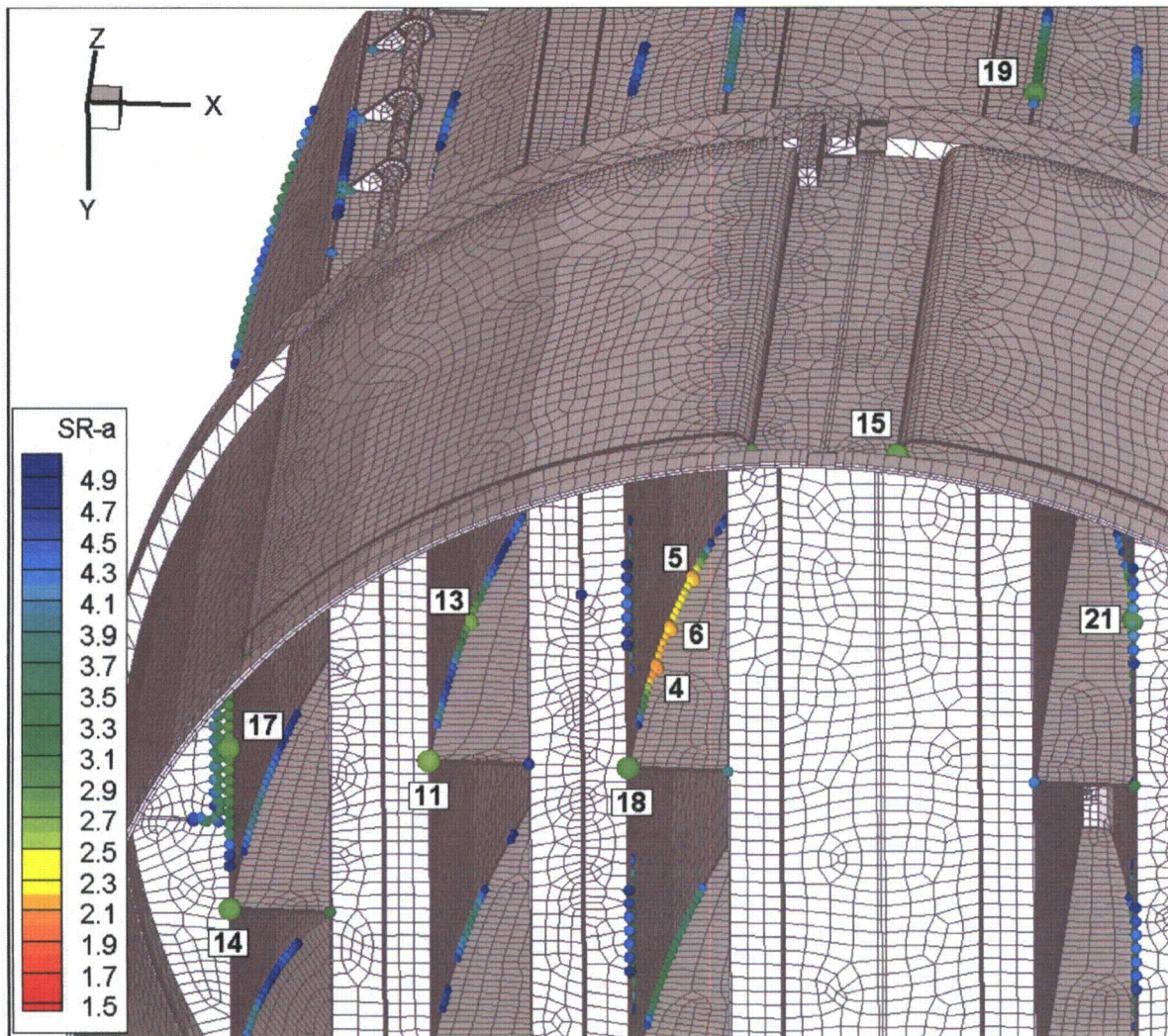


Figure 15i. Locations of minimum alternating stress ratios,  $SR-a \leq 5$ , at welds for CLTP operation with frequency shifts. The recorded stress ratio at a node is the minimum value taken over all frequency shifts. Numbers refer to the enumerated locations for  $SR-a$  values at welds in Table 9b. View around locations 4-6, 11, 13-15, 17-19, 21 and 22.



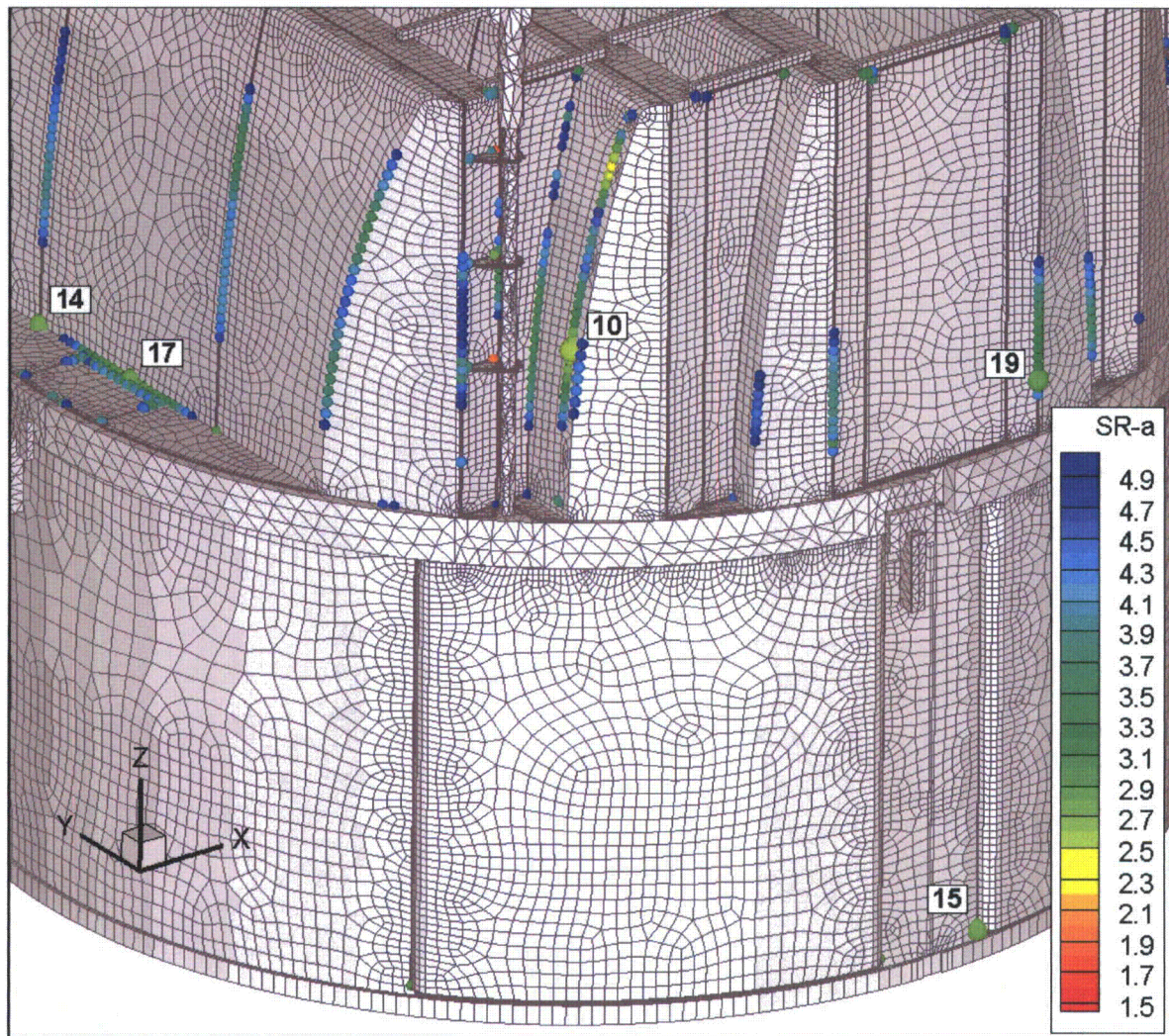


Figure 15j. Locations of minimum alternating stress ratios,  $SR-a \leq 5$ , at welds for CLTP operation with frequency shifts. The recorded stress ratio at a node is the minimum value taken over all frequency shifts. Numbers refer to the enumerated locations for  $SR-a$  values at welds in Table 9b. View around locations 10, 14, 15 17 and 19.



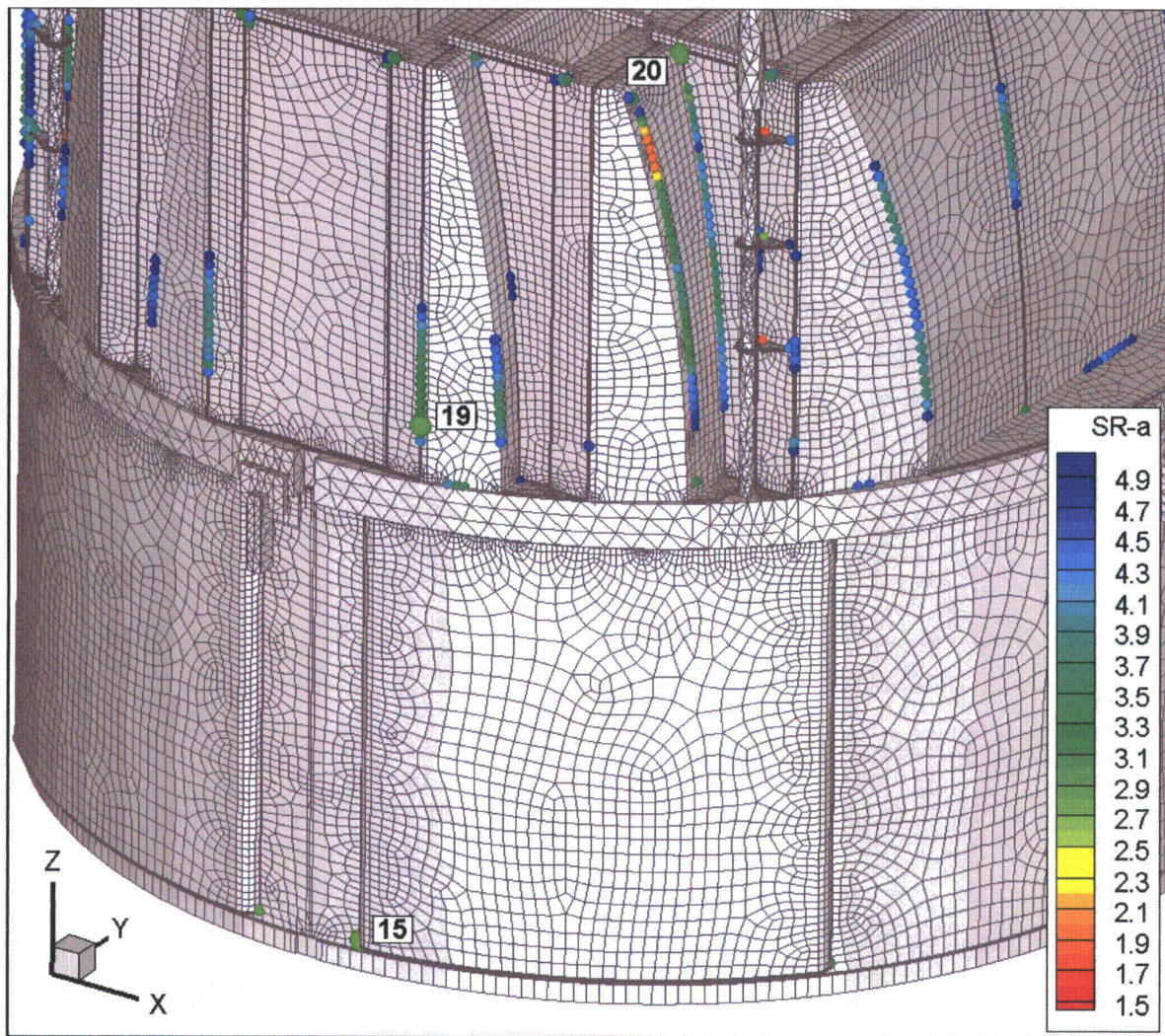


Figure 15k. Locations of minimum alternating stress ratios,  $SR-a \leq 5$ , at welds for CLTP operation with frequency shifts. The recorded stress ratio at a node is the minimum value taken over all frequency shifts. Numbers refer to the enumerated locations for SR-a values at welds in Table 9b. View around locations 15, 19 and 20.



### 5.3 Frequency Content and Filtering of the Stress Signals

The frequency contribution to the stresses can be investigated by examining the power spectral density (PSD) curves and accumulative PSDs for selected nodes having low alternating stress ratios. The accumulative PSDs are computed directly from the Fourier coefficients as

$$\Sigma(\omega_n) = \sqrt{\sum_{k=1}^n |\tilde{\sigma}(\omega_k)|^2}$$

where  $\tilde{\sigma}(\omega_k)$  is the complex stress harmonic at frequency,  $\omega_k$ . Accumulative PSD plots are useful for determining the frequency components and frequency ranges that make the largest contributions to the fluctuating stress. Unlike PSD plots, no “binning” or smoothing of frequency components is needed to obtain smooth curves. Steep step-like rises in  $\Sigma(\omega)$  indicate the presence of a strong component at a discrete frequency whereas gradual increases in the curve imply significant content over a broader frequency range. From Parseval’s theorem, equality between  $\Sigma(\omega_N)$  (where N is the total number of frequency components) and the RMS of the stress signal in the time domain is established.

The selected nodes are the ones having the lowest alternating stress ratios (at a weld) in Table 9b. These are:

- Node 89649 – located on the lifting rod brace/vane bank end plate connection. The associated PSDs are shown in Figure 16a.
- Node 98275 - located on the middle hood reinforcement strip. The associated PSDs are shown in Figure 16b.
- Node 95636 – located on the weld joining the inner hood and hood support. The associated PSDs are shown in Figure 16c.
- Node 95428 – located at the bottom of the weld joining the submerged drain channel and skirt. The associated PSDs are shown in Figure 16d.
- Node 95267 – located on the welded common junction between the outer hood, hood support and outer cover plate. The associated PSDs are shown in Figure 16e.

These are the nodes labeled 1, 2, 4, 12 and 14 in Table 9b for alternating stresses on a weld and accompanying Figure 15g-k.

In each case, since there are six stress components and up to three different section locations for shells (the top, mid and bottom surfaces), there is a total of 18 stress histories per component. Moreover, at junctions there are at least two components that meet at the junction. The particular stress component that is plotted is chosen as follows. First, the component and section location (top/mid/bottom) is taken as the one that has the highest alternating stress. This narrows the selection to six components. Of these, the component having the highest Root Mean Square (RMS) is selected.

The first node (89649), is dominated by two broad peaks centered at near 139 Hz and 98 Hz for the -5% shifted case. From the accumulative PSD it is evident that frequency shifting

attenuates the 98 Hz peak slightly, but this reduction is dominated by a larger increase about the 139 Hz peak. Frequency shifting has a more pronounced effect on node 98275 which has dominant frequencies at 119.5 Hz and 134.5 Hz. The former peak grows substantially with the frequency shift whereas the second one attenuates. Despite the +10% shift the locations of the peaks (i.e., the peak frequencies) do not change significantly. This is characteristic of a broad spectrum signal forcing a particular mode. The third node is dominated by a 45.7 Hz peak. This peak is identified with a vibration mode of the inner hoods. It is interesting to note that the shifted response yielding the limiting alternating stress ratio actually produces an RMS value for this stress component that is lower than that without the shift (note that the RMS is obtained from the maximum value of the accumulative PSD curve). This occasionally happens when the time response has one or a small number of isolated peaks that contribute directly to the alternating stress intensity (which is the maximizing peak to peak stress fluctuation), but makes a negligible contribution to the RMS. A similar, though less pronounced, behavior is observed in the fourth location (node 95428) on the submerged drain channel/skirt weld which contains the same peak together with a larger one at 54.2 Hz. Finally for node 95267, the dominant stress contribution occurs at 54.6 Hz.

Another way to characterize the dominant frequencies is to plot the dominant frequency over the dryer surface. For each finite element node the frequency associated with the largest stress harmonic (at any frequency shift) is recorded. A contour map of this dominant frequency is shown in Figure 17. This map is useful in a qualitative sense for identifying what dryer components appear most responsive to particular frequencies. For most of the dryer, including the central section of the outer hoods, the middle and inner hoods, and most of the skirt the dominant frequencies are in the 50-55 Hz range as indicated in Figure 17a. From Figure 17b the outer sections of the outer hoods show peak frequencies near 70-80 Hz. The section of the middle hood outboard of the closure plate where high stresses are observed, reflects dominant frequencies in the 110-120 Hz (Figure 17b) and 160-180 Hz frequency ranges (Figure 17c). The highest frequency responses occur on the closure plates connecting the outer vane banks and middle hoods.

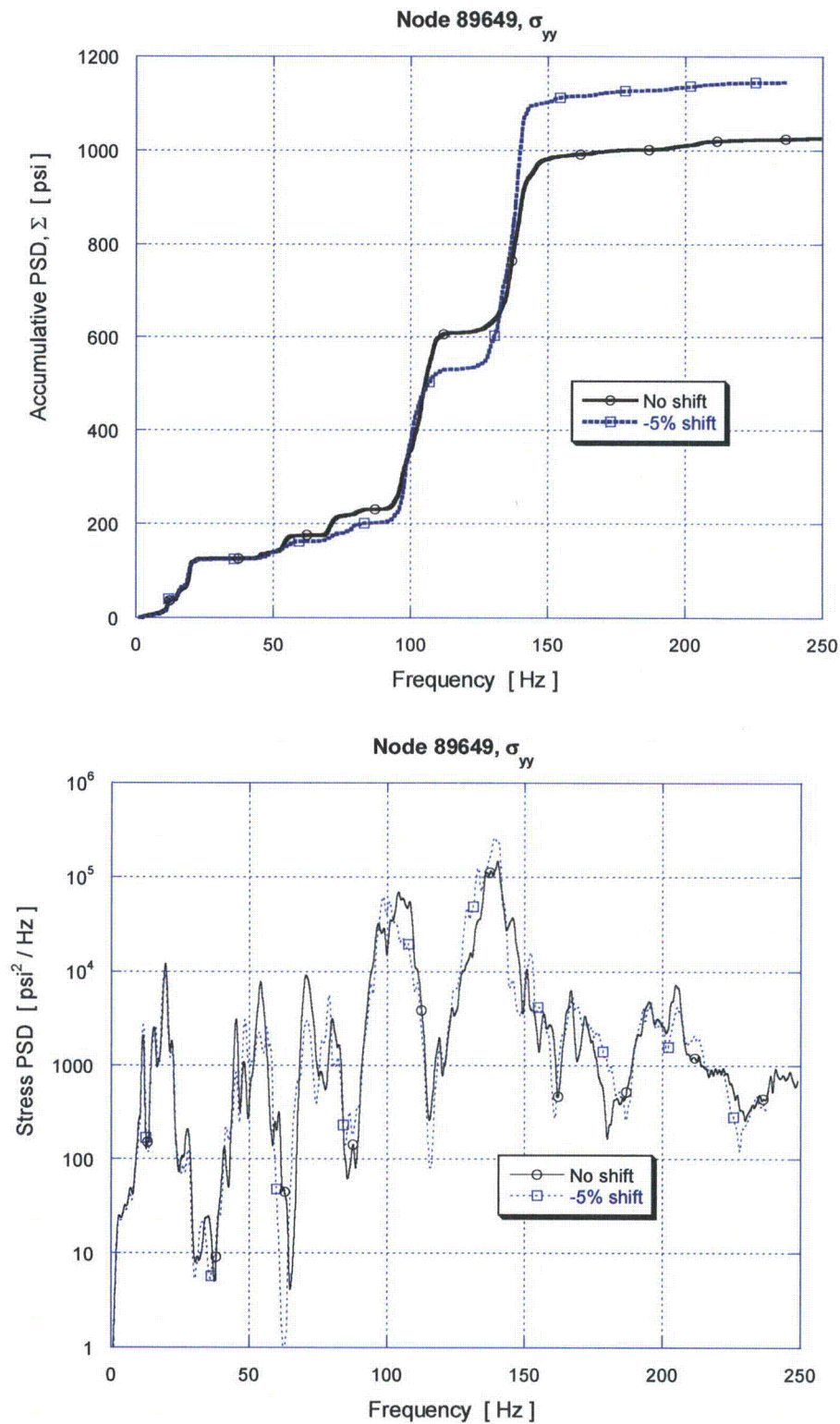


Figure 16a. Accumulative PSD and PSD curves of the  $\sigma_{yy}$  stress response at node 89649.

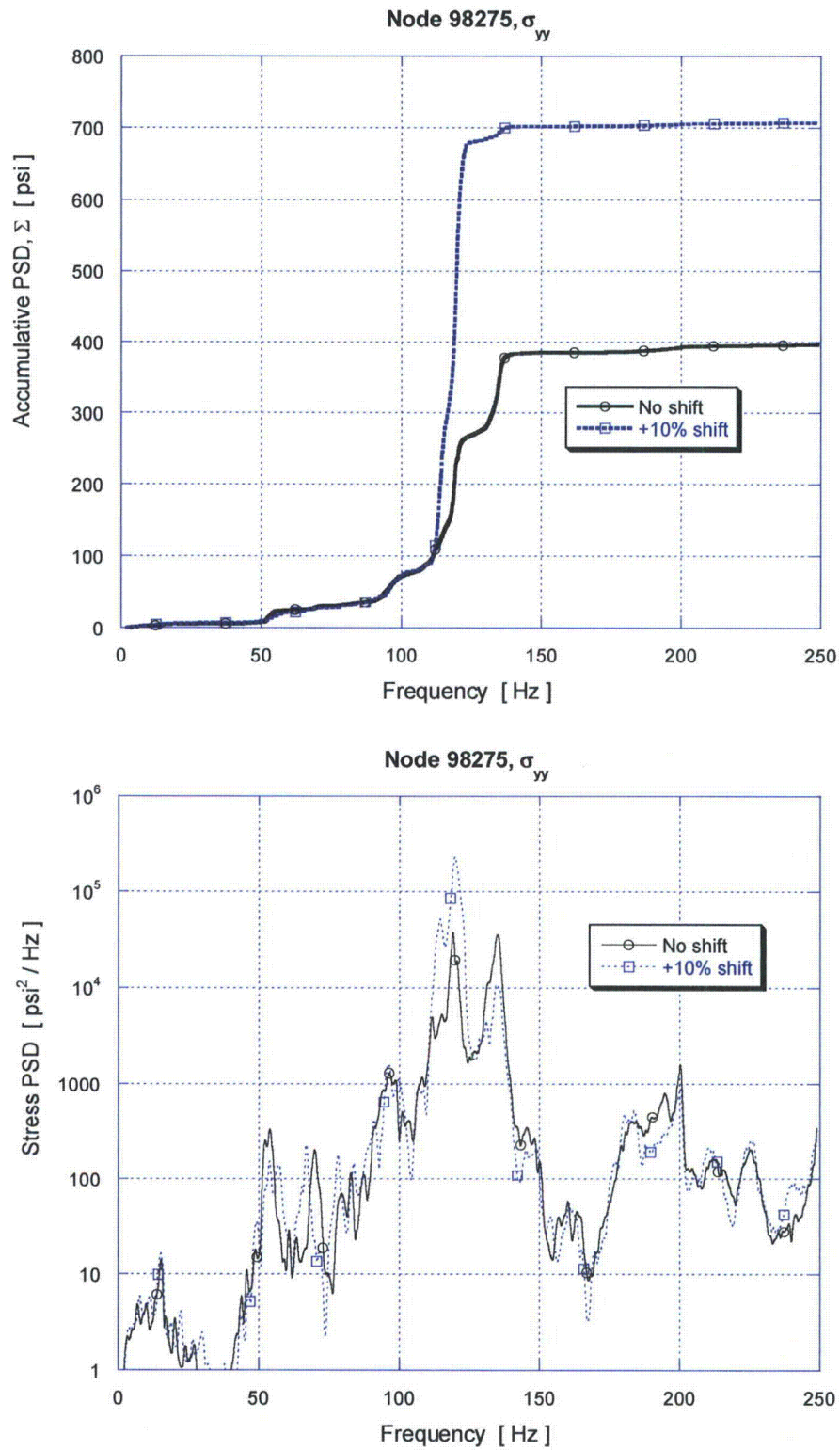


Figure 16b. Accumulative PSD and PSD of the  $\sigma_{yy}$  stress response at node 98275.



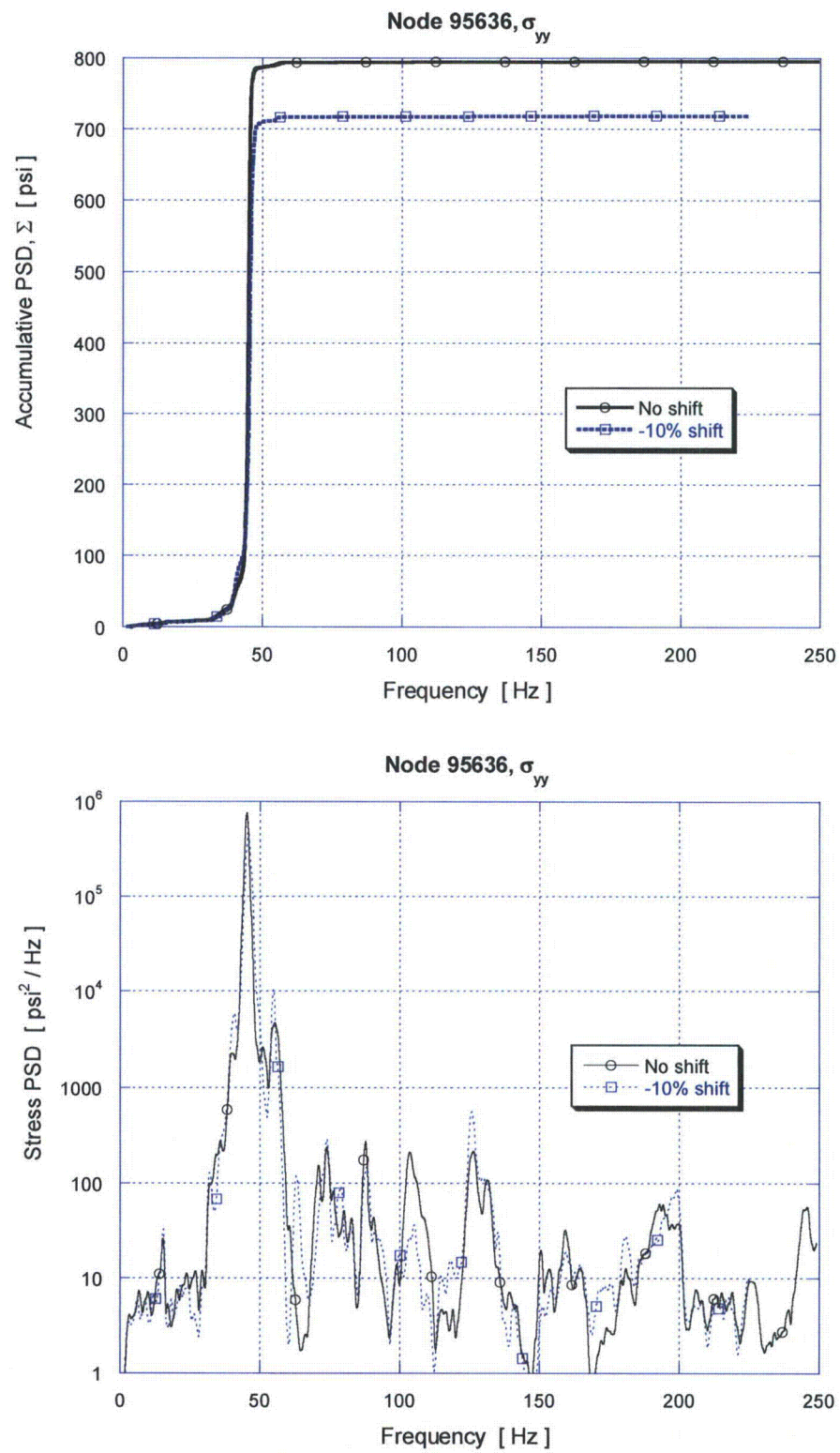


Figure 16c. Accumulative PSD and PSD of the  $\sigma_{yy}$  stress response at node 95636.

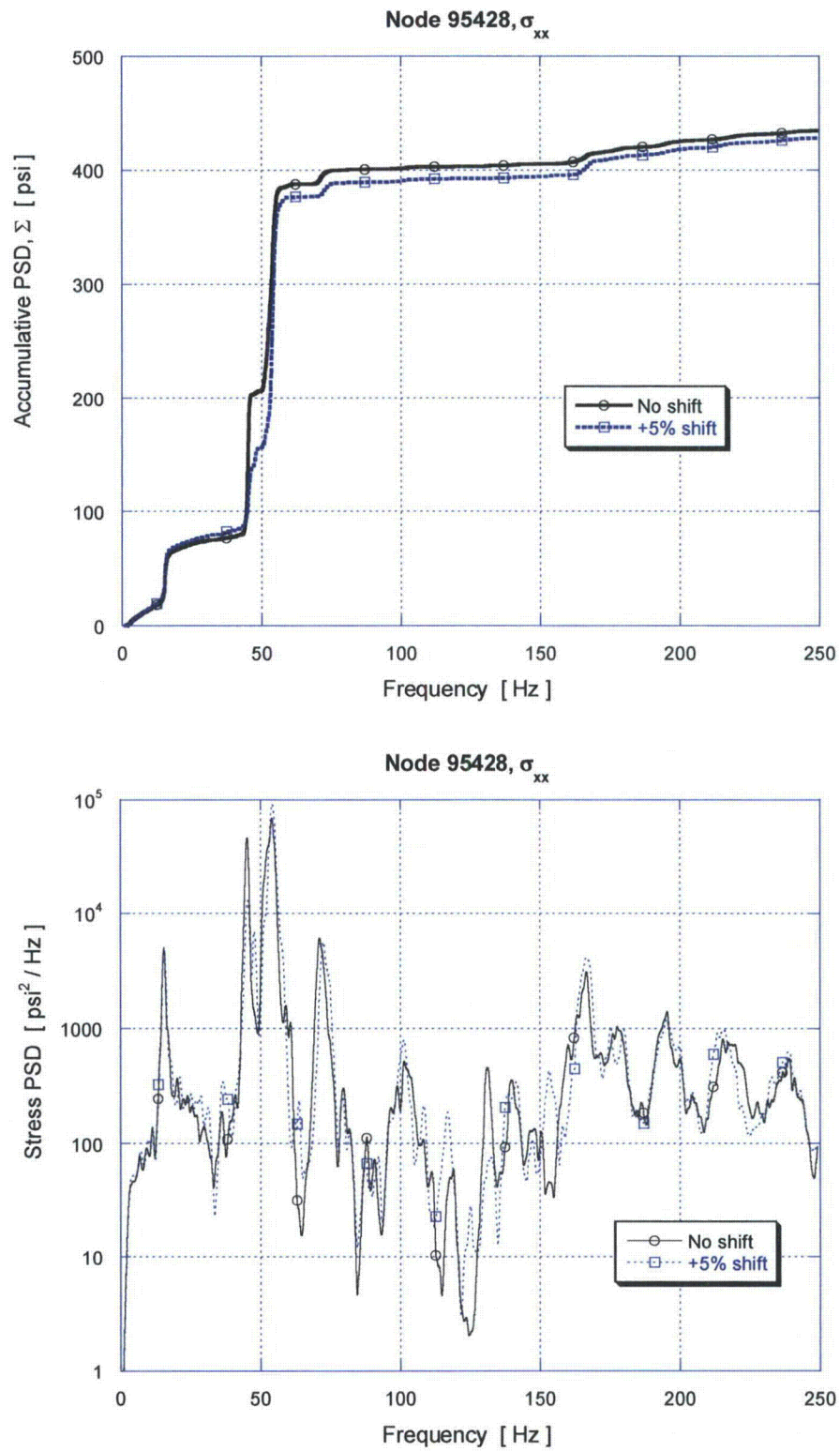


Figure 16d. Accumulative PSD and PSD of the  $\sigma_{xx}$  stress response at node 95428.

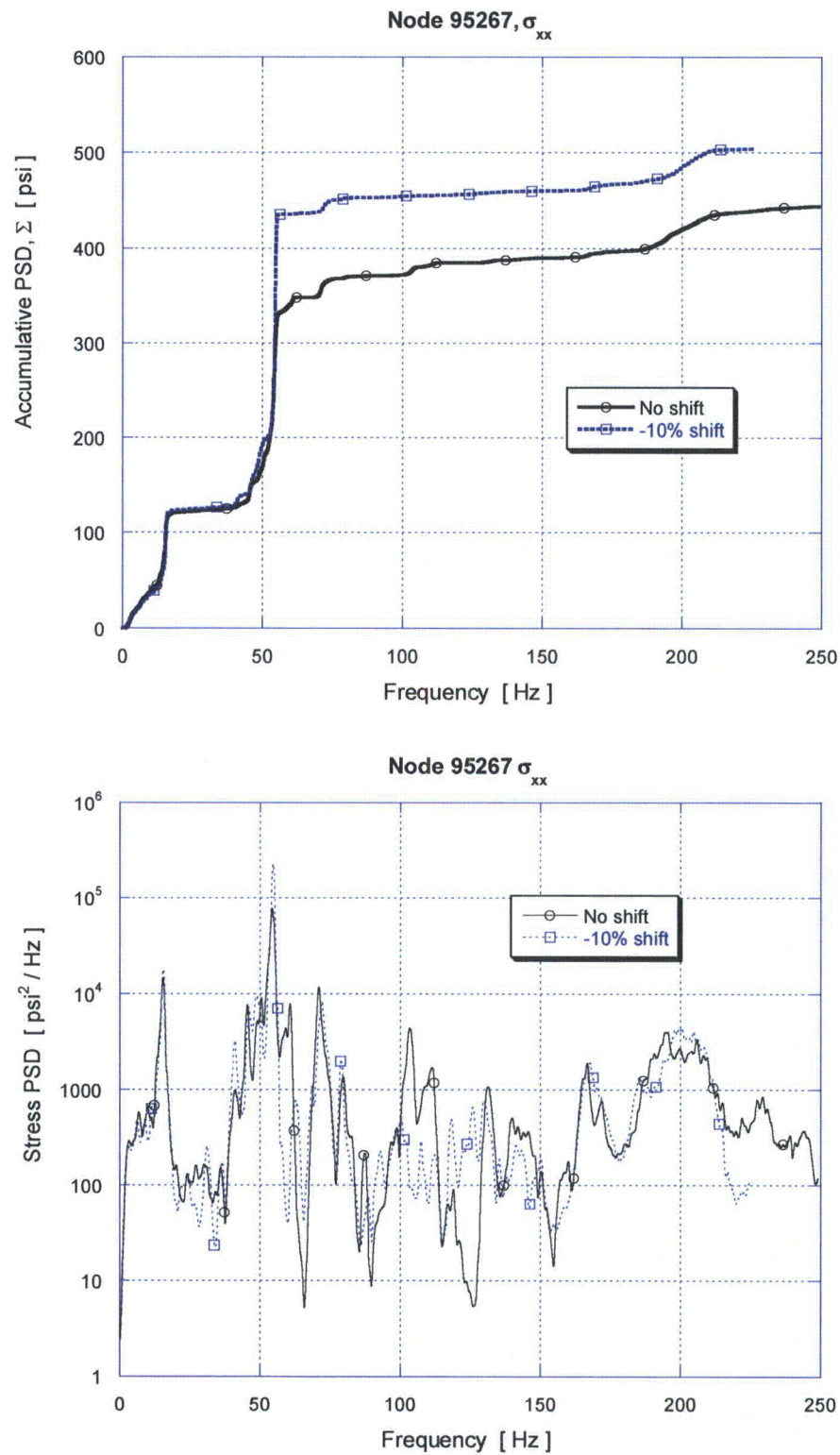


Figure 16e. Accumulative PSD and PSD of the  $\sigma_{xx}$  stress response at node 95267.



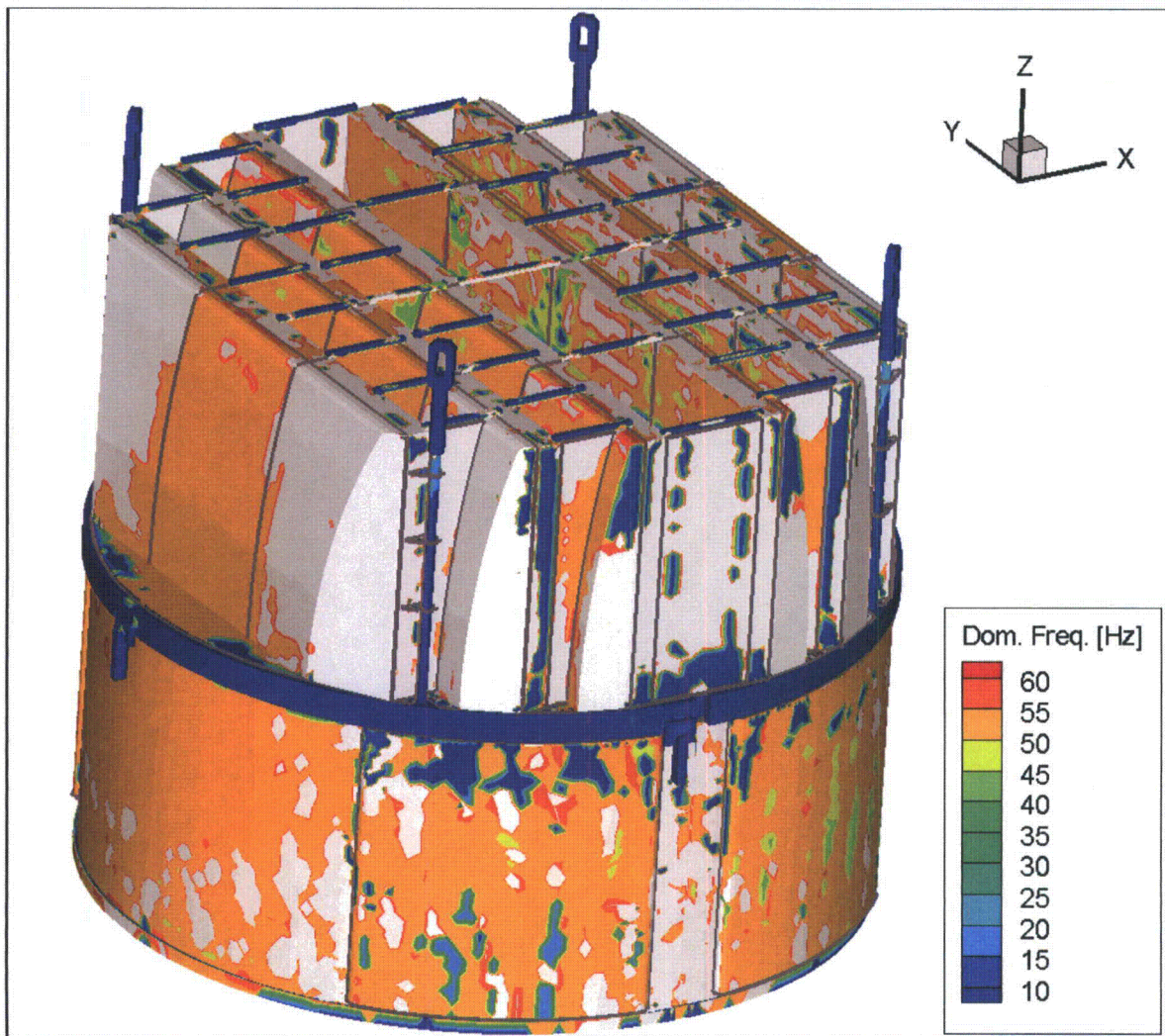


Figure 17a. Contour map showing the dominant frequencies (i.e., the frequency with the largest stress harmonic). This shows locations with dominant frequencies in the range 10-60 Hz.

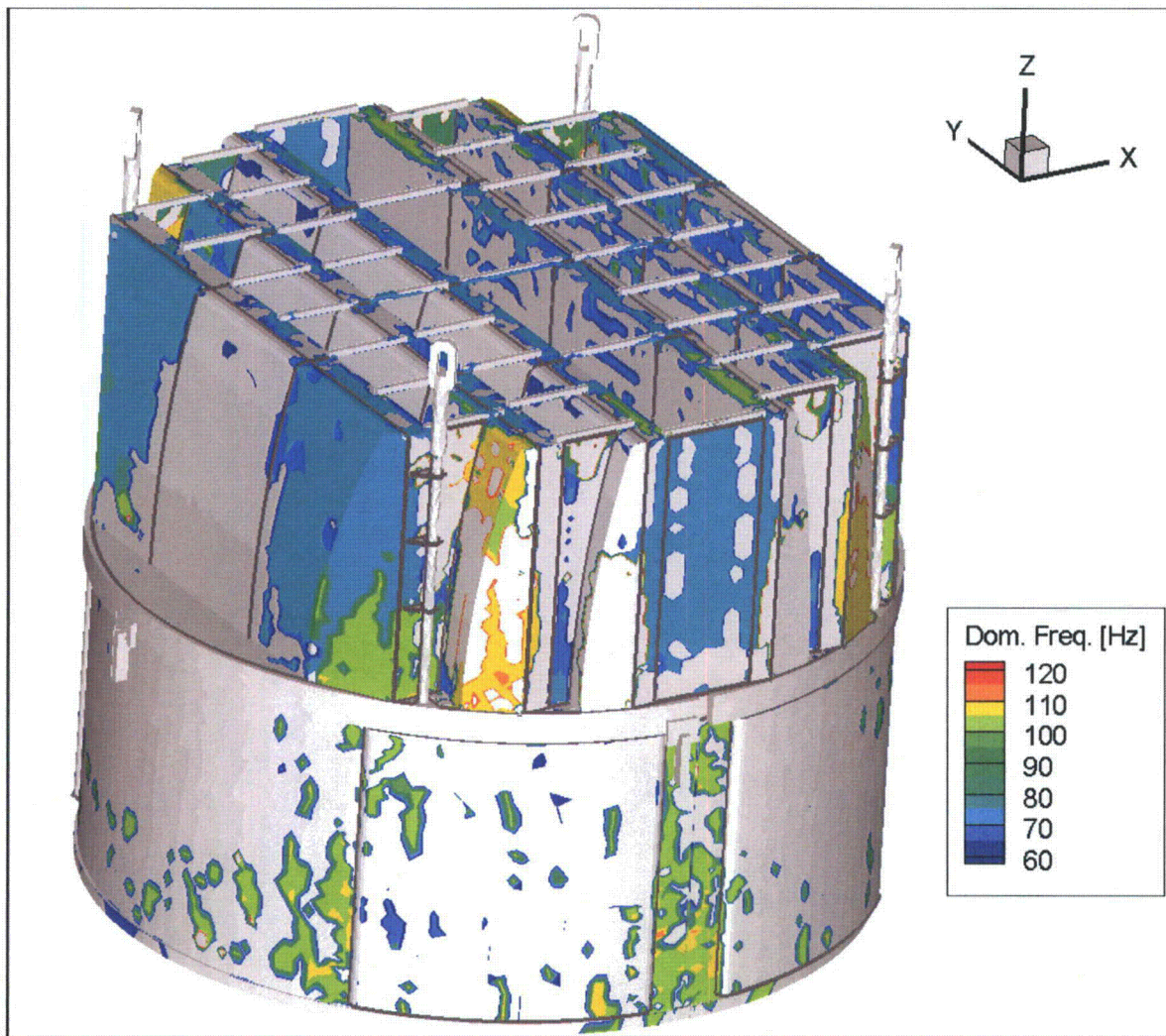


Figure 17b. Contour map showing the dominant frequencies (i.e., the frequency with the largest stress harmonic). This shows locations with dominant frequencies in the range 60-120 Hz.



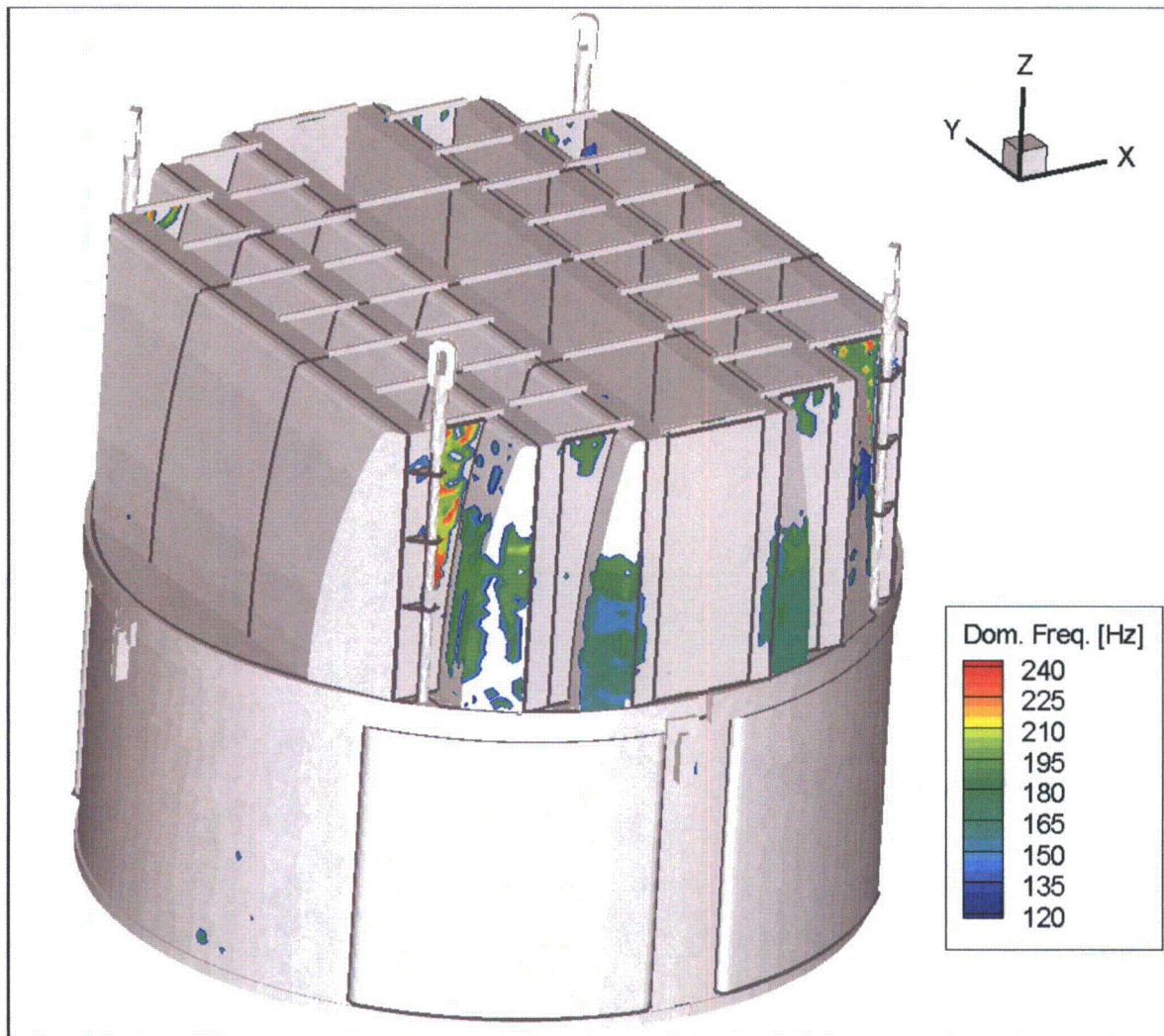


Figure 17c. Contour map showing the dominant frequencies (i.e., the frequency with the largest stress harmonic). This shows locations with dominant frequencies in the range 120-240 Hz.